High Volume Fraction Polymer Nanoparticles as Inkjet Ink Model Suspensions: from Synthesis to Rheological and Printing Characterisation

Mohmed Ashraf Mulla

School of Chemical and Process Engineering

University of Leeds

Submitted in accordance with the requirements for the degree of

Doctor of Philosophy

June, 2018

The author declares that the work in this dissertation was carried out in accordance with the requirements of the Universitys Regulations and Code of Practice for Research Degree Programmes and that it has not been submitted for any other academic award. Except where indicated by specific reference in the text, the work is the candidates own work. Work done in collaboration with, or with the assistance of others, is indicated as such. Any views expressed in the dissertation are those of the author.

Acknowledgements

I owe a great many thanks to a lot of people, without whom this project would never have reached fruition. I will attempt to thank them all, here goes...

First, thanks to my supervisor, Olivier. Olivier, without your help I would never have made it this far. Your patience and motivation have helped me achieve everything I wanted to from this project.
I would also like to express my gratitude for my initial supervisors: Simon, thanks for taking a chance with me. Grace, I can't thank you enough for getting me started and helping me realise how proactive I should be!
Next, my thanks to the Cambridge contingent: Steve, Simon, Graham, Prof Hutchings and all those I have been fortunate enough to meet and work with. Special mention to Steve, you were fantastically helpful and patient with the jetting experiments.
I want to extend my gratitude to Amy, Simon, Francesco, Alex, Kazi, Noa, Doojin, Shivani, Yuno, and the many others I was fortunate enough to meet in Okinawa. Amy, Simon, I feel very privileged to have worked with such talented researchers. Simon, you are truly inspiring to work alongside. Abhishek, Antonio, Alberto, Tori, Mariana and Mira, thanks for making a secluded quiet lifestyle, not quite so quiet.
Thanks to all past and present members of the Colloid and Polymer group. There are too many to name here, you know who you are.
During my time at Leeds I met many friends and talented Chemists/ Engineers. In rough chronological order: Grace, James H, EJ, Kirsty, Alison, Soyeb, Andy, Susanne, Ian, James S, Jess, Wei, Tom, James G, Yuanyuan, Tom, Calum, Huagui, Kai, Tim to name but a few. Thank

you all for making my time at Leeds very enjoyable!
Special mention to Jonny (JP), although its mainly the numerous AofE's, Zombies and the crazy trips I remember, its your help that I truly appreciate - be that proof reading, writing a speech or even a grant proposal - you were always there to sound out ideas with. Thanks for always being fantastically optimistic at every opportunity, I'm very lucky to count you as a friend. Lets hope our laid back attitude never changes !
Never forgetting, Phil, Harriet, Joel and now little Billy - you guys kept me sane throughout all of this. Thanks for always being around when I needed a break, and then pushing me when I needed a kick. Phil, you've been there since the beginning - here's to years from now, when we're still as hopelessly idiotic !
Of course my thanks also to the EPSRC for provision of a PhD studentship through a DTA scholarship, (grant number EP/H018913/1 Innovation in Industrial Inkjet Technology (I4T)). I would also like to thank the RSC for awarding me with a Mobility grant, which funded my trip to Japan. And not forgetting the SCI for the travel grant, enabling my travel to Harvard.
Last but by far the least, I owe everything to my family. Thank you all for always supporting me. You all made my life so much easier.

Abstract

Inkjet technology, a printing technique in which the digitally controlled drop formation affords accurate deposition at speed, is of great advantage for material preparation in several fields, such as printed biomaterials or electronics. However, there is a need to better understand the underlying fluid behaviour of colloidal dispersions, particularly when the solids content within the ink is increased, a highly desirable and cost-saving trait for industrial applications. More specifically, this applies to the speed and material diversity which can be attained, compared to conventional printing methods. Further, extensional deformation of colloidal particle dispersions has received little attention in the literature, despite the clear need to better understand the fluid response under these conditions. This holds particular relevance for inkjet printing, where the focus is to increase the material diversity.

To this end, high solids content sub 100 nm monodisperse model poly(methyl methacrylate) polymer particles have been prepared. These particle dispersions are normally prepared via complex polymerisation routes, requiring several sequential steps. However, research presented herein reports how a more straight forward chain transfer mediated emulsion polymerisation process is quite capable of preparing particle dispersions with these hard to attain properties. The developed method is a new route for high solids content latex preparation, and was fully explored and tuned to prepare particles in the 40-70 nm size range.

The particle dispersion shear rheology was then examined from a theoretical perspective. Moreover, the stability of particle dispersions at

extremely high effective volume fractions is also explored, with the implications upon the shear rheology and jetting behaviour examined. Finally, extensional viscosity of the particle dispersions was determined using a bespoke microfluidic cross slot device. The jetting behaviour was then observed using a drop on demand micro-fab set-up.

Contents

List of Figures

List of Tables

List of Symbols

Acronyms

μEP	Micro emulsion polymerisation
AA	Acrylic acid
AAm	Acrylamide
$AIBA$	2,2-Azobis(2-methylpropionamide) dihydrochloride
$AIBN$	2,2'-Azobisisobutyronitrile
AOT	Sodium bis(2-ethylhexyl) sulfosuccinate
APS	Ammonium persulfate
$ATRP$	Atom transfer radical polymerisation
BA	Butyl acrylate
BMA	Butyl methacrylate
c.s.	Co-solvent ... (where ... represents the co-solvent)
CEP	Conventional emulsion polymerisation
CIJ	Continuous Inkjet
CS	Co-surfactant
CTA	Chain transfer agent
$CTAB$	Cetyltrimethylammonium bromide
$CTMA$	Cetyltrimethyl ammonium chloride
D	Deformation rate tensor
$DLVO$	Derjaguin-Landau-Verwey-Overbeek theory
DOD	Drop on demand
EDL	Electric double layer
FCC	Face centred cubic
$Fmon$	2-Napthyl methacrylate
HD	Hexadecane

$HEMA$	Hydroxyethyl methacrylate
KPS	Potassium persulfate
mEP	Mini emulsion polymerisation
MMA	Methyl methacrylate
NMR	Nuclear magnetic resonance spectroscopy
NPA	N-propargylamide
$p(MMA)$	Poly(methyl methacrylate)
$PLED$	Polymer light emitting diode
$PNPs$	Polymer nanoparticles
PS	Polystyrene
PSD	Particle size distribution
PSS	Poly(styrene sulfonic acid) sodium salt
PVA	Poly(vinyl alcohol)
R_c	Represents hydrocarbon chains
$RAFT$	Reversible addition fragmentation chain transfer
SDS	Sodium dodecyl sulfate
St	Styrene
$Tween80$	A non-ionic surfactant based on sorbitol and oleic acid
$V-50$	2,2-azobis(2-amidinopropane) dichloride
$V-59$	2,2-azobis(2-methylbutyronitrile)
VA	Vinyl acetate
VCz	N-vinylcarbazole
$w.r.t.$	With respect to
[X]	Concentration of X

Greek Symbols

$[\eta]$	Intrinsic viscosity of particles in medium	$\mathrm{Pa \cdot s}$
α	Aspect ratio	n/a
$\dot{\gamma}$	Shear rate	$\mathrm{s^{-1}}$
$\dot{\varepsilon}$	Extensional rate	$\mathrm{s^{-1}}$
ϵ_0	Dielectric constant	F/m
ϵ_r	Permittivity of free space	n/a
η	Apparent viscosity	$\mathrm{Pa \cdot s}$
η_0	Zero shear viscosity	$\mathrm{Pa \cdot s}$

η_∞	Infinite shear viscosity	$\mathrm{Pa}\cdot\mathrm{s}$
η_c	Suspension viscosity	$\mathrm{Pa}\cdot\mathrm{s}$
η_E	Extensional viscosity	$\mathrm{Pa}\cdot\mathrm{s}$
η_L	Solvent viscosity	$\mathrm{Pa}\cdot\mathrm{s}$
η_r	Relative viscosity	$\mathrm{Pa}\cdot\mathrm{s}$
η_r^{cf}	Colloidal force viscosity contribution	$\mathrm{Pa}\cdot\mathrm{s}$
η_r^{hs}	Hard sphere viscosity contribution	$\mathrm{Pa}\cdot\mathrm{s}$
Γ	Excess interfacial concentration of surfactant	n/a
κ^{-1}	Debye length	m
λ_c	Characteristic relaxation time	Pa
μ	Newtonian viscosity	$\mathrm{Pa}\cdot\mathrm{s}$
μ	Viscosity	$\mathrm{Pa}\cdot\mathrm{s}$
ϕ	Volume fraction of particles	n/a
ϕ_f	Freezing particle fraction	n/a
ϕ_G	Volume fraction of glassy state	n/a
ϕ_M	Melting particle fraction	n/a
ϕ_m	Maximum packing fraction	n/a
$\phi_{eff,EG}$	Effective volume fraction in ethylene glycol co-solvent	Pa
ϕ_{eff}	Effective particle volume fraction	n/a
ϕ_{EG}	Volume fraction in ethylene glycol co-solvent	Pa
$\phi_{m,eff}$	Maximum effective packing fraction	n/a
ρ	Density	$\mathrm{g/cm^3}$
σ	Shear stress	Pa
σ^*	Complex stress	Pa
σ_p	Particle stress	Pa

Roman Symbols

ΔP_E	Excess pressure drop, extensional contribution	Pa
ΔP_s	Pressure drop, shear contribution	Pa
ΔP_t	Total pressure drop in the cross-slot device	Pa
a	Closest distance between two charged particles	m
A_n	Interfacial area	m
b	Dimensionless proportionality constant	n/a
cmc	Critical micelle concentration	M

d	Microchannel depth	m
d_H	Hydrodynamic diameter	m
g	Surface tension	N/m
G'	Elastic modulus	Pa
G''	Viscous modulus	Pa
H	Separation distance	m
h	height	m
k_B	Boltzmann constant (1.3806 x 10^{-23})	J/K
k_BT	Thermal energy (4.11 x 10^{-21} at 25°C)	J
m	Mass	g
N_D	Nozzle diameter	m
N_p	Total number of particles	n/a
PDI	Poly dispersity index	n/a
R	Gas constant	$\mathrm{J \cdot mol^{-1} \cdot K^{-1}}$
r	Radius	m
r_{eff}	Effective particle radius	m
r_{hs}	Equivalent hard sphere radius	m
Re	Reynolds number	n/a
T	Absolute temperature	K
Tr	Trouton ratio	n/a
U	Flow velocity	m/s
U_J	Jet velocity	m/s
U_{Max}	Activation energy	J/mol
UV	Ultraviolet light	nm
V_c	Volume of a sphere	$\mathrm{m^3}$
$V_{eff,c}$	Effective volume of a sphere	$\mathrm{m^3}$
$V_{efft,c}$	Effective total dispersed phase volume	$\mathrm{m^3}$
$V_{t,c}$	Total dispersed phase volume	$\mathrm{m^3}$
w	Microchannel width	m
W_m	Minimum amount of work	N
We	Weber number	n/a

Si Units

F	Farad

J	Joule
K	Kelvin
kg	Kilogram
m	Meter
M	Molar
N	Newton
Pa	Pascal
s	Second

Publications and Conferences

M.A. Mulla, H. Zhang, H.Y. Yow, O.J. Cayre, S. Biggs, Colloid particles in Inkjet formulations in: S. Hoath (Ed), Fundamentals of Inkjet Printing: The Science of Inkjet and Droplets, Wiley-VCH, 2016.
M.A. Mulla, H.Y. Yow, O.J. Cayre, S. Biggs, A new route to high solids content sub 100 nm monodisperse latex particles, *manuscript in preparation.*
M.A. Mulla, O.J. Cayre, Inkjet printing model latex particles, *manuscript in preparation.*

Conferences

90th ACS Colloid and Surface Science Symposium, oral presentation, *Inkjet Printing Colloidal Fluids*, Cambridge, MA, USA, 2016.
Science of Inkjet and Printed Drops, oral presentation, *Preparation and Characterisation of Colloidal Inkjet Inks*, London, UK, 2015.
15th European Student Colloid Conference, oral presentation, *Preparation, Characterisation and Printing Model Colloidal Inkjet Inks*, Krakow, Poland, 2015.
International Association of Colloid and Interface Science, oral presentation, *Preparation and Characterisation of Colloidal Inkjet Inks*, Mainz, Germany, 2015.
UK international colloids conference, poster presentation, *Preparation of Model Colloidal Inkjet Inks*, London, UK, 2014.

Innovation in Industrial Inkjet technology consortium, oral and poster presentations, *Presentations to Industrial and Academic sponsors*, Cambridge, UK, 2013-2015. (monthly review meetings (researchers), and quarterly technical review meetings (Industrial partners))

Project Motivation and Overview

This project is part of a collaboration between the Universities of Leeds, Cambridge and Durham for the investigation and innovation in Industrial Inkjet technology, strongly supported by 8 UK based companies.[1]

The collaboration was formed to better understand the inkjet printing process, by investigating the formulation and behaviour of printed drops. The aim of the consortium was to widen the range of materials that can be printed using this technique, with particular focus on high solids content colloidal fluids. And in so doing, extend the status of the technique from a niche technology to one widely used commercially.

Within this aim, the consortium focuses on three main themes of the inkjet printing process;

Theme I focuses on the formulation, rheology and jetting behaviour of colloidal dispersions: A theoretical and practical understanding of the formulation of high solids content colloidal dispersions, their behaviour in an inkjet system, and upon deposition onto a substrate.

Theme II focuses on the understanding and control of dynamic micro-scale drop impact, spreading and fixing: this involves investigating the processes controlling the functionality and structure of the printed features. The features examined include the chemistry and surface treatment of the substrate, surface morphology, interactions between successive droplets, and the fluid dynamics of wetting.

Theme III focuses on developing a model to describe all aspects of the fluid behaviour leading to the formation of drops, and the fate of the drops. The model, based on the underlying physical theory, was to be validated by precise practical measurements by incorporating the knowledge from the previous two themes.

The overall aim of this project, within the consortium was to examine and understand the jetting behaviour of high solids content particle dispersions, for application in commercial manufacturing processes.

This required the preparation of colloidally stable model particle dispersions in the sub-100 nm range, with a monodisperse size distribution. To this end, a novel route to prepare model high solids content p(MMA) latex particle dispersions was designed and finely tuned: p(MMA) was chosen as the density difference between the particles and solvent would be small and thus would improve overall stability.

The shear viscosity was examined from a fundamental perspective, with the importance of the effective volume fraction highlighted. In the same vein, the electrolyte concentration is found to have a large impact on the formation of repulsive driven glasses at high particle effective volume fractions.

The elongational viscosity of the dispersions was then examined and related to the jetting behaviour.

Thesis Overview

Traditionally, a thesis might begin with a literature review which paves the way for the novel research that follows. However, in this project such a review would have to encompass many different topics, relating to polymer synthesis, colloid stability, fluid flow and microfluidics. Such a review would be far too large with difficult segues between each topic, and frankly tedious to understand without first presenting the results for each topic. Therefore, a concise literature review is presented within the introduction of each results chapter.
The following is a brief outline of the research presented within this thesis;

Chapter 1: introduction to basic concepts related to colloids, polymers and inkjet printing, laying the foundations for the research presented in the following chapters.

Chapter 2: is concerned with latex particle synthesis, and includes the results obtained from a thoroughly refined method to prepare monodisperse particles with a sub-100 nm size, at a high solids content.

Chapter 3: covers the characterisation of particle dispersion stability and shear viscosity.

Chapter 4: is concerned with the elongational rheology of particle dispersions, and the methods used to obtain this data. The chapter also assesses the printing ability of these dispersions, with the aid of a micro-fab jetting set-up at Cambridge University

Chapter 5: summary of the results obtained within this research project, and possible future directions.

Preface

In formal scientific writing we are taught to avoid personal pronouns. I briefly deviate from convention here, and ask you please to indulge me. I have decided to include this preface to give readers an insight into the directions I took with this project and account for the research that didn't make the cut. I am hoping that from reading this, the reader can perhaps understand how the research evolved into finished product.

Perhaps the most appropriate description of this project, in a word would be 'eclectic'. The research spans multiple fields within chemical engineering, specifically particle synthesis, to shear and elongational rheology (microfluidics) and inkjet printing. My project remit was to Inkjet print colloidal dispersions, and characterise how x, y, and z, variables affected the printing process from jetting through to drop deposition, ideally ending up with a guide, of sorts, to printing high solids content particle dispersions. The idea was to prepare the particles in house, where we could control the physiochemical properties.

A point I would like to emphasise here, which may be common to all PhD and long term projects, is that the struggles encountered during the project are rarely evident in the final presented work. On this point, although only being responsible for a small proportion of the thesis word count, considerable time was invested in optimising the polymerisation of a suitable polymer particles. Albeit a necessary investment given the success of the whole project hinged upon synthesis of suitable particle dispersions!

The aim was to use as little surfactant as possible, so we could control the surface tension of the dispersion when we used them to examine the jetting behaviour and drop drying. Therefore, I focussed quite a bit of attention on trying to reproduce a synthesis route from the literature where the authors prepared particles using a

surfactant free method. However, in the end I found this could not be reproduced, whether that was due to unreported reaction conditions or the authors had harnessed the powers of the dark arts I cannot say! But I can assure the readers that considerable effort and time was spent carefully reproducing these experiments.

On a similar and perhaps more appropriate note, significant effort was exerted preparing fluorescent particles. The plan was to use these particles to examine drop drying behaviour and the variables that can be manipulated to improve the particle distribution in the deposit: where the hope was track the particles using fluorescent microscopy. Ultimately, this proved to be time and effort wasted, as by the time the synthesis had been satisfactorily tuned, our collaborators with the equipment required to explore this, were no longer interested in this area. I no longer resent this time drain (I gained useful synthetic experience), though I can assure you I did, briefly at the time.

I also invested time in investigating how the addition of various free polymers would affect the drop deposition and the jetting behaviour, and examining particle and non-adsorbing free polymer mixtures both from a stability and rheological perspective. However, the jetting experiments failed, irrespective of the slow destabilisation observed for these dispersions, and consequently the data is not included here. This was most likely due to the depletion flocculation interaction forming large aggregates which clogged up and/or dried up with the nozzle, preventing jetting behaviour to be observed .

The focal point of this project, jetting particle dispersions, always felt like an eternal struggle against nature. From experience I can say with some authority, it is very difficult to flow colloidal dispersions through small crevices. I spent a long time getting to grips with the jetting set-up, particularly with the nozzles, which are fantastically difficult to clean when clogged. With this in mind, it is important to clarify that all efforts were made to include only carefully collected, and importantly reproduceable data - by the end I was intimately familiar with the instrumentation and well equipped to deal with almost any issues the instrument could present!

Chapter 1

General Introduction

The following is some fundamental information required to fully understand the concepts discussed throughout this thesis.

1.1 Inkjet Printing

Inkjet technology was developed in 1970s, and has been in commercial use since the 1980s, and is even now an ever present personal printing tool.[2] The concept of inkjet printing can be traced as far back as the nineteenth century.[3] Inkjet printing involves digitally controlling the generation, manipulation and accurate deposition of micron sized ink drops, at a controlled rate. Although inkjet technology is mainly used for printing purposes (graphics and conventional printing), it has the potential to be used in the manufacturing process. It could be applied in the chemical, biochemical, or pharmaceutical industry as an accurate dispensing tool.[4,5] Or if the material for 3D printing is available in the form of a liquid initially, could also be used to build 3D objects.[6,7]

Inkjet printing has the advantages of being a very flexible method for printing small amounts of material, which can easily be used for mass fabrication. It was used to produce polymer emitting light diode displays using poly(3,4-ethylenedioxythiophene) (an semiconducting aqueous solution), as the ink.[8] The device was used to display a logo. The technique has also been used in liquid crystal display manufacture to produce the colour filters.[9] Various coloured inks (both pigments and

dyes) were printed on each pixel to prepare a multicolour display.

Inkjet technology has also been investigated for 3D printing using metallic or ceramic colloidal dispersions.[6] 3D printing would allow manufacture of complex components or could be used for rapid prototyping. These are prepared using an ink that includes particles and a binder in the formulation.[7] Good drop deposition is crucial for preparation of complex structures. The viscosity of such inks increases due to the inclusion of binders, and generally the inks are found to be shear thinning.[10] These inks have a time dependent rheology which further complicates the deposition process. This is a promising technique, but has been shown to lead to a few issues with the most important one solids loading. Ideally a high solids ink, would create a better final product. Inefficient drying is also a big issue with this kind of technique.[11]

An alternative technique for 3D printing involves printing a binder solution, acting as the ink, to create a 3D object by binding ceramic powder. This technique works by printing layer by layer to create the final 3D object. Various types of binding solutions have been tested for 3D printing using inkjet to print. Solutions with varying viscosity (2.9-9 mPa.s) and surface tension (26.2-50.2 mNm^{-1}) have been printed with solids loading between 10-20 vol%.[10]

Inkjet printing is, therefore a very versatile method and has been used in many fields including plastic electronic manufacture, 3D ceramic printing, drug delivery devices to name but a few. It is a technique with huge potential, particularly for applications orientated for manufacturing processes.

The inkjet printing technique must be suitably prepared for a given application, from the print-head, ink and the substrate to be jetted onto.[2] For a given application the requirements must first be established, which then enable selection of the most appropriate hardware and ink.

There are some limitations for the inkjet printing process which must also be addressed for wider applicability, relative to its main use in graphical printing.[12] The resolution which depends on the accuracy of the deposited drop, as well as the size of the dried drop. The precision which depends on the both on the print head and the drop in flight. The drop whilst in flight is affected by electrostatic and aerodynamic effects. The biggest limitation however, is the material diversity in the available inkjet-able inks, particularly high solids content colloidal dispersions;

fluids that are attractive for manufacturing applications.[1] These include functional fluids used to prepare a range of materials, including solar cells, flexible electronics, biomaterials etc.[13,14]

1.1.1 Inkjet inks

Currently, there are four main types of inkjet inks that are commonly used, phase change, solvent based, water based, and UV curable inks.[15–18] Less prevalent inks, such as oil based, or hybrid inks of the four aforementioned inks do exist but are not extensively studied.

Phase change inks are sold in solid form, but are melted in the printer prior to being jetted.[19] These inks, therefore exhibit a fast drying time (upon deposition), show good opacity, and they are also very environmentally friendly. However these are inks are not very durable and also have a poor resistance to abrasions. An example for the application of these inks, is in the field of barcode printing where they are printed onto non-porous substrates.

Aqueous (or water) based inks are relatively inexpensive and environmentally friendly, and are normally used for desktop printing (i.e. home/work use).[17] They are not prevalent in industrial applications as these inks require specially treated or porous substrates or even lamination, otherwise durability is very poor. Also these inks are unsuitable for non-porous substrates.

UV curable inks when printed remain as stable liquids, on the substrate until they are irradiated with a particular wavelength and intensity of light.[18] They have been in use for many years, and the inkjet printing of these inks is now a robust and well established technique. They are used in many applications including product coating, package decoration and labelling. However, the UV curing hardware increases the costs and facilities (space, power) required to implement these inks.

Solvent based inks are traditional the inks of choice, and have been around for years.[16] They produce an excellent print quality, have great durability and can be used on a range of substrates. They also have a fast drying time (can be accelerated by heating), and are generally cost effective. However because of this fast drying, they require high maintenance as they could potentially block print head nozzles. There are also some environmental concerns surrounding these inks.

Pigment based Inkjet Inks

Originally, the inks used for graphics printing were dye-based inks, but as the deficiencies of such inks became clear, pigmented inks soon began to replace these.[20] Dyed ink although has good print quality, it has very poor image durability. Water-, light- and weather-fastness were very quickly highlighted as the weaknesses for such inks. Pigments, used in paints, plastics and coatings, are known to perform much better in this respect while producing a quality final product.[21] The colour of the paint and the finish is from the pigments used. They hold the paint together, for a smooth finish, and also protect the painted surface from corrosion and protect somewhat from weathering. Note some inks used today are still dye based, however due to the increased understanding of the mechanics; these inks have significantly improved properties relative to the older dye based inks.[22]

Pigmented inks are prepared by dispersing pigments with a diameter between 50-200 nm to produce a colloidally stable dispersion.[23] In order to create a stable dispersion the pigments must be stabilised is some manner. This is normally achieved by either steric or charge stabilisation. Surfactants or some polymer derivatives can be used to achieve this stability. In some cases the pigment surface is modified, by addition of functional groups to create a surface charge to stabilise the dispersion in that manner.

There are a few issues that should be considered for pigmented ink formulation, including stability, viscosity, surface tension of dispersion, size, etc.[12] Ink stability is a big issue, as depending on the application the ink may be used over a period of weeks to months. All pigment dispersion will eventually settle, destabilising the ink but by controlling the pigment properties the shelf life can be increased. Using a smaller particle size would increase the shelf life, as settling is proportional to the square of the particle diameter.[24] The density difference between the particle and the dispersant should as small as possible to again reduce the rate of settling.

The pigment size is also an issue during jetting, where the micro jets can be as small as 10 μm in diameter. Using larger particle can cause irreversible damage to the jets, generally the smaller the particles the better the overall performance will be. The viscosity and the surface tension of the dispersion are also an issue during

jetting. For adequate inkjet print-head filling and droplet ejection the dispersion is required to be of relatively low viscosity ($\sim$ 1-20 mPa.s).[12]

High solids loading is required for some lightfast pigments, which could then affect the viscosity and stability of the dispersion.[17] Lightfast pigments here refer to those pigments where the colour intensity produced is a bit dull, therefore would require more pigments to produce a final deposit with desirable colour intensity.

These are just some of the issues that are required to be addressed for inkjet ink preparation. Some of these have been overcome though as proved by the readily available inkjet pigment ink from various global manufacturers, including Cabot, Ciba, Toyo ink etc.

A good understanding of the ink rheology is required for inkjet applications, in order to prepare inks that both perform well for their respective application, and can still be inkjet printed (behave well in the print-head, upon jetting and deposition). However, very few authors have systematically studied this behaviour for the inks being investigated, instead opting to use simple rheology data (shear rate vs. viscosity) to prepare inks with appropriate viscosity for inkjet printing.[25]

1.1.2 Drop generation

Inkjet printers generate drops by two methods, continuous inkjet (CIJ), and drop on demand (DOD) printing.[2]

CIJ is generates a continuous stream of drops regardless of whether they are required or not, Figure 1.1. The unrequired drops are deflected into a collection gutter by an electric field, from where the ink is recycled and used again. This is a potential wasteful process as the ink may become contaminated. The drops generated by this method are $\sim$ 100 μm in diameter, which are normally two times larger than the nozzle diameter. Drops are positioned by either moving the substrate, or by steering the drop when in flight, and typically have a velocity of $\geq$ 10 ms^{-1}.

DOD is a more economic method, as it only generates ink drops when they are required, Figure 1.2. The drops are positioned by moving the print-head to where they are required and then printed. The surface tension of the ink is important for this method, as the ink in the nozzle is held in place by surface tension. This is the preferred method, and the most studied method for inkjet printing, as it can be used

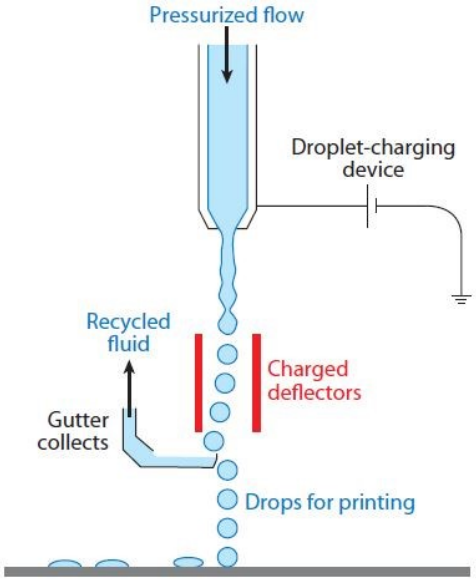

Figure 1.1: Schematic diagram of a continuous inkjet print-head. Reprinted from ref (2).

to control the size and velocity of the generated drops. Therefore it is the method concentrated upon in the consortium, and will also be the focus of this project.

Printing using inkjet technology involves jetting the ink onto a substrate with 1 mm standoff distance. The ink is jetted through a nozzle, where the drops are formed, and must have enough forward momentum to reach the substrate. Controlling the piezo print-head timing can be used to tailor the drops produced to the ink properties, to achieve the adequate viscosity for example.[26] Newtonian fluids for example have a narrow range of conditions, where the properties are useful for jetting. The print-head temperature can be increased to attain the best possible properties (i.e. viscosity) of the fluid for optimum jetting behaviour, which is unattainable at ambient temperatures.

Non-Newtonian fluids, such as linear polymer suspensions, are of great interest for manufacturing purposes, to be used for example for the production of flexible electronics and solar cells. Good jetting behaviour of a certain fluid appears to be rather straightforward and predictable, from the empirical outcomes for DOD printing.[26] It is probably because of this that normally, prior to printing, the fluid is only considered for the final application rather than the jetting process as a whole.

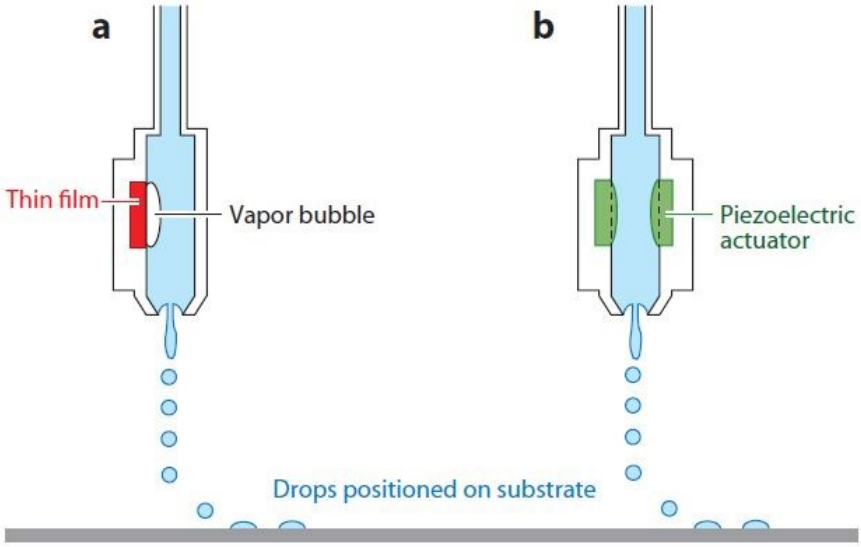

Figure 1.2: Schematic diagram of a drop on demand print-head. Reprinted from ref (2).

In that, deposition behaviour is focussed on more so than jetting, when formulating an ink, as long the ink displays the adequate properties specific to the print-head when jetted.

However in reality this is not adequate, rather good jetting behaviour cannot be sufficiently predicted from single characterisation parameters, such as low shear rate viscosity.[26] Good jetting behaviour, here, refers to the link between the rheology, drop formation and the printing of complex (non-Newtonian) fluids. The piezo producing the jet typically has small deformations relative to the nozzle (20 nm vs. 30 μm), which then suggests the jetting may well be affected by the linear viscoelastic response of the fluid.

This thesis is concerned with the study of polymer (colloidal) particles, more specifically their preparation, the various physiochemical properties they exhibit and their use as a model system to examine Inkjet printing behaviour. Therefore, in the following sections the fundamental properties of colloids, surfactants and polymers are discussed and the underlying science thus, creating the foundations for the overall research presented within.

1.2 Colloids

There is no formal definition of a colloid that describes, fully the numerous classes and examples of colloidal systems. However, these systems are characterised as a dispersion of two immiscible components, where one of the components has a size $\leq$1 μm in at least one dimension.[24] This size restriction means colloids have significantly large surface areas per unit volume. Colloid science is the study of the interactions between the two (or more) phases, and in most cases can be more aptly termed colloid and interface science.

Examples of colloids are found in a whole myriad of everyday products including cheese, butter, toothpaste, paint, inks. They are also many examples of naturally occurring colloids including milk, blood, clouds, mist and dust.

Polymer particles, also known as latex particle are another example and an important class of colloids for this thesis. Both naturally occurring, and synthetic polymers are used to prepare materials that have become ubiquitous in daily life. Examples include protective clothing, packaging, foods including gelatine, contact lenses and shoes.

1.3 Polymers

Polymers, also known as macromolecules, where the essential constituents are numerous monomer repeat units. They can be further classified in terms of the arrangement of the monomer units for clarity (figure 1.3).[27] The nature and arrangement of the monomer as well as the number of monomer repeat units (molecular weight) all affect the behaviour of the resulting polymer suspension.[27,28]

1.3.1 Monomers

Monomers, a contraction of *mono* meaning one, and *mer* meaning part, are the constituent molecules of a polymer (where polymer is a contraction of *poly* meaning many, and *mer* meaning parts). There are numerous monomers available for polymer preparation, where the wide variety of chemical and physical properties which can significantly affect the subsequent polymer.[28]

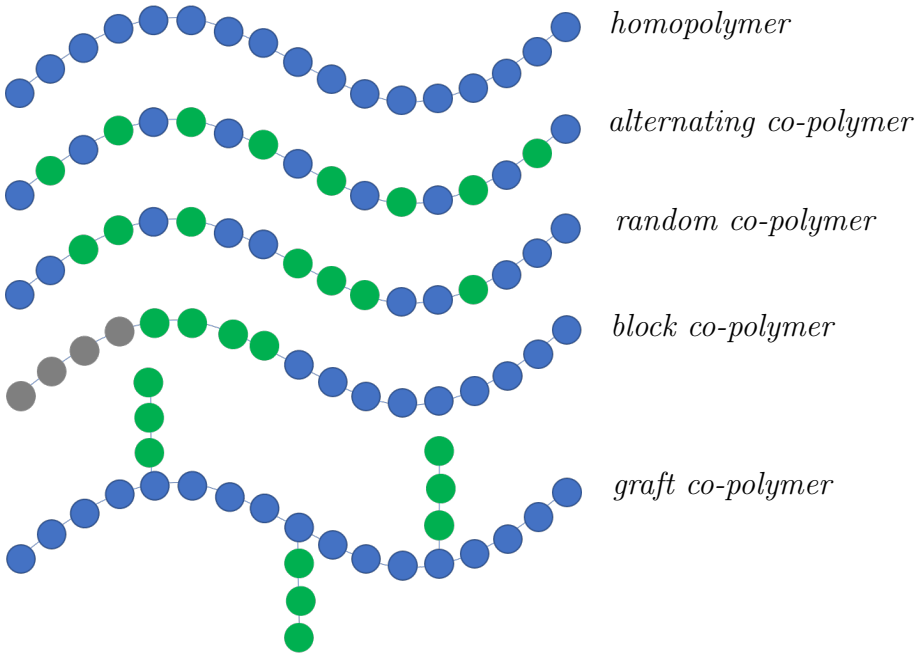

Figure 1.3: The arrangement of the monomer/s on the polymer backbone can be further used to classify the polymer molecules

Monomers can, broadly speaking be categorised by polarity; non-polar monomers (poly(styrene)), water insoluble but polar monomers (poly(vinyl acetate), poly(methyl methacryalte)), or water soluble polar monomers (poly(vinly alcohol), poly(ethylene oxide)). The monomer chemical functionality is important when selecting monomers, as it may contain certain moieties which are then imparted onto the subsequent polymer; these can then enable certain behaviour when in solution including a thermal or pH response. Polymers with an ionisable group are known as polyelectrolytes (such as poly(acylic acid)), where of course the dispersion environment pH, determines the degree of charge for the polymer.

1.3.2 Molecular weight distribution

The molecular weight of polymers cannot be well described by a single value, as it is very difficult to synthesise polymers with the same molecular weight. Similarly to naturally occurring polysaccharides, the molecular weight of synthetic polymers is better described as a weight distribution.[28]

The molecular weight is typically either expressed as a number (M_n) or weight average (M_w) molecular weight. The molecular weight distribution, which is more commonly known as dispersity, is the ratio of the two values, M_w and M_n. M_n is the statistical average molecular weight, calculated using the following equation (where N_i is the total number of molecules with the molecular weight M_i);

$$M_n = \frac{\Sigma N_i M_i}{\Sigma N_i} \tag{1.1}$$

M_w accounts more so for the molecular weight relative to M_n, where the larger the molecular weight the higher the contribution to M_w. It is calculated using the following equation;

$$M_w = \frac{\Sigma N_i M_i^2}{\Sigma N_i M_i} \tag{1.2}$$

1.4 Amphiphiles

Amphiphiles are a unique and important class of chemical compounds, as they posses both a solvophobic and a solvophilic part.[24,27] The solvophilic group has a strong affinity to the solvent, whereas the solvophobic group has little or no attraction to the solvent; examples include surfactants and amphiphilic co-polymers. It is this dual nature encompassed within the molecule that leads to the extremely interesting phenomena, described in the following section, that occurs at an interface and in the bulk.

The behaviour of the solvophilic and solvophobic groups varies with solvent type and conditions. So as an example, in water the solvophilic group will typically be the polar end of the molecule, whereas the solvophobic group will typically be the non-polar end. As water is the most common solvent available, and the most used when investigating amphiphiles, herein to avoid any confusion the polar and non-polar groups will referred to as they would be in an aqueous environment, i.e. the solvophilic group as hydrophilic group and the solvophobic group as the hydrophobic group.

Surfactants

Surfactants (a contraction of *surf*ace-*act*ive *a*g*ents*), are an important example of amphiphiles. Surfactant are used in many everyday products including textile processing, cosmetic products, medications, to name a few.[29–31] They are considered to be amongst the most versatile products from the chemical industry.[32]

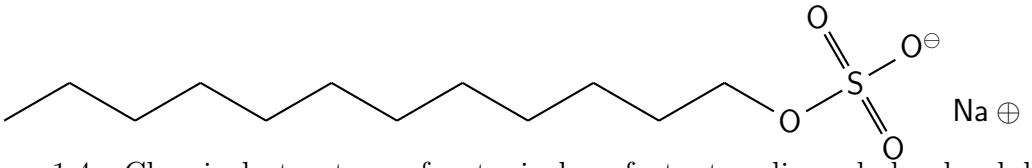

Figure 1.4: Chemical structure of a typical surfactant sodium dodecyl sulphate (SDS)

Surfactant solubility in an aqueous environment is typically dependent on the ionic interactions or hydrogen bonding of the hydrophilic head group with the aqueous phase, and on the characteristics of the hydrophobic part of the molecule (i.e. degree of saturation, and chain length).[24,27] Therefore surfactants are normally classified in terms of the nature of their hydrophilic head group, from an-/cat-ionic to zwitter-/non-ionic. They are typically driven to adsorb at the interface between two phases (such water/air or water/oil) by their amphiphilic nature.

The water molecules located at an interface, such as the water/air interface are in a different environment to the water molecules in the bulk. The molecules on the surface have unequal short range attraction,in the various directions, and therefore undergo a net inward pull into the bulk. This gives rise to a force acting at the interface called surface tension, which minimises the interface as much as possible.

$$W_m = gA_n \tag{1.3}$$

The surface free energy per unit area, surface tension, g is defined as the minimum amount of work , W_m required to create a new area of the interface, A_n, Equation 1.3.

In a surfactant solution where the concentration of the surfactant is below the critical micelle concentration (cmc), the surfactant molecules are present in the bulk as surfactant monomers, and concentrate at the interface reducing the free energy of the system and the surface tension and thereby change the amount of work required

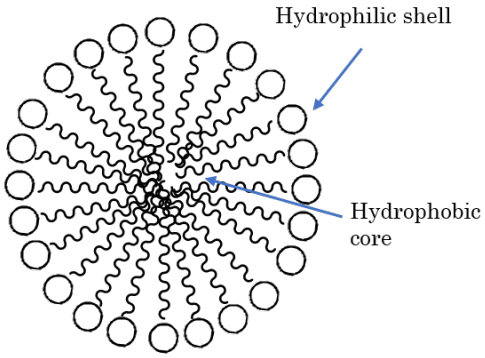

Figure 1.5: A *representation* of a surfactant micelle in an aqueous solvent

to create a new unit area of the interface. The Gibbs isotherm, Equation 1.4, shows the interfacial tension depends on the surfactant concentration;

$$\Gamma = \frac{1}{RT}\frac{\delta g}{\delta InC} \tag{1.4}$$

The surface tension is decreased with increasing surfactant concentration up to a point where increasing the concentration no longer has any effect. The concentration at which the surface tension is no longer altered is known as the critical micelle concentration (cmc). This is the concentration at which the surfactants form organised aggregates known as micelles. Above the cmc surfactant molecules exist both in monomeric and micellised form and are in a constant rapid exchange between the three states (in the bulk, at the interface and in micelles).

Micelles are organised surfactant molecules with the hydrophobic tails orientated to the interior forming a hydrophobic oily core, with the hydrophilic heads on the outside forming the outer shell. The cmc of a surfactant can be determined by measuring any physical property of a surfactant solution, including molar conductivity, osmotic pressure, light scattering intensity and surface tension. A plot of the measured property against the surfactant concentration shows a break, this is the cmc. As an example if conductivity is measured, the plot shows an increase in conductivity with concentration until the cmc is reached when it is no longer affected by increasing surfactant concentration, Figure 1.6. This is because surfactant monomers act as electrolytes, whereas micelles do not, and an increase in conductivity is only observed until micelles become present within the system.

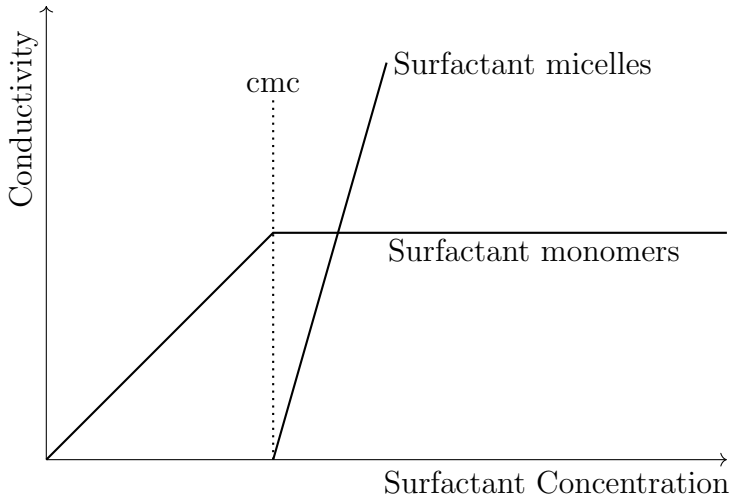

Figure 1.6: Change in conductivity as surfactant concentration increases, up until the CMC is reached where the micelle concentration begins to grow.

One of the most important properties of a surfactant is the ability to form micelles, Figure 1.5. Micelles are the reason why for example a water immiscible phase can be dispersed above the saturation concentration of the species, as the surfactants self-assemble in water and contain the water immiscible phase within the assembled structure, the micelle.

1.5 Interactions and Stability of Colloids

The stability of colloids is controlled by particle-particle interactions, which are dictated by particle size, shape and concentration, and the surface properties of the particles.[33–35]

1.5.1 Attractive interactions

All molecules and atoms are subject to dispersion or Van der Waals forces. Similarly attraction between colloid particles is due to Van der Waals forces.[33–35] These forces, in electrically neutral atoms originate from the instantaneous dipole formed due to electron density fluctuations. For two colloidal particles in close proximity, the sum of all the atomic interactions lead to an effective attraction known as the colloidal

Van der Waals interaction; the strength of this interaction is determined by the dielectric properties of the particles and the background medium. The Van der Waals attractive potential, U_{VdW} for two spherical colloidal particles with a radius, r and an inter-particle distance, H, is given by;

$$U_{VdW} = -\frac{A_H}{6}\left(\frac{2r^2}{H^2+4rH} + \frac{2r^2}{(H+2r)^2} + ln\left[1 - \frac{4r^2}{(H+2r)^2}\right]\right) \tag{1.5}$$

Where A_H is the Hamaker constant, which is determined from the density and the polarisability of the material.

1.5.2 Electrostatic repulsion interactions

Electrostatic stabilisation is provided by an ionic or ionisable surfactant/emulsifier, or by some other means that creates a charged surface on a colloid. This stabilisation is generally only significant in an aqueous environment. It is based on the mutual repulsive forces when two similarly charged surfaces approach each other, known as the electrostatic repulsion interaction, U_{ER} and is given by;[33–35]

$$U_{ER} = -\frac{y^2e^2}{4\pi\epsilon_0\epsilon_r H} \tag{1.6}$$

Where y is the sum of colloid surface charges, e the elementary charge, and ϵ_0 and ϵ_r represent the dielectric constant and permittivity of free space respectively.

A charged particle in an aqueous environment affects the ion distribution in the direct vicinity, which causes the particle to be surrounded by a volume of counter-ions and co-ions, creating the so called electrical double layer, EDL.[33] Note, away from the colloid surface the two ion types attain a constant average.

The EDL can be broken down into two layers, the stern layer and the diffuse layer, see Figure 1.7. The stern layer is the inner region made up of strongly bound counter ions. The diffuse layer is the outer region made up of loosely associated counter-ions and co-ions, where the concentration of ions decreases with distance. The slip plane (Figure 1.7), between the two layers, is a boundary within which the ions, though not tightly bound, remain with particle in this region.

The extent of the potential at this boundary is used to describe the stability of the system, and is more commonly known as the Zeta potential (the potential

typically varies from 10-100 mV). The screening of the particle surface charge due to the adhered ions therefore reduces electrostatic repulsion. Equation 1.6 is therefore modified to account for the EDL, where κ represents the quantification of thickness of the double layer;[33]

$$U_{ER} = \frac{y^2 e^2}{4\pi\epsilon_0\epsilon_r H(1+\kappa r)^2} \cdot \frac{e^{\kappa H}}{2r+H} \tag{1.7}$$

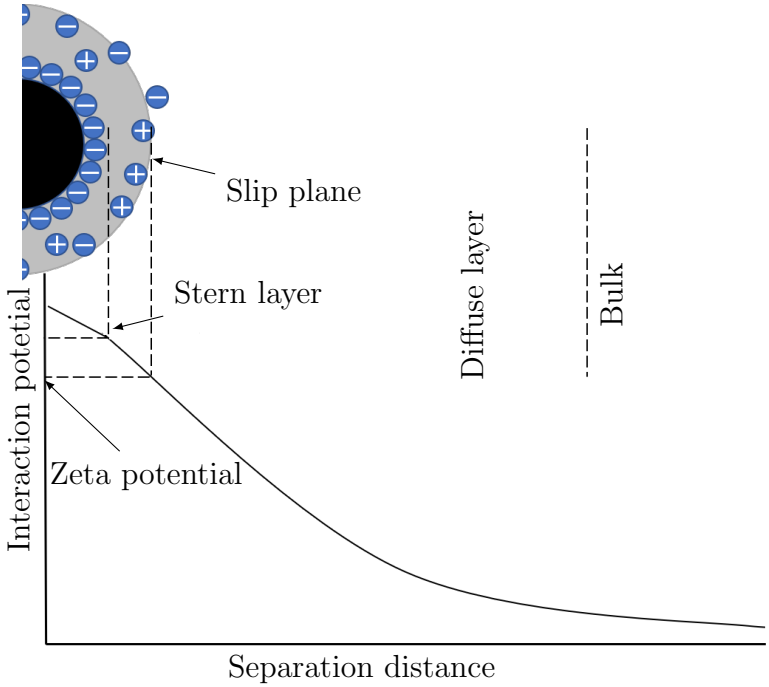

Figure 1.7: A graphical representation of the electrical double layer, depicting the stern and diffuse layer with the slip plane, for a positively charged particle.

When two particles approach each other there is an overlap of the double layer, which causes long range electrostatic repulsion. The approximate exponential decay is depicted in Figure 1.8. The EDL thickness determines the extent of this decay and is calculated as the Debye length(κ^{-1});[33]

$$\kappa^{-1} = \sqrt{\frac{\epsilon_0\epsilon_r k_B T}{2N_A e^2 I}} \tag{1.8}$$

Where I is the ionic strength of the medium, $k_B T$ is thermal energy and N_A is Avagadro's constant.

The Debye length depends on the electrolyte concentration and valency (ionic strength). The larger the Debye length, the slower the inter-particle potential decay and the longer the range of inter-particle interaction.

1.5.3 DLVO theory

The Derjaguin-Landau-Verwey-Overbeek (DLVO) theory is a classic theory describing charged colloidal particle suspension stability.[33–35] The theory takes into account Van der Waals attraction forces and electrostatic repulsion forces, and focuses on balancing the two opposing forces;

$$U_H = U_{VdW} + U_{ER} \tag{1.9}$$

The interactions that occur in a colloidal dispersion, between drops or particles, can either be attractive or repulsive. The attractive forces are driven by Van der Waals forces, while repulsive forces are driven by electrostatics

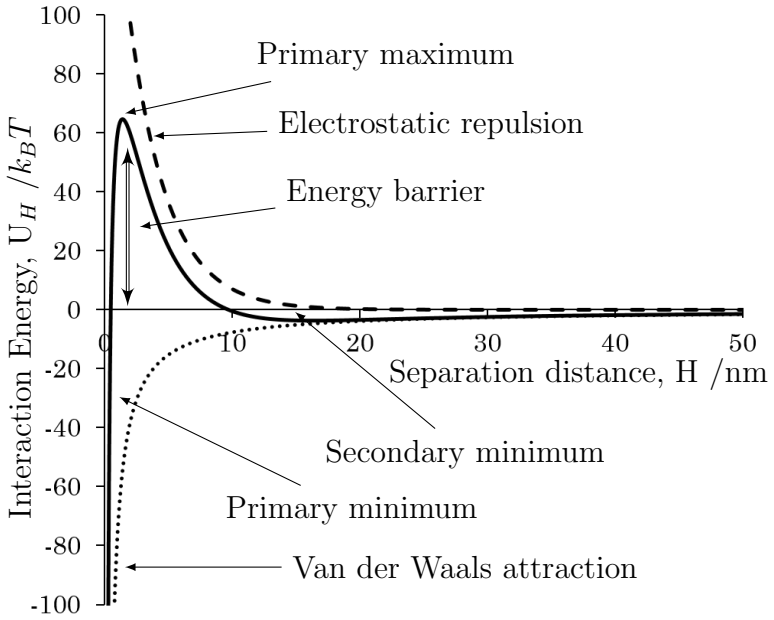

Figure 1.8: A graphical *representation* of the overall interaction energy (solid line) as a function of the inter-particle distance according to DVLO theory.

Long range Van der Waals attraction arises from electronically or orientationally polarised molecules when particles approach one another. The magnitude of the

attraction is determined by the Hamaker constant, particle size and the inter-particle distance. Electrostatic repulsion arises from the EDL acquired by charged particles. The overlap of the EDL for two particles in close contact causes an enhanced osmotic pressure between the volume in the EDL and the bulk, thus resulting in a repulsive interaction.

Figure 1.8 shows that at small inter-particle distances, (H) the Van der Waals interaction (primary minimum) is dominant and causes coagulation. The energy barrier must be overcome by the approaching particles kinetic energy, from Brownian motion to cause permanent coagulation. The secondary minimum is due to the combined effect of the Van der Waals attraction and electrostatic interaction and is observed in most systems. If the two approaching particles do not have sufficient kinetic energy to overcome the energy barrier, they fall into this secondary minimum, where aggregation can occur depending on the inter-particle bond energy. If the bond energy is sufficiently high, the particles are weakly aggregated, and they can be redispersed by applying a small amount of energy to the system.

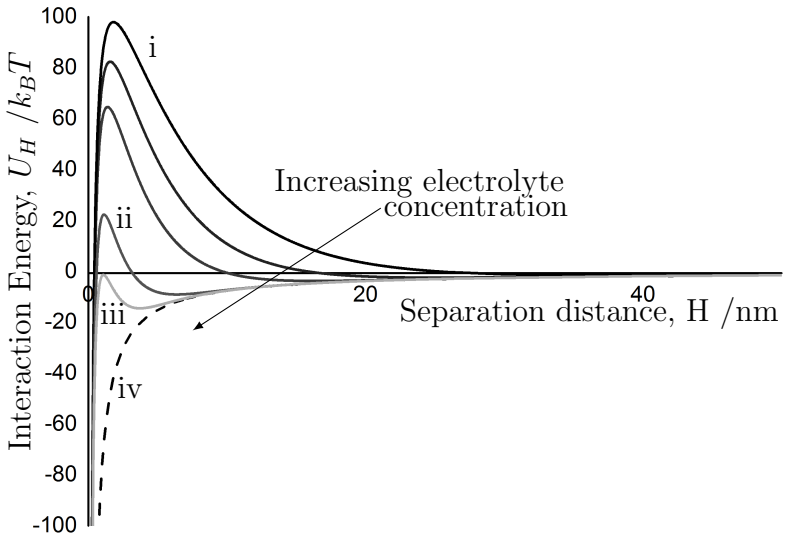

Figure 1.9: Change in DLVO potential due to electrolyte concentration. Calculated for 150 nm spherical silica particles with a surface potential of 40 mV, with electrolyte concentrations 0.0025, 0.005, 0.01, 0.04, and 0.08 M, in water.

The DLVO potential for a system is affected significantly by the ionic strength

of the medium, for a given Van der Waals attraction and particle size. Figure 1.9 depicts this effect for spherical silica particles with a diameter 150 nm, where the electrolyte concentration increases, from i to iv. From the plot, at the electrolyte concentration for i the primary maximum is sufficiently large enough that a stable dispersion is expected. At ii, the electrolyte concentration is larger, though there is still a significantly large primary maximum preventing irreversible aggregation, a more shallow secondary minimum exists. This minimum if sufficiently deep can lead to weak aggregation occurring, though this can reversed by agitation. For electrolyte concentrations at iii and iv, the DLVO potential indicates irreversible aggregation, where the dispersion is unstable due to the now dominant Van der Waals attraction.

Of course the above examines the case for dispersions in polar solvents. In contrast for apolar solvents colloids and particles require steric stabilisation, due to the difficulty associated with dissociation in such solvents. Although it is possible for dissociation to occur in apolar solvents, it is rather difficult due to the nature of such solvents (lacking in charge dispersion on solvent molecules).

1.6 Summary

A brief introduction and discussion of the inkjet printing was given, and the fundamental concepts required to understand the upcoming observations were discussed. The limitations of the technique were discussed and the lack of material diversity available for inkjet printing highlighted. In order to address and expand the material diversity, particularly for manufacturing purposes, this project aims to examine the printing behaviour of a model colloidal dispersion.

Therefore, the aim of this thesis is to characterise and understand the jetting behaviour of a model colloidal particle dispersion, with particular focus on the particle concentration. In order to achieve this, a particle synthesis route was designed to prepare a high solids content particle dispersion, with a sub-100 nm size range with a monodisperse size distribution. The novel preparation method was systematically investigated from a theoretical perspective. The dispersions were then used to examine the shear and elongational viscosity, as well as the jetting behaviour.

The concepts discussed here, become important later, particularly when considering the synthesis route with the need for surfactant in the formulation and implications for the stability and observed viscosity.

The following chapters deal with the 3 main themes covered in this project, particle synthesis, rheology, and jetting. The rheology is split into two, shear and elongational, with chapter 3 dealing exclusively with shear rheology, as well as dispersion stability. Elongational viscosity is discussed within chapter 4, where it is more appropriate as the results are discussed in terms of the observed jetting behaviour.

Chapter 2

Synthesis of High Solids Content Latex Particles

2.1 Background & literature review

2.1.1 Overview

Polymer nanoparticles (PNPs), also known as latex particles have a wide range of applications in numerous fields including medicine/biotechnology where for example biodegradable polymeric nanoparticles are used as drug delivery systems.[36] They are also taken advantage of in electronic/ photonics, and conducting materials/sensors, where for example conjugated polymers are used as semiconductors for lightweight thin film electronic devices.[37,38] They have also been used for pollution control/ environmental technology where for example polymer particles are used for soil remediation.[39] In most instances the surface area of these particles, and the ability to optimise these for specific applications, somewhat explains the pivotal role they play in the aforementioned fields.[40,41] The preparation method plays a vital role in achieving PNPs with the desired properties for a particular application.

PNPs can be prepared either by direct polymerisation of the relevant monomers or grown further from preformed polymers. The method employed to synthesise the PNP is chosen on the basis of the desired particle characteristics including particle size, application, reaction media etc.

In the following sections, different routes for latex preparation are discussed, along with the costs and benefits of each route. More attention is given to the routes of most importance for this work, i.e conventional-, surfactant free-, chain transfer-emulsion polymerisation. Other routes, including micro- and mini emulsion polymerisation are mentioned briefly but the requirement of relatively high surfactant concentrations for latex preparation, in this case means these are unsuitable for this work.

The particle dispersions prepared and discussed in this chapter are further used as model inks later, to examine the inkjet printing technique.

2.1.2 Emulsion polymerisation

Emulsion polymerisation is the most common method used to prepare waterborne resin/particles with various physiochemical and colloidal properties.[42] Synthetic rubbers, paints, adhesives, paper coatings, toughened plastics to name a few, can be prepared by emulsion polymerisation.

Hoffman and Delbruck are the authors of the earliest patent, for synthetic latex preparation granted in 1909.[43] Hoffman and Delbruck polymerised aqueous emulsions of dien monomers to prepare a product that somewhat resembled natural rubber. These emulsions were stabilised by gelatine, starch, egg white, flour and blood serum, but this process followed by some other similar studies are not emulsion polymerisation reactions as we know them.

However it was Dinsmore who first produced synthetic rubber stabilised by soap in 1929, then followed by Luther and Huck who similarly produced synthetic rubbers but, with an added initiator[44,45]. They were polymerising emulsified monomer, and as such are the first authors, in the literature to do so. Emulsion polymerisation then grew rapidly and latex production at the industrial scale began in the 1930s.

The major developments in Emulsion polymerisation were in World War II, when styrene and butadiene were copolymerised to produce synthetic latexes to replace natural latexes. With intense collaboration between industry, academia and government laboratories many types of latex were prepared.

World War II was the reason for the development of emulsion polymerisation, due to the necessity of synthetic latex for boots, and the need for much higher

polymer concentration solutions which could not prepared from previous routes due to a viscosity restriction at ∼10wt.%. However emulsion polymerisation, is even now used to produce millions of tons of synthetic latex which is used in a wide variety of applications. The use of synthetic latex grew, along with the understanding of the underlying science and the possibilities it opened up: from the variety of monomers available, to the various desirable properties for the resulting polymers.

The following sections elaborate on the main components, kinetics and mechanism for conventional emulsion polymerisation, followed by a discussion on particles, and the properties of these dispersion obtained via this route. The mechanism described is the one proposed by Harkins[46] and Smith and Ewart[47].

Conventional Emulsion Polymerisation - Mechanism

The formulation of a conventional emulsion polymerisation system includes, dispersion medium (typically water), surfactant, initiator, and the monomer.[48] These are the main components of an emulsion polymerisation, with other additives, including acids/bases, buffers, chain transfer agents etc. often used in conjunction. The monomer in this route mainly exists as emulsified droplets, approx. 1-10 µm in diameter dispersed in the aqueous medium. A very small amount of the monomer (approx. 0.04 %) is dissolved in the aqueous medium and, provided the concentration of the surfactant is above the critical micelle concentration (CMC), a small amount of the monomer (1 %) is incorporated within the micelle cores. Note this is for hydrophobic monomers such as styrene and methyl metharylate. The polymerisation commences when the initiator is added, which dissociates into free radicals, where dissociation is increased at higher temperatures. The radicals are then captured by the micelles, which have a huge oil-water interfacial area and are therefore the polymerisation loci.

According to the aforementioned theories by Harkins and Smith and Ewart, the polymerisation occurs in three stages.[46–49]

The Initial stage:

This is also known as the nucleation or the particle formation stage. The polymerisation reaction begins upon generation of free radicals. These first react with the dissolved monomer polymerising a few monomer units creating oligomers. Once a critical chain length is achieved the hydrophobicity of the oligomers drives these

growing chains to precipitate within the micelles, where the growing chain continues propagating with the available monomer.

These can now be considered as particle nuclei, which continue to grow by acquiring more monomer from the monomer droplets. The monomer diffuses through the aqueous phase to the particle nuclei. As these nuclei grow there is an increased demand for surfactant molecules to coat the particle surface in order to maintain adequate colloidal stability. Some of the surfactant micelles disband and supply the surfactant to the growing particle swollen micelles. Again to help maintain stability the surfactant stabilising the monomer droplets would also desorb from the surface, as monomer droplets reduce in size as the monomer is used in growing particles.

The nucleation stage is considered to be complete once the surfactant micelles are used up i.e. no longer exist. This occurs very early in the reaction, at about 10-20 % conversion. Particle size and particle size distribution is controlled by this stage. Large latex particles with a narrow size distribution can be obtained by using a low surfactant concentration, as the lower the surfactant concentration the lower the nucleation period and the narrower the resulting size distribution.

However, using a lower surfactant concentration does not adequately stabilise the system and can give rise to aggregation. It should be noted that there could be some polymerisation occurring in the large monomer droplets, this is only a very small proportion due to the small surface area of these droplets for radical diffusion, as compared to that available for the monomer swollen micelles. Smith and Ewart showed that the number of particles nucleated per unit volume of water is proportional to the concentration of the surfactant and initiator in the system to the 0.6 and 0.4 powers respectively. Surfactant concentration is therefore the most important factor controlling particle nucleation.

The Particle Growth stage

During this stage, monomer concentration in the monomer swollen particles is constant, as the monomer diffusion from the monomer droplets is continuous. This stage ends when the monomer droplets are used up, i.e. they disappear, typically this is just after the halfway stage of the reaction ($\sim$ 50-80 % conversion).

At this stage, the following expression is widely used to calculate the rate of polymerisation, R_{pi} for relatively insoluble monomers;

$$R_{pi} = k_p[M]_p\left(\frac{nN_P}{N_A}\right) \tag{2.1}$$

Where k_p is the chain propagation rate constant, $[M]_p$ monomer concentration in the particles, n the average number of free radicals per particle, N_p number of particles nucleated per unit volume of water, and N_A is Avagadro's constant. the assumptions made to derive this model are;

- Particle nucleation or coagulation do not occur, and the number of particles remains constant
- Particles are relatively monodisperse
- Free radicals do not desorb from particles
- When an oligomeric radical enters a particle, the bimolecular termination of the polymeric radical is instantaneous.

These assumptions imply that either only one free radical or no free radicals exist in the monomer swollen particles. Therefore for the systems that follow these kinetics n is equal to 0.5, and the monomer concentration is relatively constant in the monomer swollen particles (where monomer droplets are still present). As a result, a constant rate of polymerisation is achieved during this stage, Figure 2.1.

The Completion stage

At this point, the monomer swollen particles contain all the unreacted monomer and the surfactant is mostly used to stabilise the monomer swollen particles. Polymerisation continues until the monomer is used up, 100 % conversion. The rate of polymerisation decreases along with monomer concentration. As the monomer is polymerised, within the swollen particles, viscosity increases within the particle, which slows down the polymerisation rate for the remaining monomer. Once polymerisation is complete, the system is a dispersion of solid latex particles stabilised by surfactant.

The above described mechanism is for the case where the surfactant concentration is above the cmc, however particles have been synthesised in systems where the surfactant is below the cmc, where another mechanism describes the reaction,

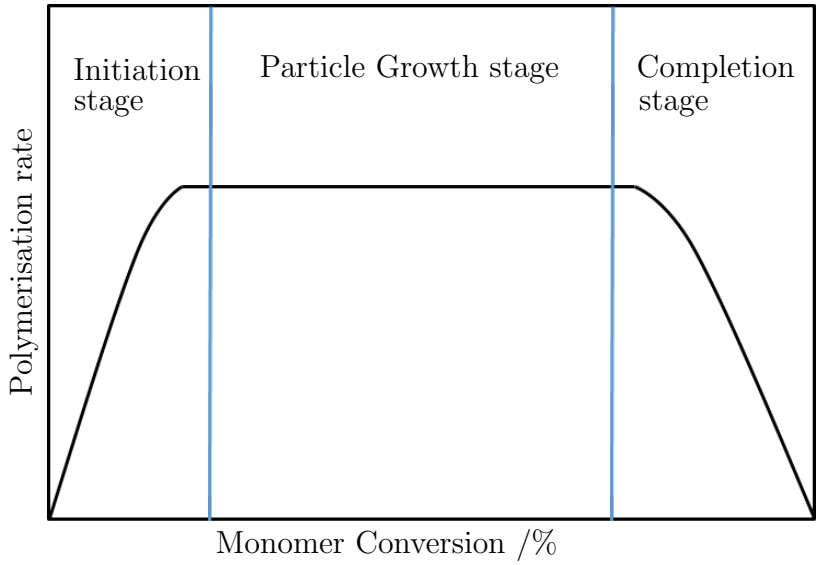

Figure 2.1: Graphical representation of the typical rate of polymerisation, during emulsion polymerisation as a function of monomer conversion

Section 2.1.3. The kinetics of the polymerisation process are further examined and can be found in the Appendix A.1.

2.1.2.1 Other Emulsion polymerisation routes

The polymerisation process can be classified by the initial emulsion type, macro-, mini-, and micro-emulsions (this is for oil in water systems). The characteristics of these initial emulsions differ subtly, but lead to significant differences in the properties of the final polymer particles. The size of the dispersed droplets, emulsion stability and the mechanism for particle nucleation are some of the properties affected by the initial emulsion type.

Macro-emulsion polymerisation; also referred to as conventional emulsion polymerisation (CEP), is the route discussed in detail so far (Section 2.1.2). Characteristically, it consists of a significant amount of free/micellised emulsifier, where the monomer exists in relatively large droplets (1-100 µm). The emulsion, though kinetically stable, is thermodynamically unstable, therefore phase separation is rapid without constant agitation. As discussed earlier, nucleation occurs outside of the monomer droplets, which generally act as monomer-reservoirs due to their very small

interfacial area. This route has been shown to yield PNPs with a huge range of sizes from 100 μ to 20 nm, see Table 2.1

Micro-emulsion polymerisation (μEP); this route involves preparing a micro-emulsion (thermodynamially stable) prior to the polymerisation step, where the monomer droplets are between 10-100 nm.[50–56] The monomer is dispersed with the aid of both a surfactant and co-surfactant (such as short chain alcohol penta-/hexa-nol). Such emulsions contain an excessive amount of emulsifier, thus micelles are excess and do not deplete throughout the reaction. Primary radicals are therefore preferentially driven into the monomer swollen micelles, due to the latter's significantly high surface area, relative to forming nucleated centres in the bulk aqueous phase. This route generally leads to an increase in micelle size during polymerisation, usually due to coagulation between inactive and active micelles or monomer diffusion from inactive micelles to active micelles. The latter is more likely, as usually on average a single polymer chain is attributed to each micelle with a molecular weight $\geq$ 1000000 (particle size $\leq$ 50 nm).

Mini-emulsion polymerisation (mEP); this route requires a mini-emulsion to be prepared prior to polymerisation, which can remain stable for hours or months depending on the specific emulsion.[40,55,57–64] Therefore, such systems require high energy input (eg homogenisation), and a large amount of surfactant to prepare the initial emulsions. The monomer in such systems exists in droplets with sizes ranging from 50-100 nm. To ensure the stability of these droplets, a co-surfactant is required to aid the emulsifier. Normally the co-surfactant used in such systems is a long chained fatty alcohol (e.g. cetyl alcohol). The addition of such a co-surfactant then reduces the spacing between each emulsifier molecule, as it does not penetrate the oil/water interface strongly due to its preference for the oil phase; thereby decreasing the interfacial area. The total surface area of the monomer droplets is significantly high, and as no monomer free micelles exist in this system, these become the locus of polymerisation. The final PNPs obtained have a similar size range to that of the initial monomer droplets. Table 2.1 lists some studies from the literature, making use of the different routes to PNPs.

Table 2.1: Selected literature comparing various polymer latex synthesis routes

Route	**Monomer**	**Initiator**	**Stabiliser**	**Particle Size**
CEP[65]	St	APS/$Na_2S_2O_3$	PS-b-P(PEGMA)	217-494 nm
CEP[66]	BA/St	$K_2S_2O_8$	SDS	42 nm
CEP[67]	St	KPS	CTAB	20-40 nm
CEP[68]	MMA	APS	SDS	40 nm
CEP[69]	VCz	KPS	SDS	50-200 nm
CEP[70]	St	KPS	SDS	20 nm
SFEP[71]	St with c.s. Acetone	V-50	n/a	248 nm
SFEP[72]	MMA with c.s. Acetone	KPS	n/a	45 nm
SFEP[73]	MMA with c.s. Acetone	$NaHSO_3$/ $CuSO_4.5H_2O$	n/a	165 nm
SFEP[74]	HEMA	KPS	PVA	100 nm
mEP[57]	AA	AIBN	Span 80 with Tween 80 as CS	80-150 nm
mEP[58]	St	KPS	SDS with a fluorinated block copolymer CS	80 nm
mEP[59]	MMA	KPS	SDS with PMMA polymer CS	118 nm
mEP[62]	St	V-59	CTMA with HD CS	100 nm
μEP[50]	VA	KPS	AOT	<40 nm
μEP[51]	MMA/BMA	KPS	SDS	40-96 nm

2.1.3 Surfactant free emulsion polymerisation

Surfactants modify the surface tension of liquids (see Section 1.4), which can be an undesirable effect for some applications; they can also considered a contaminant

in some applications specifically in the biomedical field.[75–78] PNPs prepared by the conventional method discussed earlier, use surfactants to stabilise dispersions. Surfactant removal from these systems can be a very time consuming process, and it is very difficult to get 100 % surfactant removal by conventional methods (dialysis).[79,80] It also increases manufacturing cost, which is highly undesirable. Surfactant free emulsion polymerisation (SFEP) is a variation of the conventional emulsion polymerisation process, where the polymerisation is carried out in the absence of surfactant or at surfactant concentrations below the cmc.[81,82]

Stabilisation of the PNPs, which would otherwise be afforded by surfactants, now arises from the use of ionisable initiators or ionic comonomers. With the absence of surfactant, aggregation does tend to occur during synthesis which can increase particle size relative with CEP methods. The micellar nucleation mechanism (discussed earlier Section 2.1.2) is no longer applicable for these systems, rather the process relies on the homogeneous nucleation mechanism.[82]

The formulation of these systems commonly include a water soluble ionisable initiator, monomer and the dispersion medium, which is normally water or a mixture of water and a volatile solvent. Ionic comonomers may also added to the formulation to give full or partial stabilisation. As aforementioned, a small concentration of surfactant may be present to enhance dispersion stability, however surfactant is not responsible for nucleation and growth of particles.

Similarly to conventional emulsion polymerisation free radicals from the initiator are first generated. These free radicals then react with the monomers to form an active centre and begin propagating, however once the active monomers grow to certain length (oligomeric active centres) they become hydrophobic and coil up to minimise contact with water and in so doing forming the particle nuclei. Primary particles are formed by the limited aggregation of unstable particle nuclei, which are then stabilised by absorption of either the comonomers, or the ionisable initiator molecules. NB when present at low concentrations, surfactant may also adsorb to the water/polymer interface to provide additional stability. Generally an ionic initiator is employed to impart stability to the growing particles; these initiators produce polymer chains with anionic charges which lead to an increase in the surface charge density thereby imparting colloidal stability to the particle dispersion. However, care must be taken since these species also increase the ionic strength of the aqueous

phase and if a careful balance is not achieved the surface potential and therefore the electrical double layer will be greatly reduced and the imparted stability will no longer be sufficient. A few of the reported cases for PNPs synthesised via this route are displayed in Table 2.1

Preparing sub 100 nm latex particles using this method is considered to be challenging.[74,83] One possible approach would be to reduce the monomer concentration used, however this in turn would reduce the solids content in the final dispersion. Microwave assisted polymerisation has been shown to be very capable in preparing PNPs, where acetone is used as a co-solvent.[81] The particles prepared in this manner are monodisperse 50 nm crosslinked latex particles, with a high solids content for SFEP (14 nm at 5.6 wt.%, and 41 nm at 12.6 wt.%). These particles were comprised of hydroxyl functionalised PMMA copolymers. The use of cross linkers is essential for this method, in that they lead to enhanced reactivity, and control for microwave reactions.

Another example of SFEP involves copolymerisation of Styrene with 10(9)-hydroxyl-9(10)-allyl ether octadecanoic (HAEOA) acid to produce a monodisperse particle dispersions.[84] The HAEOA is a surfactant monomer, and as such acts both as a stabiliser and a monomer. The reaction is initiated by exposure to microwave radiation. The surfactant monomer does not affect the rate of polymerisation nor the polymerisation mechanism which proceeds via homogeneous nucleation.

2.1.4 Controlled/Living radical polymerisation

Some of the limitations of the aforementioned polymerisation methods include the inability to produce particles with a controlled size distribution, chain architecture, composition and specific functionality. Fast radical-radical termination reactions in the polymerisation reaction are at the root of the polydispersity issue. This polymerisation method is used to prepare well defined polymers with controlled structures, architecture, functionality and molecular composites.[50] Controlled/living radical polymerisation (CLRP) and conventional emulsion polymerisation are similar in that they both proceed by the same radical mechanism, and can both be employed to polymerise similar monomers. CLRP however, extends the life time of growing

chains, give inherently faster initiation and termination rate decreases significantly with time.

Fundamentally, the concept of CLRP is to minimise chain termination as much as possible. CLRP relies on an intermittent species whose formation of active propagating species reduces chain termination. The key is to establish a rapid dynamic equilibrium between the dead chains (no longer propagating) and the propagating active centres. The persistent radical effect is used to reversible trap radicals (in activated centres) in an activation-deactivation process;

$$P_n^{\cdot} + X \underset{k_{act}}{\overset{k_{deact}}{\rightleftharpoons}} P_n X \tag{2.2}$$

where $P_n^{\cdot}$ is the propagating active centre of length n, X depicts a general stable radical species such as nitroxide[85] or a cobalt porphyrin[86], with a deactivating rate constant, k_{deact} and activating rate constant, k_{act}.

The propagating active centres are trapped by the stable radical species, and then reactivated either spontaneously with a catalyst or light radiation to reactivate the active centre. The radical species X cannot terminate with itself, it can only couple with a propagating centre. Of the three most promising CLRP methods, nitroxide mediated polymerisation[87] (NMP), atom transfer radical polymerisation[88] (ATRP), and reversible addition fragmentation chain transfer polymerisation[89] (RAFT), NMP follows the persistent radical effect. A stoichiometric amount of the stable radical species is required for this synthesis method, as the final polymers are all terminated with this species. ATRP also follows this effect, except it is a catalytic process, therefore requires less than a stoichiometric amount of a redox active catalyst. NMP and ATRP are beyond the scope of this work and therefore will not be discussed in much detail, RAFT however is of relevance and is discussed in more detail below.

RAFT polymerisation

RAFT polymerisation in its essence, is emulsion polymerisation mediated by a chain transfer agent (CTA), also known as RAFT agent[90];

$$P_n^{\cdot} + RY \overset{k_{ex}}{\rightleftharpoons} P_m Y + R^{\cdot} \tag{2.3}$$

Where $P_n^{\cdot}$ and $P_m^{\cdot}$ are propagating chains of length n and m respectively and Y represents a transfer agent.

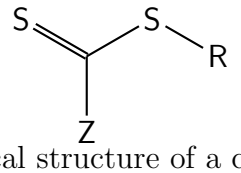

Figure 2.2: Chemical structure of a chain transfer agent.

The mechanism of RAFT is different from CEP, in that it also incorporates chain transfer activation and equilibrium reactions, to the three stages of CEP, which have been discussed earlier in this chapter. In RAFT the intermittent species, common for all CLRP methods is the RAFT CTA agent.[50]

The chemical structure of a CTA, Figure 2.2 contains three important groups: the stabilising group, Z, the leaving group R, and a thiocarbonyl group, $C = S$ (responsible for driving the chain transfer mechanism). During polymerisation the thiocarbonyl group reacts with a propagating chain, thereby terminating the active centre, but producing another radical species in the process, which then goes on to become an active propagating chain. The terminated chain on the CTA can again be activated, by the thiocarbonyl group reacting with another propagating chain. This equilibrium then enables the polymer chains to grow relatively equally leading to a final polymer dispersion with a low molecular weight polydispersity. Typically for emulsion polymerisation the CTA concentration is required to be 10 times that of the initiator, to act effectively during the reaction.

The following equation describes the ideal situation, where the number average molecular weight, M_n increases linearly with conversion, f and can be used to confirm polymerisation control by predicting the final molecular weight of the polymer[50]:

$$M_n = \frac{[M]_0 M_{MW} f}{[CTA]_0} \tag{2.4}$$

Where $[M]_0$ is the initial monomer concentration, M_{MW} the molecular weight of the monomer, and $[CTA]_0$ is the initial CTA concentration.

RAFT polymerisation is not very well developed for dispersion polymerisation; most of the literature on this topic report problems due to the CTA, where RAFT polymerisation is extended into *conventional* emulsion polymerisation.[91] Poor colloidal stability, high polydispersity, and lack of molecular weight control in the final particle dispersions are the problems normally reported as being associated with this method.[92,93] These problems are typically thought to be due to poor CTA transfer through the aqueous phase.[92,94]

It has been shown that these problems can be overcome by ensuring the CTA does not need to migrate through the aqueous continuous phase. One of the approaches overcomes these issues by using seed particles, which contain all the CTA, prior to polymerisation.[95] Mini emulsion polymerisation can also be used to similar effect, given that the CTA would be present in the monomer swollen micelles, which are then directly converted into particles.[96]

Together, suggests RAFT polymerisation cannot be very well implemented into conventional emulsion polymerisation for particle synthesis. Regardless of the mechanism occurring the CTA will still have to migrate from the monomer droplet/monomer swollen micelles/ aqueous phase, to the newly formed particles for the reaction to proceed under RAFT control. However, these issues could be circumvented if the CTA was exclusively made available in the growing particles, with no need for any migration thus leaving the reaction under RAFT control.

A rather interesting approach to achieve this control would be to first prepare amphiphilic diblock copolymers.[97] These would act as surfactants and would then self-assemble into polymer-micelles. Therefore, no surfactant would be required in these systems. The diblocks would still have the original RAFT functionality available and therefore polymerisation can proceed within these micelles, and CTA migration is no longer required.

This approach does mean however that monomer droplets in the dispersion must be avoided until the diblocks are locked into position. If monomer droplets were available in the system prior to polymerisation, the diblocks would also act to stabilise these. This would imply that once polymerisation begins, droplet nucleation

would be very likely to become significant. Whereas in conventional emulsion polymerisation the surfactant molecules desorb from the monomer droplets, the diblocks would not. They would instead grow, which would immobilise them to the droplet surface and reduce the amount of monomer released from the droplets and therefore cause significant droplet nucleation. However, this can avoided by ensuring monomer is added slowly, i.e. so no monomer droplets are formed, until the diblocks become locked with the growing particles. Latex particles prepared in this manner would be stabilised by the anchored diblocks, where relatively monodisperse particles as small at 45 nm at 20 wt% solids content can be prepared.[97]

An amphiiphilic CTA has been shown to be quite efficient in producing PNPs.[97] The strategy implements RAFT control in CEP, where the CTA is used initially to prepare a diblock with both a hydrophilic ad hydrophobic component sufficiently balanced to self assemble into polymer micelles. Once these are formed, the hydrophobic blocks are made to grow with slow addition of another more hydrophobic monomer. The polymerisation leads to PNP formation, as growth of the hydrophobic block locks in the polymer chains. Monomer starved conditions were used here, in that no monomer droplets are allowed to form so that the CTA remains within the particles attached to the polymer chains. Control is maintained over the entirety of the reaction without loss of colloidal stability thus producing hairy triblock core shell particles. This strategy can be used to prepare a range of particle sizes (45-190 nm), with solids content $\sim$15 wt.%.[97]

Surface active CTAs are quite interesting and have some potential for RAFT polymerisation, as they also act as particle stabilisers (surfactant is not used in these systems).[98] The surface active CTA is composed of a dithiobenzoyl main structure and a benzoic hydrophobic carboxylate hydrophilic moiety, acting as initiator, surfactant and CTA. Activated by UV radiation, the CTA was successfully used to prepare p(MMA) particles. Increasing the CTA concentration lead to lower molecular weight, particle size and molecular weight distribution dispersions. Particles obtained from this strategy are in the range 300-400 nm.

2.1.5 Synthesis of high solids content monodisperse nanoparticles, with low surfactant concentrations

Emulsion polymerisation and its analogues are used to prepare an increasingly wide variety of polymers, for use as adhesives, binders (non-woven fabrics), textiles, paper additives, construction materials and paints to name but a few applications.[55,99] A higher polymer content is always advantageous for most of the aforementioned applications; i.e. transport and storage costs are reduced, an improved reactor (synthesis) efficiency, product formulation is more flexible, and surface coverage (for thin film formation) is improved with reduced drying times.[40,41,57,100,101] Although, there are many advantages for preparing high solids content latexes, the increase in viscosity of the polymer dispersions comes with its own problems. Indeed as the dispersion viscosity increases, problems arise from mixing, stability, mass transfer and heat removal.[102] This problem has been addressed, broadly speaking with two different approaches.

The maximum attainable volume fraction for monodisperse spherical particles is 0.64; this is the maximum number of particles that can be squeezed into a given volume.[55,100,103] N.B. only spherical particles are considered in this review. At this volume fraction, the viscosity approaches infinity and the spherical particles begin to come into contact with each other. The remainder of the formulation must also be considered, if for example a surfactant has been employed the space occupied must also be considered; i.e. the maximum packing volume fraction is reduced.

Therefore, if the aim is for a maximum possible solids content with low viscosity, a bimodal particle size distribution (PSD) is employed. There have been several studies devoted to high solids content latex preparation, generally seeking appropriate packing behaviour between two size populations.[104] Typically, more often a large difference between the small and large particle population is sought, as it is at these conditions where a low viscosity can be attained.[103–106] This is a good solution for high solids content latex preparation where the PSD is not an issue for application, or even where a bi/trimodal PSD is a useful feature for its end application.[100]

However, there is growing demand for preparation of small (< 100 nm) latex particles with a narrow monomodal PSD (this is the focus of this project; ruling out targeting multimodal systems to maximise packing).[68,76–78,107–115] Such particles

possess an increased surface area to volume ratio, surface functionality, and penetration.[116] There are many fields where these properties are sought, some of which are controlled release systems, stimulus responsive materials, biomedical separations, anti-corrosive coatings, and polymer-carbon nanotube dispersions.[116–124] For these systems most of the literature focuses on preparing PNPs at the maximum solids concentrations where the particles are colloidally stable.

This demand has driven a huge interest in developing a strategies for preparing particle systems with these properties.[68,76–78,107–115] In can be gleaned from the mechanism for particle formation (Section 2.1.2), that in order to decrease particle size, the rate of nucleation must be increased, whilst the particle growth rate must be decreased. Coagulation must also be avoided to ensure a small PSD. Several routes have been shown to be capable of preparing PNPs with just these constraints; including a system in which the monomer is dispersed so that it exists only within the micelles, which can then be photopolymerised to yield small particles (2-3 nm) with a narrow PSD (though at only a 0.6-1.4 wt.% solids content - targeting small particle size at low surfactant concentrations, with solids content being the drawback).[125]

However the synthesis process becomes much more challenging when taking into account all of the constraints imposed by the application that require such particles;

- sub 100 nm particle size
- High solids content
- Monodisperse PSD
- Low surfactant concentration

The requirement for a low surfactant concentration has been discussed in Section 2.1.3, while the remaining 3 have been the subject of this section.

In order to prepare small particles with a monodisperse PSD requires some adjustment, from method selection to surfactant/initiator/monomer concentration. However, with all 4 constraints in place the synthesis is much more demanding, as the the constraints are all inter-dependant. Indeed on the surface these constraints are almost conflicting. As the solids content is increased and a smaller particle size targeted, there is an increase in the frequency of particle collisions; this would normally be dealt with by increasing the stabiliser content to improve particle stability. However, this is restricted, as a low surfactant concentration is a prerequisite, therefore another strategy is needed. Such systems are the theoretical

aim of polymerisation reactions, and many authors have attempted to do exactly this, with varying rates of success. Several different strategies have been used to meet these conditions, with some of the more successful discussed herein.

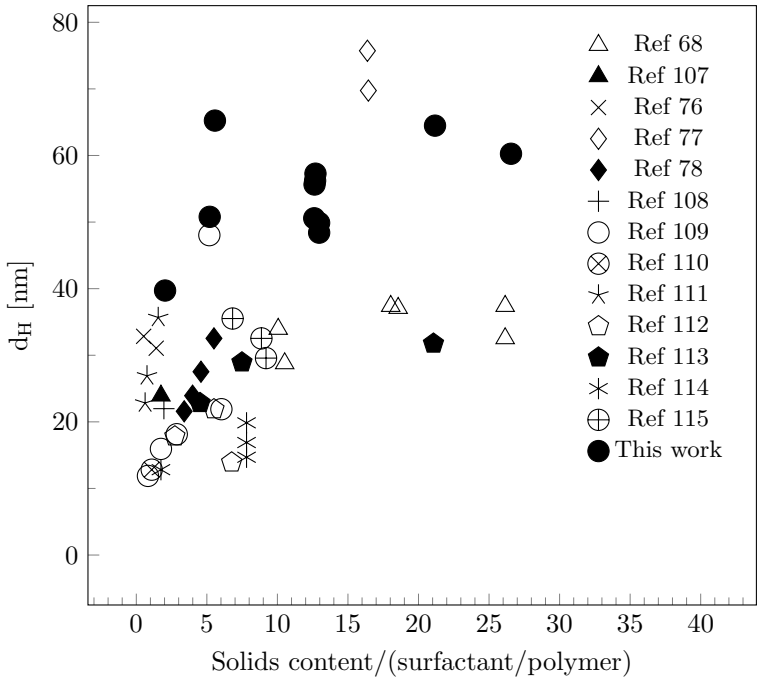

Figure 2.3: Overview of the literature focusing on high solids content monodisperse PNP preparation. Reproduced and modified from ref 68.

The most prominent work in this area is shown in Figure 2.3, reproduced from ref 68.[68]. The figure plots particle size, against the solids content(g), normalised by the surfactant:polymer ratio.[68,76–78,107–115] The figure aids the visualisation of the challenge addressed here, where the fourth quadrant is the target for most of the research i.e. a high solids content small PNP dispersion using little surfactant. A more detailed examination of some of the more successful approaches are discussed below.

A method based on CEP has been used to prepare particles that almost meet the above constraints quite well (ref 78 in the above plot).[78] The approach modifies the CEP route by using an extremely hydrophobic cobalt complex, bis[(difluorooryl-)-dephenyl glyoximato] cobalt. The role of the cobalt complex is known to aid control over the molecular weight distribution and is used in catalytic chain transfer

polymerisation.[126–130] In the above case however, it is used to enhance nucleation efficiency for CEP. This technique appears to work well, and has been shown to produce particles as small as 10 nm, albeit with less than ideal high solids content. The control arises from the action of the cobalt complexes within the monomer swollen micelles, where it transfers a radical from an actively growing polymer chain to a monomer molecule, creating a monomeric radical. The monomeric radical desorbs into the aqueous phase, where it grows into an active nucleating centre. Thus, the complex decreases the particle growth rate, while increasing the nucleation efficiency. When targeting higher solids content (> 40 wt.%), this strategy was shown to yield stable PNPs (33, 44 nm) at reasonably low surfactant concentrations (∼8 wt.%); although this concentration is still considerably high for the aforementioned applications.

Recently a semi-continuous CEP method has been shown to be capable of preparing PNPs within all the above constraints.[68] The strategy is a theory guided approach, where most of the particles are initially formed by CEP. Here PNPs are prepared with size ∼ 13 nm, at 18 wt.% solids content using a small amount of surfactant (0.4 wt.%).[114] Following this, more surfactant and monomer are fed into the system, and the particles are allowed to grow further. The number of particles formed initially are the maximum number of particles in the final dispersion, i.e. no new particles are formed in the second stage. The addition of more surfactant in the second stage increases the stability of the growing particles, without which particle collisions lead to coagulation and larger /more unstable particles. This had the effect of a number of smaller PNPs being formed concurrently, thought to be due to some radicals desorbing from the growing PNPs and polymerising monomer in the aqueous phase thereby creating new PNPs. However, even taking this complication into account, this strategy readily prepares PNPs with a size 32 nm at solids content up to 36 wt.%. The results from this study can be found in figure 2.3 as Ref 68. Despite these results, the monodisperse PSD criteria requirement is not met.

The other strategy appearing to meet the above synthesis criteria well in figure 2.3, Ref 110 similarly uses a semi-continuous monomer starved polymerisation route to prepare particles at small sizes with a narrow PSD and high solids content.[113] The strategy was used to successfully prepare narrow PSD PNPs in the

range of 23-32 nm using surfactant at 5-1 wt.%. However, this work failed to prepare particles at sufficiently high solid content ($\sim$ 24 wt.%).

2.1.6 Conclusions and outlook

This review has explored the various polymerisations routes to prepare PNPs in an aqueous solvent, spanning conventional emulsion polymerisation, surfactant free emulsion polymerisation and RAFT polymerisation. Covering such a broad and active topic thoroughly cannot be achieved within the limits of this thesis. Still, considerable effort has been made to cover the most important fundamental aspects, along with some of the more influential research articles from recent literature.

What are the main challenges of creating monodiserse, sub-100 nm, surfactant free, high solids in aqeuous solvents?

There is little doubt that advances are being made in this field and some fascinating systems conceived to meet the rising demand for PNPs with specific functionality and size: specifically the requirement for sub-100 nm particles with monodisperse distribution and high solids content, while using as little surfactant as possible. However, in some areas, particularly RAFT polymerisation, academics can perhaps be accused of concentrating a little heavily on preparing ever more complex systems with high functionality (amphiphilic block co-polymers) where perhaps a stripped down approach would yield a desirable system.

The challenge lies in either protecting the particles against aggregation with stability arising from a component other than surfactant, or controlling the overall number of particles such that each particle grow at the same rate, thereby leading to monodisperse final distribution.

2.1.7 A novel one pot synthesis route to high solids content monodisperse sub-100 nm PNPs

In this research two methods are employed, surfactant free- and chain transfer mediated- emulsion polymerisation, to prepare monodisperse sub 100 nm PMMA nanoparticles. The two methods are vigorously tested, by examining the various component concentrations to determine the effect on the final particles prepared.

In order to avoid the use of surfactants, and therefore a more practical route, a SFEP strategy was initially tested. As will be seen later, this approach was found to be unsuitable for PNP preparation at the sub-100 nm size range with a monodisperse PSD.

A second route, CEP mediated with a CTA is shown, herein to yield PNPs at significantly high solids content, where the size is sub 100 nm and monodisperse. To the authors knowledge, the PNPs prepared here show both a higher solids content, and a smaller (monodisperse) size than what has been done previously, *at the surfactant concentrations used here*. The prepared dispersions are characterised in terms of their stability, size and PSD.

2.2 Methods and Materials

The following section outlines the materials and methods used for the preparation and characterisation of p(MMA) latex nanoparticle dispersions. The preparation routes used here, SFEP, and CTA mediated emulsion polymerisation are described, as well as the techniques used to characterise the resulting particle dispersions; including scanning electron microscopy (SEM), electrophoretic mobility and dynamic light scattering (DLS).

Material	**Supplier**	**Purity /%**
Sodium dodecyl sulfate (SDS), fig 1.4	Acros Organics	92.5-100 based on total alkyl sulfate content
Methyl methacrylate (MMA)	Fisher Scientific Ltd	99
Sodium hydrogen carbonate	Fisher Scientific Ltd	99.85
Ammonium persulfate (APS)	Sigma-Aldrich	98
2,2-azobis(2-methylpropionamide) dihydrochloride (AIBA)	Acros Organics	Not available
4-cyano-4-((dodecylsulfanylthiocarb-onyl)sulfanyl)pentanoic acid	Sigma-Aldrich	97
2-Napthyl Methacrylate (Fmon)	Sigma-Aldrich	Not available
Acetone	Sigma-Aldrich	$\geq$ 99.8

Table 2.2: Materials used for Latex particles synthesis

Water

The water used in this research was purified by a millipore reverse osmosis unit and treated with a Milli-Q reagent water system, to yield ultra pure water. The surface tension was measured to be 72.2 mN/m at 21 °C, which is in good agreement with the literature value (72.4 mN/m at 20 °C).[131] The water had a resistivity of 18.2 MΩ.cm at 25 °C, which again corresponds well to the known resistivity of ultrapure water (18.2 MΩ.cm at 25 °C).[131]

Glassware

All glassware was twice cleaned with a solution of Decon 90 (a surface active cleaning agent) then with Milli-Q water. Each piece of glass was then finally washed with acetone and dried in an oven at 50 °C. This was to ensure no impurities remained particularly any surface active species.

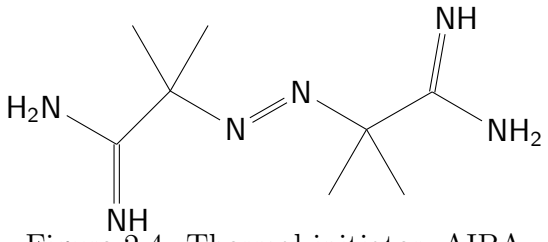

Figure 2.4: Thermal initiator, AIBA

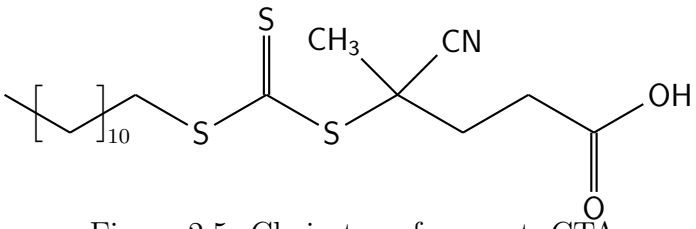

Figure 2.5: Chain transfer agent, CTA

2.2.1 Methods

2.2.1.1 Monomer inhibitor removal

MMA as received contains a trace amount of monomethyl ether hydroquinone (MHEQ) acting as an inhibitor, which keeps the monomer stable. Inhibitor removal can be achieved by either distillation, or by passing the monomer through a column of basic alumina.

Initiator was removed via both methods. For purification via vacuum distillation, MMA was heated at 35 °C, and the condensate collected for use. For inhibitor removal using basic alumina, a column was packed with basic alumina and a vacuum attached. The monomer was then fed into the column and the resulting, inhibitor free monomer collected. The inhibitor-free monomer was used within 2-3 weeks, as the monomer was typically found to self polymerise approximately 4 weeks following purification.

Comparison of the two methods

Both removal methods were tested for their efficiency by using the *purified* monomer from each removal method to prepare particle dispersions, at fixed experimental parameters.

There was no discrepancy found in the final particle size, however a significantly higher amount of coagulum was observed for particles generated that were purified via alumina column. It is speculated that this was the case due to incomplete removal of MHEQ inhibitor via the basic alumina column method. In fact, the effect was very apparent in this case due to the synthesis targeting high solid contents. For this reason it was decided monomer purified via distilled monomer would be used for all subsequent synthesis experiments.

2.2.1.2 Surfactant free emulsion polymerisation

The following describes how a p(MMA) nanoparticle dispersion was typically prepared via SFEP;

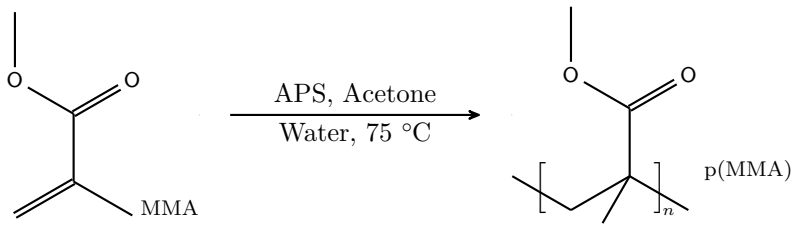

Figure 2.6: Surfactant free emulsion polymerisation reaction scheme

APS (0.124 g) was added to a mixture of acetone/ Milli-Q water (40:60) and the solution stirred (400 rpm). MMA (5.2 g) was then added drop-wise (0.3 g/min) and the mixture degassed (N_2, 40 min). The temperature was then increased to 75 °C and the polymerisation was allowed to run for 4 hrs. Upon completion, the resulting particle dispersion was passed through glass wool before collection and storage (< 10°C).

2.2.1.3 CTA mediated emulsion polymerisation

The following describes how a p(MMA) nanoparticle dispersion was typically prepared via CTAmEP;

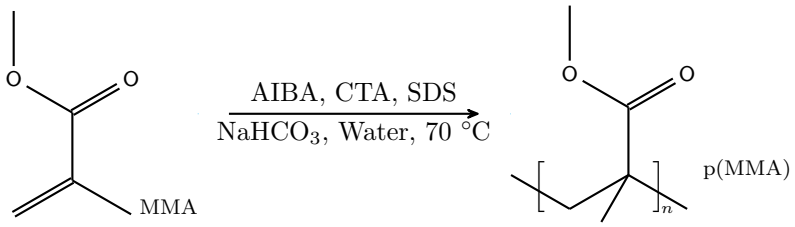

Figure 2.7: CTA mediated emulsion polymerisation reaction scheme

Initially a stock solution was prepared by adding the CTA (0.003 g) to MMA (51 mL) and the solution degassed (N_2, 1 hr) with magnetic mixing (400 rpm). SDS (1 g) and $NaHCO_3$ were dissolved in Milli-Q water (29 mL). Next, MMA (19 g) was added drop-wise (0.8 g/min) to the mixture, under magnetic mixing while the reaction media was simultaneously deoxygenated (∼40-60 min). The stock solution (12.5 mL) was then added drop-wise (0.8 g/min) to the mixture. AIBA (0.02 g) dissolved in Milli-Q water (10 mL) was next added, drop-wise to the reaction media, and the temperature increased to 70 °C. The polymerisation was then allowed to run to completion (2 hr), and upon completion the resulting particle dispersion passed through glass wool before collection and storage (< 10 °C). Note, here more than 5 wt.% coagulum constitutes significant coagulum presence.

2.2.1.4 Solids content

Solids content is defined as the ratio of the amount of solid (here, polymer particles) in the dispersion, to the total amount of the dispersion, by weight (usually) or volume and is expressed as a percentage. For the sake of completeness the following figure displays the conversion to volume for the most commonly referred values in upcoming figures, for p(MMA) dispersions;

$$10\ wt.\% \equiv 8.5\ vol.\%$$
$$20\ wt.\% \equiv 16.9\ vol.\%$$
$$30\ wt.\% \equiv 25.4\ vol.\%$$
$$40\ wt.\% \equiv 33.9\ vol.\%$$

Figure 2.8: Conversion from weight to volume % for p(MMA) dispersions

2.2.1.5 Dialysis

The prepared particle dispersions were 'cleaned' by dialysing in Milli-Q water, using dialysis (cellulose) tubing (8000 MWCO, pore size). Approximately 60 mL of the prepared particle dispersion was placed into pre-cut and pre-wet dialysis tubing (closed with dialysis clips). This was then placed in a 2 L *tall* beaker, and filled to maximum capacity with Milli-Q water (the external phase). The external phase was replaced approx. twice every 24 hrs. This procedure removes surfactant, salt and also any unreacted monomer from the particles dispersion, while ensuring particles do not escape into the external phase. For each latex dispersion, the particle size was determined both prior to, and following dialysis. No significant difference was found in the polymer particle size following dialysis for all samples: although in order to account for EDL, samples are measured with a fixed background electrolyte concentration, clarified in the following section.

2.2.2 Particle characterisation

The prepared particles were analysed using dynamic light scattering, electron microscopy, nuclear magnetic resonance spectroscopy and electrophoretic mobility (zeta potential) measurements. The techniques are all individually examined below;

2.2.2.1 Dynamic Light Scattering (DLS)

DLS is an important and powerful non-intrusive technique, used to determine the size and size distributions of particle and polymer dispersions.[132] The technique measures scattered light from light irradiating the dispersed particles/polymers, and the time dependant intensity fluctuation recorded at the detector.[133,134] These intensity fluctuations are caused by Brownian motion of particles, and are then related to constructive and destructive interference events. The diffusion coefficient (D_c) of the particles/polymers is then inferred from this data. The hydrodynamic diameter (d_H) is then determined using the Stokes-Einstein equation[134];

$$D_c = \frac{k_B T}{3\pi\eta d_H} \tag{2.5}$$

Where k_B is Boltzmann's constant, T the absolute temperature and η the viscosity.

It must be noted, that the size measured using this technique d_H, is actually the diameter of an equivalent sphere with the same translational diffusion coefficient as the measured particle.

As mentioned in the previous chapter (Section 1.5), for a colloidal particle there is an associated volume which moves with the particle called the electrical double layer (EDL).[33] Thus, the hydrodynamic size obtained here includes EDL thickness contribution, which then means the electrolyte concentration significantly affects the d_H.

For this reason, for particle size measurements the particle dispersions were diluted in water (10 mM NaCl) to ensure the EDL thickness should be broadly dampened, to a similar level for all particle measurements.

All reported measurements are an average of 3 measurements where each measurement consists of 10 runs. The reported polydispersity index (PDI) is a measure of the distribution broadness as measured by the instrument. This is a dimensionless value, and is defined as the squared ratio of the particle size distribution and mean particle size. Size measurements were performed on a Zetasizer Nano ZS (Malvern Instruments Ltd) and a Brookhaven BTC DLS. Note, PDI, when shown in the upcoming figures, is plotted on the Y2 axis with a log scale, this was done to avoid confusion from the size data plotted on the Y1 axis: it is kept in to highlight size distributions in the sample dispersions.

2.2.2.2 Electrophoretic Mobility

For a given colloidal dispersion, the surface charge can be determined by measuring the zeta potential.[33,135] This is the potential at the slip plane, close to the particle surface (see Section 1.5, Figure 1.7 for further details) as it moves within the solvent. The particle, under an applied electric field, will respond by travelling to the electrode of opposed charge (determined by the surface charge). This diffusion rate is dependant on the particle size, surface charge, and the applied electric field strength. The velocity of a particle dispersion in a unit electric field is the electrophorectic mobility, U_E.[135] The following equation is then used to convert U_E to zeta potential, ζ;

$$U_E = \frac{2\epsilon_0 \zeta f(\kappa r)}{3\eta} \tag{2.6}$$

$f(\kappa r)$ is Henry's function, where κr is essentially the ratio of the EDL to the particle radius, limited to measurements in aqueous media with moderate electrolyte concentrations. Typically, at these concentrations the EDL thickness is a few nm, and $f(\kappa r)$ is assumed to be 1.5. This is known as the Smoluchowski approximation, applicable for any concentration and shape of dispersed particles.[136,137]

ζ is widely used as an indication of dispersion stability, where the particle charge is (negative or positive) sufficiently high, electrostatic repulsion renders the suspension stable.[138] Whereas, if the opposite were true the particles would be more likely to aggregate (and sediment or cream depending on the density difference) and the dispersion considered unstable (for charge stabilised dispersions). For any ζ measurement the pH of the dispersion must be known, as the surface potential of the colloidal system is affected by both the pH and ionic strength. The plot of ζ as a function of pH, for most colloidal dispersions would pass through a ζvalue of 0 mV at a given pH. This is the point at which the dispersion is expected to be most unstable, and is better known as the isoelectric point.

ζ measurements were determined using phase analysis light-scattering with a Zetasizer Nano ZS (Malvern Instruments Ltd). The zeta potential values determined in this study are an average of 3 measurements, where each measurement is set to collect at least 30 runs.

2.2.2.3 Scanning Electron Microscopy (SEM)

SEM is an important technique to image particle surfaces and is capable of resolutions as low as 1 nm.[139] A field emission gun or thermionic sources are used to generate electrons which are then focused onto the sample using a condenser lens. The imaging is carried out under vacuum to avoid air interacting with the generated electrons; samples must be stable under vacuum and must be conductive to avoid charging effects.

The sample surface is scanned in sections forming a raster.[140] The electrons hitting the sample surface lose their energy within a teardrop shaped interaction volume, which depending on the sample characteristics can extend from 100 nm to

about 5 μm in the surface. The interaction of the electron beam with the sample causes different effects to occur including high energy backscattered electrons, secondary electrons and x-rays of which the most important one is the formation of inelastically scattered secondary electrons ($>$ 50 eV). These are detected and amplified by the detector and are then represented on a screen as grey dot. The intensity of each dot corresponds to the measured intensity.

The number of electrons reaching the detector will vary with the topography and composition of the sample surface (hence the need for additional conductive coating), giving rise to more or less bright spots which then allow the image to appear as a 3D image. The image on screen is synchronised with the electron bundle scanned across the sample surface where the linear magnification is realised from the ratio of length of the monitor and the size of the raster. A magnification of up 500,000 x can be achieved by changing the size of the raster on the sample surface. The chemical composition and orientation of the sample can also be determined by detection of x-rays and high energy back scattered electrons, in addition to the secondary electrons.

High resolution SEM for the particle dispersions produced in this study was performed on a Hitachi SU 8230 cold-FEG (field emission gun) SEM. Typically a drop of the dispersion (0.04 wt%) is placed onto a clean SEM stub and dried. Once dry, the sample is sputter coated in carbon (10-15 nm) using an Agar high resolution sputter coater.

2.2.2.4 Nuclear Magnetic Resonance spectroscopy (NMR)

Nuclear magnetic resonance spectroscopy, more commonly known as NMR spectroscopy, is a powerful analytical tool used to glean information of molecular structure, conformation and purity. NMR can be used to determine the molecular weight of polymers (up to $\sim$ 12000 g/mol), via end group analysis, as well as accurately determining the monomer ratios for copolymers.[141]

Here, ^{1}H NMR was used to to determine the monomer conversion of the prepared particle dispersions. The ^{1}H NMR spectra were obtained using a Bruker 500 MHz NMR spectrometer. For these measurements, a sample of the reaction media was collected and dissolved in $CDCl_3$ at concentrations approximate to 30 mg mL^{-1}, and

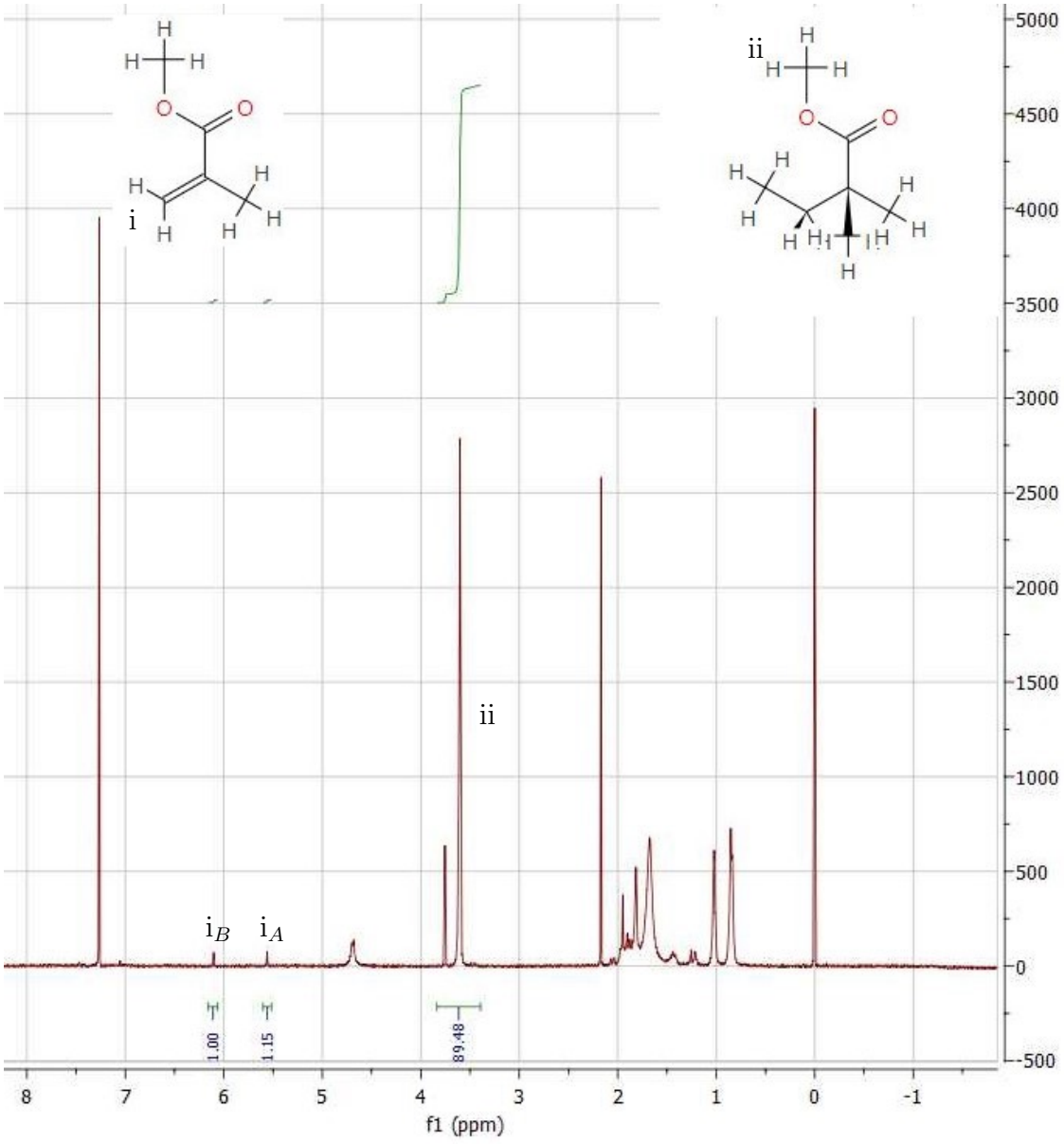

Figure 2.9: NMR spectra for a polymerisation run at 120 min, with the MMA molecular structure on the top left of the figure, and the p(MMA) structure on the top right side of the figure.

the samples stirred for 2 hr prior to analysis. The chemical shifts for the spectra were normalised to 2,2-dimethyl-2-silapentane- 5-sulfonate sodium salt (DSS, δ 0.015 ppm).

Spectra were analysed and assigned using the MestReNova 9 software (Mestrelab Research S.L.). Phase correction and background subtraction were performed manually prior to the analysis of spectra.

The monomer conversion is determined by calculating the ratio of the signals from the methoxy protons in the unreacted monomer (δ 5.55 and 6.10 ppm, i in Figure 2.9), and the methoxy hydrogens from the polymer (δ 3.6 ppm, ii in Figure 2.9). This was a good indicator of the monomer conversion rate as polymerisation proceeds, and the implications discussed in the following results section.

2.2.2.5 Attension Theta Pendent drop

The surface tension of the dialysed particle dispersions was determined using optical tensiometry.[142] The tensiometer is used to analyse the drop shape of the dispersion, hanging from a needle tip. The shape of the drop here is a result of the balance between surface tension and gravity. The liquid/air interface causes an increase in the pressure within the drop, from which the surface tension is determined using the following expression, relating to the drop shape[142];

$$g = \Delta\rho g^* R_0 / f \tag{2.7}$$

Where the shape factor, f is related to the Young-Laplace equation, and solved by the software for each drop, $\Delta\rho$ the density difference of the two phases, R_0 is the radius of the drop curvature at its apex, and g^* is the gravitational constant.

Prior to taking any sample images the instrument is calibrated with a spherical ball, with known dimensions.This technique requires no dilution, and samples are measured as they are prepared using drop shape analysis. Each sample drop is held in place and the drop allowed to settle (until real time surface tension measurement attains a constant value). Drop volume is kept constant by the instrument, which auto fills the drop if any evaporation occurs. For each measurement at least 20 images are captured and analysed, from which the average value is reported.

2.3 Results and Discussion

Latex particle synthesis is a complex process, regardless of the method used to prepare the dispersion. The size and size distribution of the final particle dispersion can be impacted by numerous experimental factors, including but not limited to: stirring speed, stirring type (magnetic/overhead), cleanliness of equipment, purity of the various components used, target solids content, oxygen content, solubility, temperature etc. As such investigating the effects of various component inclusion/concentrations becomes more difficult. With this in mind, it is imperative that all the equipment used is cleaned to a good standard (see Glassware in experimental section) before each synthesis, and that the same experimental set-up used throughout the study. Moreover, for each synthesis run the system is degassed and saturated with nitrogen prior to polymerisation. This is to ensure removal of dissolved oxygen from the continuous phase and reactants which, if available during the reaction will form radical species which can act to terminate propagating centres. A highly undesirable consequences for polymerisation.

2.3.1 Surfactant free emulsion polymerisation

The method used in this study develops a previous study.[82] Where, a range of monodisperse PMMA nanoparticles were prepared, by altering monomer, initiator and acetone concentration in the continuous phase. APS is used as the initiator, which also stabilises the particles by producing a charge on the particle surface. Table 2.3 shows some of the more successful results from the attempts made to replicate their method; the ratio of the solvent mixture (water and acetone) was kept constant at 40 vol% acetone. This was the acetone concentration reported by the authors to yield the desired particle size and size distribution. This solvent mixture has a reduced surface tension, compared with pure water, approximately 35 mN/m, Figure 2.10.

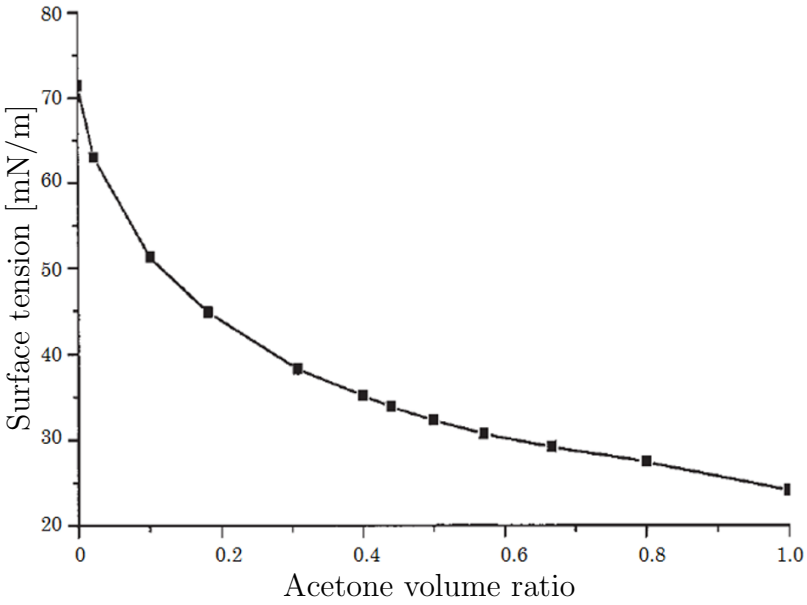

Figure 2.10: Static surface tension measurements of water:acetone mixtures, with increasing acetone concentration (reprinted from ref 143).

The reduction in surface tension aids in stabilising the particles, while the decrease in polarity causes an increase in the final particle size. The nucleating particle centres are less stable though with the reduction in polarity, as the surface potential is relatively small compared to a pure water solvent, which leads to larger particles in the final dispersion. However as monomer solubility is increased in this solvent mixture, more nucleating particle centres are formed initially. These then require the same amount of monomer as the polymerisation proceeds, using up more monomer. The increased monomer solubility overrules the effect of decreasing the dielectric constant, when the ratio of acetone to water is more than 20%.[143] Thus, overall smaller particles can be prepared in the presence of acetone than in water alone.

The results from preparing particle dispersions using this method were very inconsistent, Table 2.3. Initially the particle size targeted was 32 nm at approximately 10 wt% solids content, with a monodisperse size distribution. Run 1-3 where all the variables are kept constant, are the results from the aforementioned targets. Run 4 was slightly different, in that the target solids content was less than the previous runs, 6.6 wt% but all other variables were kept constant to the previous runs. The target size and size distribution were those from the literature, achieved using the

same variables (i.e. same target solids, initiator concentration and acetone:water ratio).[82]

Table 2.3: Results from some of the samples obtained when using surfactant free emulsion polymerisation

Sample	**Solids Content /wt. %**		$\mathbf{d}_H$	**PDI**
	Target	Final	/nm	
1	9.5	2.86	188 ± 32	0.17
2	9.5	0.48	242 ± 48	0.20
3	9.8	9.31	163 ± 24	0.15
4	6.6	3.54	243 ± 75	0.31

From the results in the above table, it is clear that run 1-3 produced dispersions with very dissimilar results. Run 1 and 2 did not achieve the target solids content, in that most of the activated monomer ended up as coagulum, more so in run 2 than run 1. Run 3 improved upon the results from the prior two runs, in that the target solids content was very nearly achieved. This is rather misleading as this suggests the particles prepared in run 3 were sufficiently stabilised against coagulation. However there is no significant difference in the variables, target solids content or initiator concentration, for this conclusion to be drawn. Rather this serves as evidence that the synthesis of nanoparticles using this method is very difficult and inconsistent. This is confirmed with run 4, where a lower monomer concentration is used, (therefore increased stabiliser content) but the results were similar again to the previous runs.

It was thought that reducing the monomer concentration may perhaps lead to desirable results, in that the initiator to monomer ratio is increased which then implies the stabilising capability of the system is increased, which should then yield improved results, if the initial cause for unsuccessful samples was inefficient stabilisation. However from the results this was not the case. At this point, it must again be highlighted that for each synthesis run, the same equipment is used each and every time, which was also cleaned in the same manner every time. Therefore the inconsistency is concluded to be due to the method rather than an experimental error.

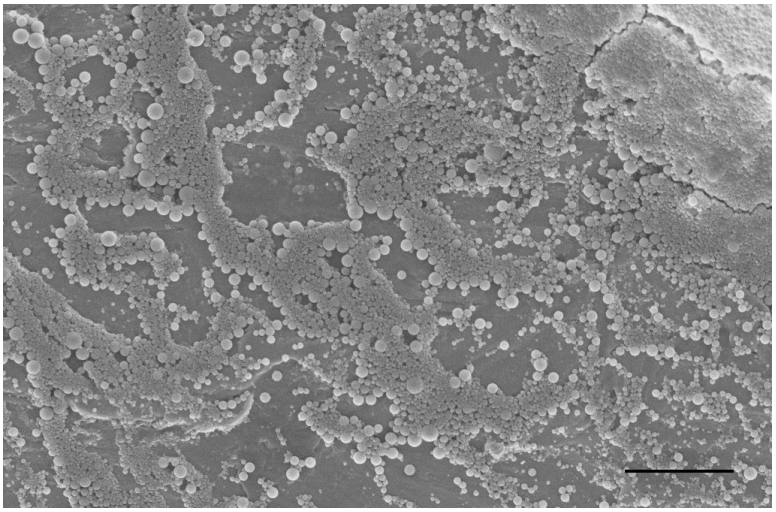

Figure 2.11: SEM image of PNPs prepared using SFEP (run 1 from table 2.3), scale bar here is 5 μm, prepared at 70 °C.

This is clear evidence that it is very difficult to prepare a sub 100 nm particle dispersion where the size is monodisperse using this method, or even reproduce any of the original results. This was thought to be due to a combination of factors. The homogeneous nucleation mechanism is assumed to be responsible for particle growth, (covered in Section 2.1.3). The mechanism assumes particles are formed by limited aggregation of particle nuclei, however in this case due to inefficient stabilisation the particle nuclei aggregate more, as they do not yet possess a charged surface to be individually stable. However as the surface tension of the solvent is reduced to favour monomer solubility, it is more likely that efficient nucleation did not occur to create the numerous particle nuclei required. The reduced number of particle nuclei can then explain this increase in particle size, as reducing the number of active particle centres leads to larger particles using the increased [monomer] available for each nucleus to continue growing to much larger sizes. However this phenomenon should still lead to a narrow size distribution. Thus a combination of the two factors are held responsible for the final dispersion characteristics.

It is rather difficult to produce a stable dispersion of latex particles using this method, due to the inadequate stabilisation of the monomer and the subsequent particles. It is even more so challenging to prepare a dispersion of monodisperse sub 100 nm latex particles; therefore this method was deemed unsuitable for preparation

of the particles sought for this project and was not investigated further.

2.3.2 Chain transfer mediated emulsion polymerisation

The method used here is another adapted from the literature.[78] In the original article the authors make use of a very hydrophobic CTA, bis[(difluoronoryl) diphenyl glyoximato] cobalt(II). This CTA is used as a catalyst and was successfully in preparing PNPs at high solids content (44 wt.%) and small sizes (33, 44 nm), although the surfactant concentrations used (∼8 wt.%) to achieve this was still undesirably high (see page 37).

Here, this method was adopted using a different CTA, and a lower surfactant concentration. The CTA used was a commercially available, 4-Cyano-4-((dodecyl sulfanylthiocarbonyl) sulfanyl) pentanoic acid. This CTA was chosen, as it is known to be very suitable for methacrylate based monomers and is also more water soluble, a desirable trait, as the CTA is required to migrate through the aqueous phase in the polymerisation process. Table 2.4 shows some results obtained, following some preliminary work, using this method (lower surfactant concentrations are used relative to the literature method).

Table 2.4: Results from some of the samples obtained using chain transfer mediated emulsion polymerisation

Run	**Solids content /wt.%**	**[CTA] /mM**	**d_H /nm**	**PDI**
1	38.83	0.34	55 ± 2	0.087
2	39.13	0.33	54 ± 2	0.078
3	37.67	0.96	50 ± 1	0.037
4	38.60	0.10	61 ± 1	0.040

From the preliminary results, it was immediately made apparent that this was a viable and reproducible method to prepare sub 100 nm latex dispersions, when using this CTA and a lower surfactant concentration. The study the method was adapted from prepared particles in the range 33-44 nm, which was also the initial target here. Unfortunately this results could not be reproduced without increasing the surfactant concentrations significantly. The particles obtained here utilise much less

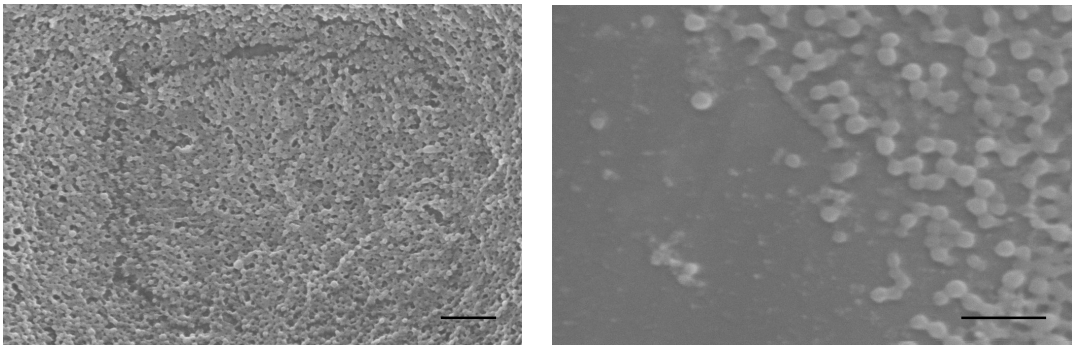

(a) Run 1 from Table 2.4, scale bar is 500 nm (b) Close up of run 1, scale bar is 200 nm

Figure 2.12: SEM images of the PNPs, run 1 from Table 2.4, prepared at a targeted 40 wt.% solids ([monomer] = 4M), at 70 °C.

surfactant relative to the original study and the resulting PNPs are monodisperse, sub 100 nm in size and are prepared at high solids concentrations; significantly higher concentrations than those found in the literature (see section 2.1.5).

The method proved to be very reproducible, and therefore was chosen for a further systematic study to prepare p(MMA) dispersions with a range of particle sizes.

2.3.2.1 Mechanism

A kinetic study was performed to investigate the mechanism for particle preparation in the presence of CTA. From Figure 2.13, it is clear that there is no significant difference in the polymerisation rate (conversion) and in both cases near complete conversion is reached within 140 min.

Typically for a polymerisation process under living (CTA) control, the rate of polymerisation is lower than for a CEP process.[93,95] This is of course due to the CTA, in that an intermittent species is formed, which establishes a dynamic equilibrium between the propagating chains and the deactivated CTA capped chains (see section 2.1.4 for full details). However in these systems the CTA concentration is 10 times that of the initiator concentration to act effectively during the reaction. Here the CTA is available in much smaller amounts, as the highest CTA concentration used (Figure 2.14) equates to $\approx$ 1:1 ratio with the initiator concentration. Increasing the CTA concentration further led to a significant amount of coagulum, and did not lead to successful particle samples. This is an interesting effect, and can perhaps

be explained by considering the standard use of a CTA. CTA is normally used to prepare polymer chains with a narrow molecular weight distribution. Here the CTA is employed as an attempt to reduce the particle size.

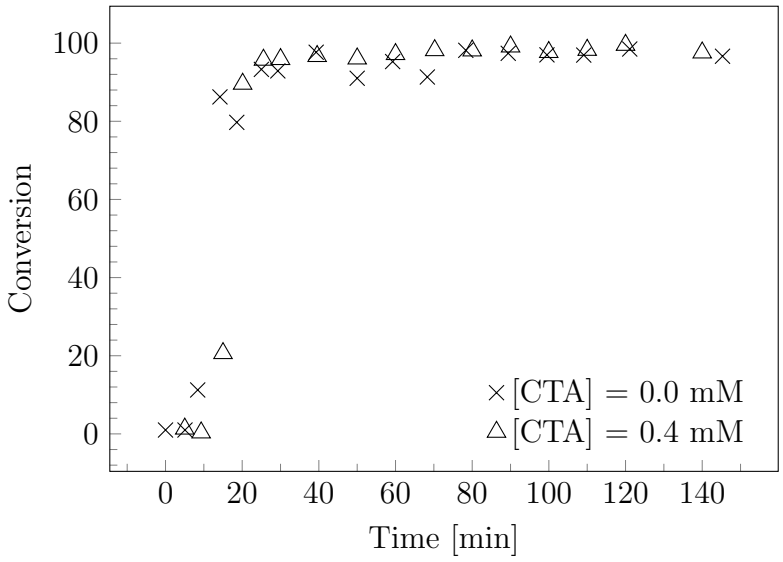

Figure 2.13: Monomer conversion with time for synthesis runs with and without CTA. The corresponding [surfactant], [initiator] are kept constant for both samples, 90 and 1.3 mM respectively.

The particle size was monitored for samples prepared with increasing CTA concentration, where all other variables were kept constant. The results are displayed in Figure 2.14 with some SEM images shown in Figure 2.15; the PDI is also displayed but is not clear for each concentration, it is merely to show all the corresponding PDIs were below 0.1. The first point depicted (the largest final particle size), corresponds to the sample where no CTA is used. The use of increasing [CTA] was seen to lower the final particle size by 33%, without loss of colloidal stability or production of a significant amount of coagulum, while maintaining a monodisperse size distribution. The final particle size decreases with increasing CTA concentration until a certain concentration is reached, where a plateau is observed.

Further increasing the CTA concentration (2 and 2.5 mM) does produce smaller particles (47 $\pm$ 1 and 44 nm $\pm$ 1, respectively); however there is a significant amount of coagulum produced. A significant increase in the overall viscosity was also ob-

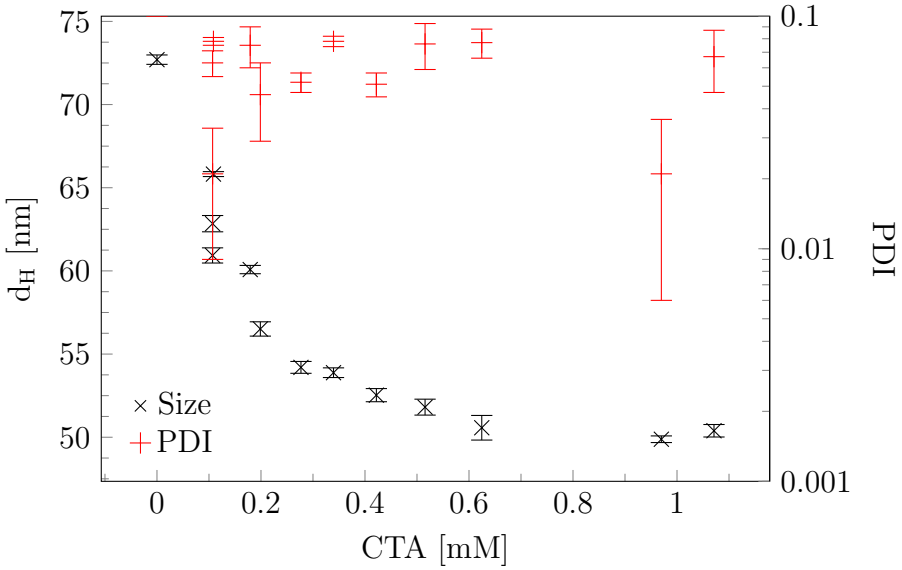

Figure 2.14: Particle size variation as a function of the CTA concentration, where the [surfactant] and [Initiator] are kept constant, 80 and 1.2 mM respectively, and 40 wt.% solids ([monomer] = 4M) is targeted for each run, at 70 °C.

served, the dispersion was almost gel-like in appearance with large 'lumps' of scattered coagulum. These could not be separated from the dispersion by filtration, due to the dispersion viscosity. Any further increase from this concentration leads to a loss of monodispersity control, significant coagulum formation, and a slow polymerisation rate.

These effects are most probably due to nucleation occurring in the large monomer droplets, which normally act as monomer reservoirs and not the locus of polymerisation. Although there is some droplet nucleation in conventional emulsion polymerisation, this is considered to be rather insignificant as the surface area of these droplets is very small compared to the surface area of the micelles (these act as the locus of polymerisation). However as the CTA is first dissolved into the monomer, it is already available in the monomer droplets and simply requires a radical to nucleate the droplet and initiate propagation. If the concentration of CTA is small and the CTA is not very hydrophobic, it is transported through the aqueous phase to the micelles and then acts to improve the size characteristics of the dispersion. If the CTA concentration is increased sufficiently high enough so that there is a high

enough concentration of CTA in the monomer droplets, droplet nucleation would become significant. The propagation reactions occurring in the monomer droplets would then lead to larger particles being formed, while the monomer swollen micelles would lead to very small particles , leading to a polydisperse final PSD.

When the CTA concentration is increased just high enough (2 and 2.5 mM) to make monomer droplet nucleation significant, the monomer droplets would still act as reservoirs and aid polymerisation in both the monomer droplet and the monomer swollen micelles; leading to small particle sizes (47 and 44 nm, respectively) as effectively more nucleating centres are present which increases the number of particles, but the loss of monodisperse PSD, as is observed here.

As a CTA is typically used to prepare polymer chains with control over the molecular weight distribution, when previous studies have attempted to use CTA to aid PNP preparation, a block co-polymer system is usually targeted (see Figure 1.3): where there is a hydrophilic block providing stability and the hydrophobic block grown within the polymer micelles. This method has been used effectively prepare particles (page 32), but with restrictions on the solids content that can be attained. To date particles in the range of 45-190 nm have been prepared at a solids concentration of $\sim$15 wt.%.[97,98]

The CTA used in this study has been greatly beneficial, and has been used to prepare a range of particles with high solids content, sub 100 nm size range and monodisperse PSD. Although only a very small amount is used, from the results it is clear this is sufficient to significantly affect the PSD at the solids content targeted here. With the CTA concentrations used here it would be incorrect to say we have a living CEP system as they are traditionally defined; i.e. where the prepared polymer chains have narrow molecular weight distribution. The particles grown here do in fact have a narrow size distribution, however not nearly enough CTA is used to, theoretically, prepare narrow molecular weight distribution polymer chains. It is likely, at the concentrations used here the CTA subtly enhances the particle nucleation efficiency by protecting growing chains from termination; though it does not affect the overall rate of termination, as the protected chains exist as dormant CTA capped chains. Therefore the mechanism for this method is as that for conventional emulsion polymerisation, the difference being in that a catalytic

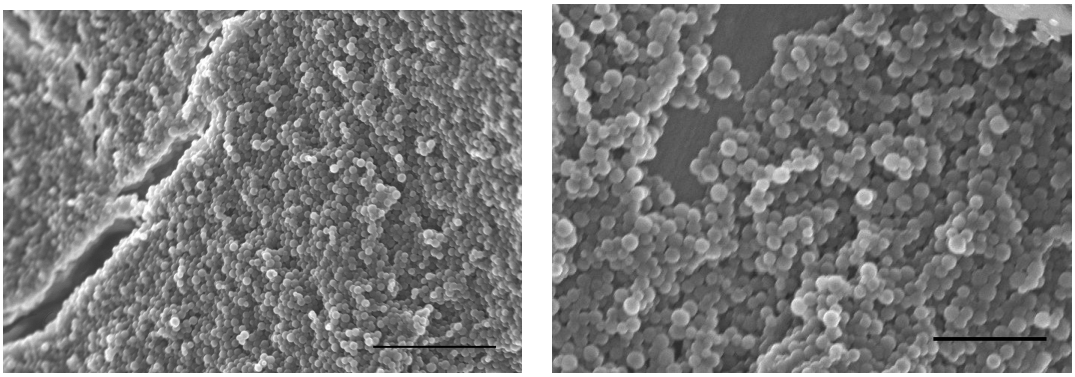

(a) 100mM SDS concentration from Figure 2.16, scale bar is 1 μm.

(b) 0.6 mM CTA concentration from Figure 2.14, scale bar is 500 nm.

Figure 2.15: SEM images of polymer nanoparticles prepared at a targeted 40 wt.% solids ([monomer] = 4M), at 70 °C.

amount of CTA is emulsified with the monomer during pre-polymerisation stage, thereby enhancing the nucleation efficiency.

The ideal concentration range, figure 2.14, where the CTA has good control over the final particles size is a relatively small but sufficient enough to warrant the use of CTA in this manner. To date, preparation of monodisperse nanoparticles at 40 wt% solids content using a CTA in this manner has not been observed in the literature, Section 2.1.5.

2.3.2.2 Surfactant concentration

Surfactant is used to stabilise, initially the monomer droplets, and then to stabilise the particles in the final dispersion (see page 23). Surfactants control to a great extent the particle nucleation efficiency and the size distribution. The particles prepared in this study are to be used as model colloidal inkjet inks, where good control over the surfactant concentration is required. Therefore the goal with this method is to PNPs with a high solids content using as *low* a surfactant concentration possible.

These requirements then make this process much more complex; with increasing solids content, both the particle surface area and inter-particle collisions, also increase significantly. These systems then require increased surfactant concentrations to stabilise against coagulation. However with the addition of a CTA to the reac-

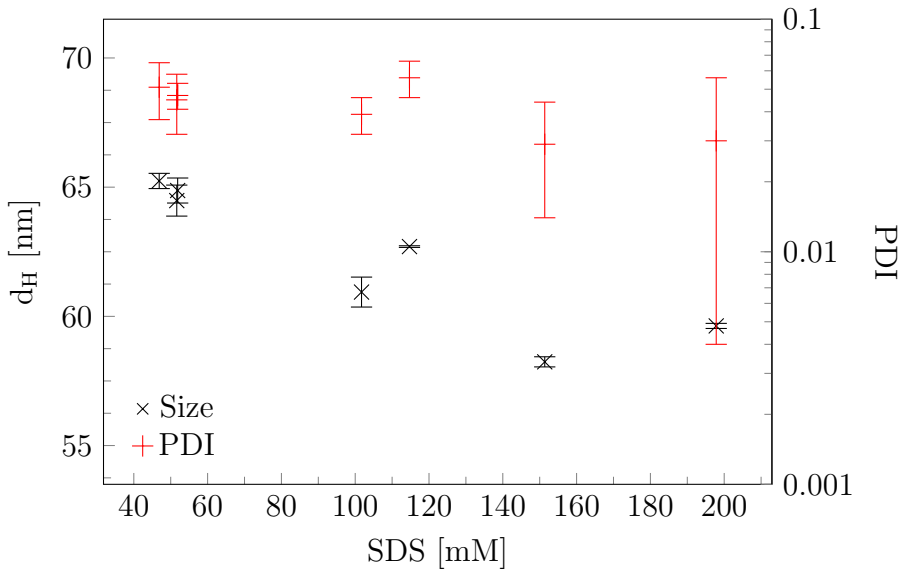

Figure 2.16: Particle size variation as a function of the SDS concentration, where the [CTA] and [Initiator] are kept constant, 0.08 and 1.2 mM respectively, and 40 wt.% solids ([monomer] = 4M) is targeted for each run at 70 °C.

tion to aid particle nuclleation efficiency, a relatively low surfactant concentration is found to be sufficient to ensure stability in the final PNP dispersion.

The change in particle size with increasing surfactant concentration can be observed in the above Figure 2.16. The particle size is usually found to decrease with increasing surfactant concentration, as is the case here. The change in particle size due to increasing surfactant concentration is ∼6 nm (64 ± 1 to 57 ± 1 nm). This decrease in particle size is due to the more readily available surfactant molecules to improve stabilisation. In that as the surfactant concentration increases, there is better stabilisation during the nucleation stage of polymerisation. The improved stabilisation increases the number of latex particles in the final dispersion, which then decreases the particle size, for a given solids content. The change in size, ∼6 nm due to surfactant concentration is then rather small considering the importance of surfactant in emulsion polymerisation.

Figure 2.16 is slightly misleading in that sense; in that, as the aim of this study is to prepare particle dispersions with as a low a surfactant concentration as possible, only small enough amounts of surfactant are utilised. Thus, the initial concentra-

tions used correspond to the largest concentration on the above plot. The surfactant concentration was then lowered further to the lowest possible concentration where stable PNPs could still be prepared point where the size was monodisperse. Using a lower surfactant concentration that the concentration depicted in figure 2.16 led to loss of monodispersePSD, and formation of significant coagulum. A slightly lower concentration (36 mM) was found to successfully prepare a stable PNP dispersion, however this was with an increase in the CTA and initiator concentration.

2.3.2.3 Initiator Concentration

The initiator in these reactions produces the radicals initiating the polymerisation process. Increasing the initiator concentration would then increase the rate of radical generation as well as the number of particles in the system, thereby reducing the final particle size; in that more radials would increase the number of activated oligomers, which then grow into particles. Increasing the initiator concentration therefore, would increase the concentration of radicals in the system and consequently lead to a reduction in the final particle size. This would also act to increase the rate of polymerisation, to a certain extent.

Figure 2.17 is used to show the change in particle size with increasing initiator concentration. A decrease in particle size is observed up to a point until a plateau is reached. It must be noted here that the lowest concentration used is the concentration that was used to prepare the 'best' dispersion from the literature method this synthesis route is based on. Best refers to the dispersion with the smallest particle size prepared. The results shown are those where all the other variables, other than the initiator concentration are kept constant, and the target solids content for each of the runs is 40 wt%.

The trend shows a significant decrease up until 4 mM AIBA is used, following this the effect on particle size is less pronounced; here a limit is reached where enough activated oligomers are produced to enter every micelle and a plateau is observed. Increasing the concentration further from this point then has a negative impact on the final particle size due to termination. This is where there is an excess of activated oligomers, which can react with one other thereby creating 'waste chains'. This in turn would lead to a more polydisperse sample, where a mixture of the terminated

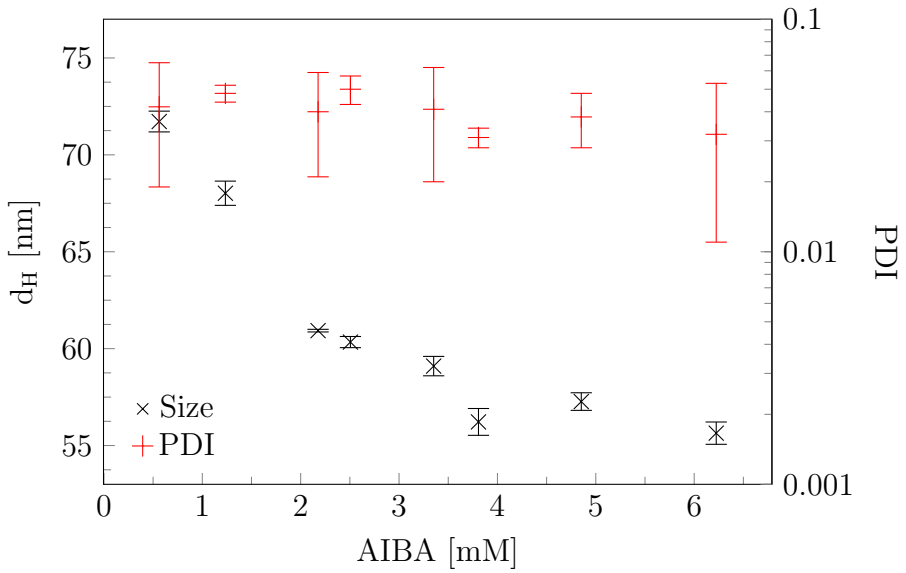

Figure 2.17: Particle size variation as a function of the AIBA concentration, where the [CTA] and [surfactant] are kept constant, 0.08 and 84 mM respectively, and 40 wt.% solids ([monomer] = 4M) is targeted for each run at 70 °C.

small oligomers contaminating the unaffected PNPs. Also if the number of initially activated oligomers decreases in the reaction, due to the termination reactions, a smaller final number of particles would be the consequence; where smaller number of particles mean larger polmer chain within the particles, leading to an increase in the final particle size.

2.3.2.4 Temperature

The rate of radical generation can also be increased by increasing the reaction temperature. Increasing the temperature increases the efficiency of the thermal decomposition of the initiator thereby increasing the rate of radical generation and the number of particles prepared. The reaction temperature used throughout the study was 70 °C, but was increased to 80 °C here to prove the effect of temperature. 59 ± 2 nm particles were prepared at 80 °C compared to 63 ± 1 nm particles at 70 °C.

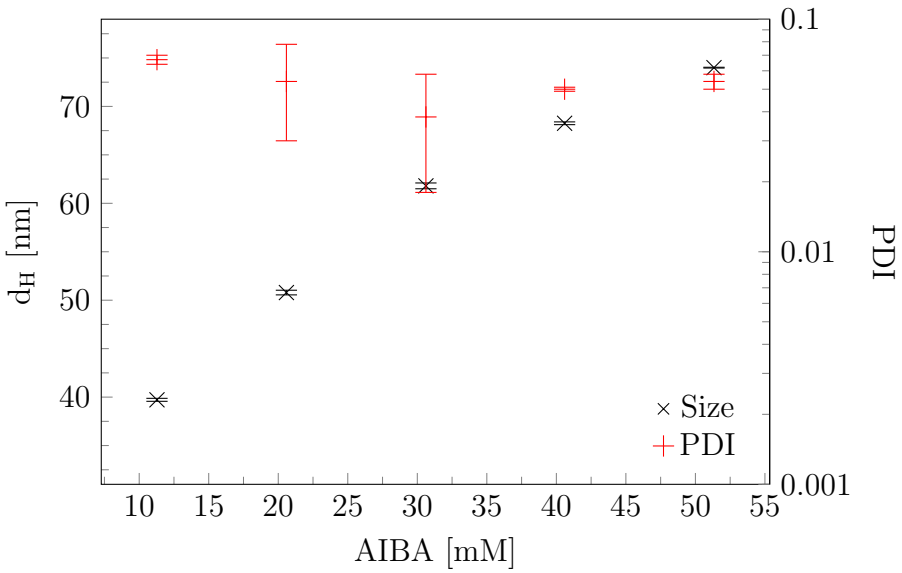

Figure 2.18: Particle size variation as a function of the Total Solids content, where the [CTA], [initiator] and [surfactant] are kept constant, 0.08, 1.2 and 80 mM respectively, for each run at 70 °C.

2.3.2.5 Monomer Concentration

The target solids content (monomer concentration) was varied to determine how this affects the final particle size, where the temperature, surfactant, and salt concentration were kept constant. The CTA is added to the monomer, and the concentration is calculated from the volume of monomer. Therefore the concentration of the CTA was kept constant *w.r.t. the monomer concentration.*

From Figure 2.18 it is immediately apparent that with a decreasing monomer concentration and a constant surfactant concentration, the surfactant stabilisation capability improves. The number of particles in the dispersions increases with decreasing solids content, leading to an overall reduction in final particle size, Figure 2.19. However as the surface area of the particles increases, the inter-particle collision frequency also increases which then requires a higher surfactant concentration to provide stability during polymerisation. This is possible when the solids content is decreased, whilst the surfactant concentration is kept constant as there is more surfactant available to stabilise the propagating particles at lower target solids content relative to when a higher solids content is targeted, adding to the fact that

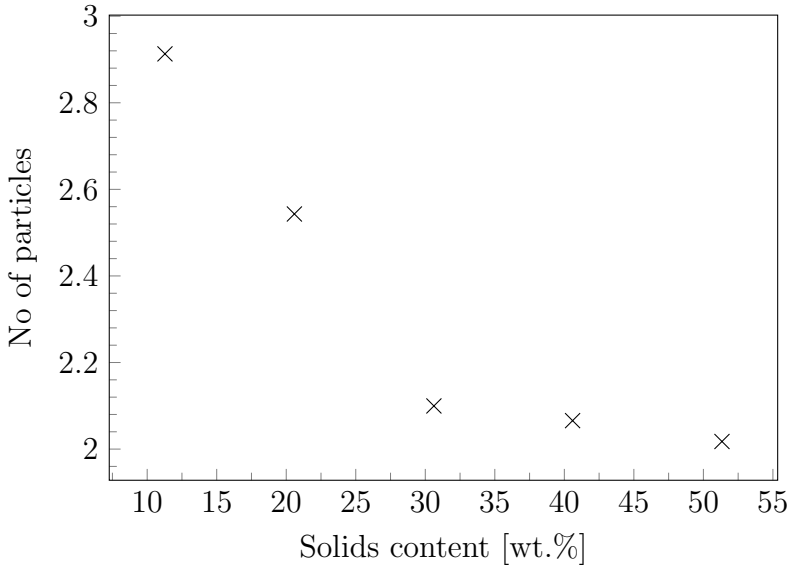

Figure 2.19: Number of particle as a function of the Total Solids content, where the [CTA], [initiator] and [surfactant] are kept constant, 0.08, 1.2 and 80 mM respectively, for each run at 70 °C.

smaller particles are prepared meaning less surfactant per particle is required.

The change in the number of particles is more dramatic from 30 - 10 wt.% relative to from 50 - 30 wt.%, as it is related to the final particle size, which is observed to vary in a similar fashion. This is to be expected, as the number of particles in each dispersion is determined from the particle size and the total solids content (polymer).

The CTA concentration is also kept constant, and so would act to improve the final particle size with decreasing monomer concentration. When the CTA concentration is varied to determine the effect on final particle size, the CTA was found to have a specific concentration range where it acted to improve the size characteristics of the particle dispersion. Increasing the concentration from the range was observed to have a negative effect on final particle size. This would be true for all the target solids content, where the ratio of CTA and monomer must within this predetermined limits for that monomer concentration, was kept as such, before the CTA starts having a negative impact on polymerisation process.

The final particle size decreases significantly with decreasing monomer concen-

tration, the final particle size is nearly halved when the targeted solids content is decreased from 40 wt% to 10 wt%. This then is the cost of increasing the solids content in the prepared particle dispersions.

2.3.2.6 Fluorescent Particles

As a proof of concept, fluorescent nanoparticles were prepared by copolymerising MMA with a fluorescent monomer, Fmon; initially these were planned for use for drop deposition experiments, however as the equipment was unavailable these were not used for any other purpose in this thesis. This was achieved by adding 0.1 and 0.05 wt% Fmon to the pre-polymerisation emulsion, Figure 2.20. Fmon is slightly similar to MMA, except for the large Napthyl group, which gives rise to the fluorescence. The polymerisation reaction rate would almost certainly have been affected, however as it was only a proof of concept experiment and a very small amount of Fmon used, the polymerisation was allowed to run as normal. The final particle size was 57 ± 1 and 62 ± 1 nm, with Fmon concentrations 0.05 and 0.1 wt% w.r.t. MMA: 55 nm particles are obtained at the same concentrations where no Fmon is added.

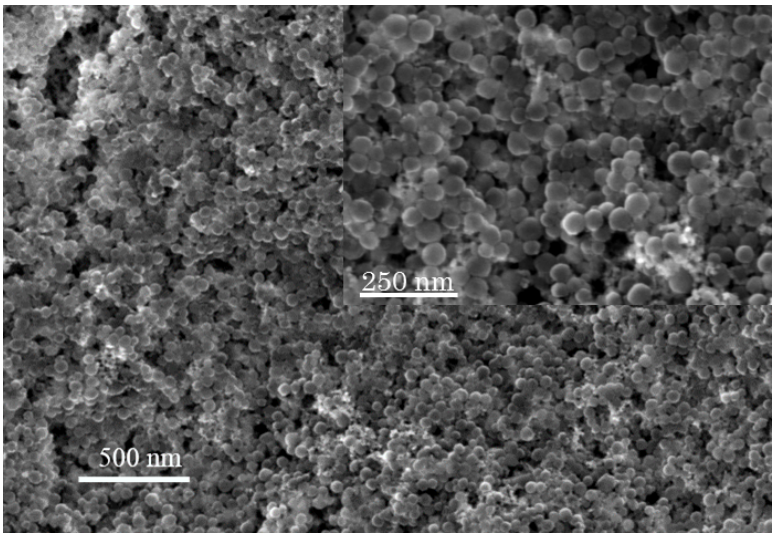

Figure 2.20: SEM image of fluorescent particles prepared at 40 wt.% solids ([monomer] = 4M), at 70 °C.

The particles were found to still fluoresce (using an optical microscope) after the

dispersions had been dialysed, and were therefore considered to be successful. However the amount of fluorescent monomer actually co-polymerised with the MMA, would need to be determined, and the fluorescent intensity quantified to prove the effective co-polymerisation of Fmon with MMA. However, this route was not explored any further as these particles were no longer required.

2.3.2.7 Zeta Potential

The zeta potential of a dispersion is normally used to indicate the stability of the system. It is a measure of the surface charge of a particle dispersion in a given medium. Zeta potential values range from +100 to -100 mV, although typically values for latex particles range from +50 to -50 mV. The magnitude of the zeta potential is used to predict the stability of the colloidal dispersion. A zeta potential of 30 mV or more is the standard potential used to describe a stable dispersion. Note the potential is either positive or negative depending on the stabilisation mechanism and resulting surface potential.

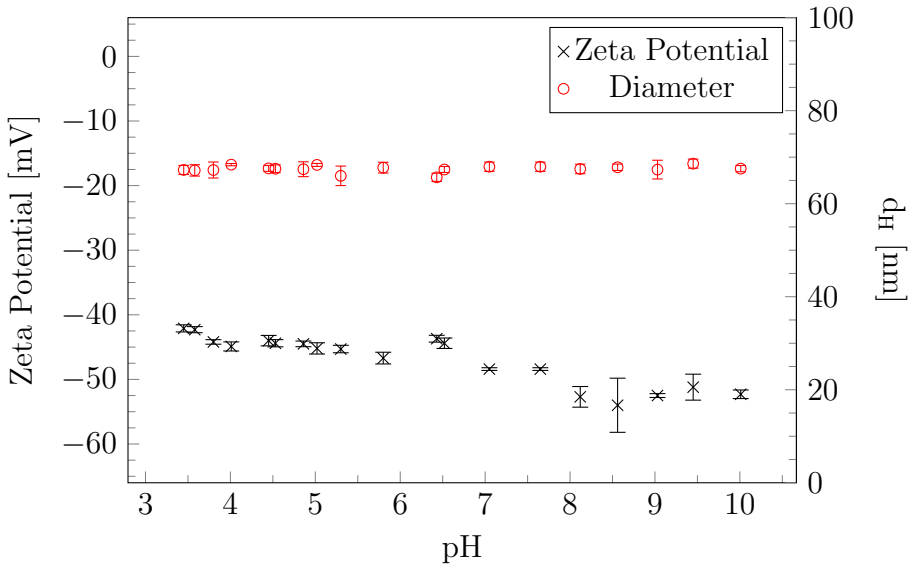

Figure 2.21: Zeta potential and Particle size as a function of pH. The particle dispersion used to determine this data, has a particle size 67 ± 1 nm and a zeta potential of -45 mV following dialysis and prior to any electrolyte addition.

The zeta potential and size of run MMEP101 was measured as a function of pH, Figure 2.21. The pH was modified with addition of either HCl to decrease the pH, or NaOH to increase the pH. NaCl was added at a 10^3 mM concentration, in order to maintain a constant background electrolyte concentration so the data is comparable across the pH range tested.

From the zeta potential plot it is clear, that above pH 3 the particles are very stable. The use of AIBA as the initiator would impart a cationic surface charge, with an approximate isoelectric point pH 7.04.[144] The negative charge is indicative of the presence of surfactant groups on the particle surface, with further confirmation from the lack of particles destabilisation over the pH range tested. The DLS data with the pH response observed from measuring the zeta potential, with no significant change in the particle size observed (normally indicative of some form of destabilisation occurring).

SDS has a polar anionic head group with a non-polar tail, which cause it to bind tightly with cationic molecules. This tightly bound interaction with the particle surface consequently makes it very difficult to remove the surfactant via dialysis. However, any free unbound SDS molecules are removed effectively via dialysis, leaving a particle dispersion in water with SDS molecules only on the particle surfaces.

2.4 Conclusions

Various routes for PNP preparation are initially discussed, and a brief history of the topic explored. As the use of polymers becomes ever more ubiquitous in everyday products, the constraints imposed by their applications and the drive to prepare particle dispersions with finely tuned properties outlined. Particularly, small (sub 100 nm) particles with a monodisperse size distribution at a high solids (polymer) content, using low surfactant concentrations.

To this end, two synthesis routes were investigated: a surfactant free emulsion polymerisation route, which is a highly desirable route as no surfactant is present in this system. However, it was concluded to be very difficult to prepare particle with the targeted properties using this method. Therefore, a chain transfer mediated emulsion polymerisation route was then investigated, using a low surfactant concentration.

The particle preparation method outlined here is one unique from the current literature, and is found to readily produce particles with the targeted properties (Section 2.1.5). In the current literature, chain transfer agents are typically used to prepare finely defined block copolymers, at CTA concentrations where the system is classified as a living polymerisation.[97,98]

Here, the relatively low chain transfer agent concentration used means the system cannot be termed living, as the living character is not observed. It is most likely that the nucleation efficiency is subtly enhanced during the early polymerisation stages. It was found to be very effective over a small concentration range, with higher concentrations shown to negatively affect the final dispersion properties. The method was also shown to be readily adaptable when copolymerising methyl methacrylate with the fluorescent monomer 2-napthyl methacrylate.

At the beginning of this chapter a challenge is posed; 'can polymer particles be prepared at high solids content, while maintaining a narrow size distribution within the sub-100 nm size range, using as little surfactant as possible?' This challenge was suitably met and the method tuned to obtain a range of particle sizes with the targeted properties, at higher solids content and lower surfactant concentrations than those found, to date in the literature.[68]

The stable high content particle dispersions obtained from this method were then used as model Inkjet inks, with easily tunable particle concentrations. The following chapters utilise these dispersions to systematically investigate the overall flow behaviour relative to Inkjet printing.

Chapter 3

Rheology and stability characterisation of particle dispersions

3.1 Introduction

This project is concerned with the use of particle dispersions to understand fluid flow behaviour for Inkjet printing applications, thus understanding the rheology and stability of these dispersions is of utmost importance. This chapter is concerned with the various dispersions used in latter chapters, with a breakdown of the sample preparation, analysis and techniques in the materials and methods section. A range of particle dispersions are used to examine fluid flow behaviour, which can be separated into 2 categories; p(MMA) particles in water at a range of particle concentrations, and p(MMA) particles in a water:ethylene glycol co-solvent at a range of particle concentrations.

This chapter deals with characterising the rheology and stability of the above mentioned colloidal dispersions, and discusses the effects of electrolyte concentration and solvent type.

3.1.1 Stability

Understanding the stability of a given colloid system is of great importance, both for use in academia and industry. A colloidal dispersion, as discussed in chapter 1, is a two phase system with a dispersed phase (the colloid) and a continuous phase (the dispersion medium). For a given colloid system with a constant volume, it follows that as the particle size decreases the surface area increases; in the colloidal size range the colloid surface properties significantly define the system characteristics. The colloid size, shape, chemical and physical properties affect the stability of the overall system.

DLVO theory is the classic theory used to examine and understand colloidal stability, discussed previously in chapter 1. The theory describes the interactions of charged surfaces in a liquid medium by combining the effects arising from Van der Waals attraction and the electrostatic repulsion (see Section 1.5). Within the results, the concepts and implications of the theory are discussed with regards to the observed data.

3.1.2 Rheology

Rheology is defined as the study of the flow and deformation of a material due to an applied force.[145] The interest and knowledge of rheology grew considerably when the numerous uses of polymer dispersions for industrial and everyday applications was realised. It is commonly expressed by the following equation;

$$\sigma = \mu\dot{\gamma} \tag{3.1}$$

Where the shear stress, σ applied is proportional to the shear rate, $\dot{\gamma}$ and the fluid is characterised by the Newtonian viscosity, μ.

The addition of a dispersed phase to the Newtonian fluid to create either an emulsion (liquid), a foam (gas) or a suspension (solid), can lead to a system with a response to shear that can no longer be considered as Newtonian, i.e. where the shear rate and viscosity relationship is no longer linear. The following considers the case where the dispersed phase is a solid, i.e. for suspensions. When investigating

the rheological behaviour of a colloidal dispersion experimentally, the common description of the system refers to apparent viscosity, η at a given shear stress or shear rate.

$$\eta = \sigma/\dot{\gamma} \tag{3.2}$$

From the equation it is apparent that μ is equal to the apparent viscosity, η for a Newtonian fluid, however this is not the case for non-Newtonian fluids where η is a function of the shear rate, $\dot{\gamma}$, i.e. when a single measurement of η does not give a good indication of the rheology of the fluid.

In the following sections, flow models relevant to this project are discussed. A flow model may be used to characterise and describe rheological data, the most simple example given earlier, equation 3.1. The observed rheological data can be described in a concise and convenient manner with a model, for example from the relationship between shear rate and shear stress, Figure 3.1. With characterisation of the effect on the rheological profile of variables, such as composition and temperature, the relationships could be applicable widely and become functional models.

There are numerous models available for characterisation with various component variables considered. They can, broadly speaking, be categorised into 3 groups: empirical, theoretical and structural models. An empirical models is found from considering the experimental data of a given system. A theoretical model provides an insight on the role of the structure, and is thus derived from considering fundamental concepts. An example of such a model is the Krieger-Dougherty model, Equation 3.5.[146] From examination of the fluid structure and usually the kinetics of change, structural models can be derived, including the Cross or the Carreau models, Equation 3.8.[146]

Theoretical models are used to understand the observed rheology, and glean information about the fluid, including, for particle suspensions, the inter-particle interactions and the particle network. The suspensions in these models account for particles in the range of 100-0.001 μm. Such suspensions are governed to a certain degree by Brownian, hydrodynamic and colloidal forces. The thermal random force, Brownian motion, is ever present for these systems. The particle motion relative

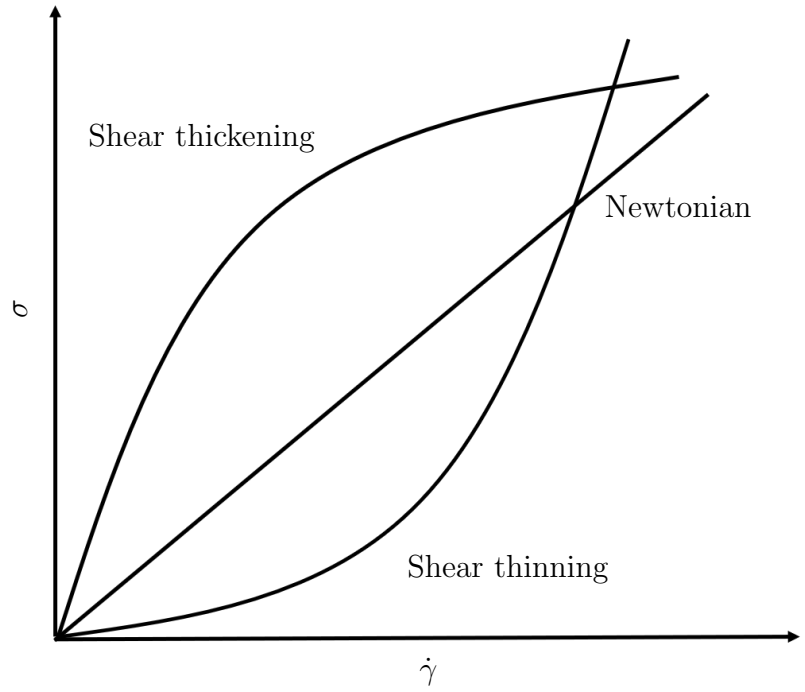

Figure 3.1: Representation of the relationship between shear stress and shear rate for three different fluid types.

to the suspending solvent in flowing suspensions is the hydrodynamic force, also known as the viscous force. Colloidal interaction forces are potential forces, and as mentioned previously include Van der Waals attractive, electrostatic repulsion and steric repulsion forces. The particle size in the suspension, up to a large extent affects the magnitude of these forces, and in turn the bulk rheology. A combination of the three forces determines the flow behaviour of particles in the 1-0.001 μm range, while the flow behaviour for larger particles is predominantly determined by the hydrodynamic forces.[147]

Therefore suspension viscosity is dependant on the solvent and the suspended colloids, and of course the shear rate, $\dot{\gamma}$. Generally the suspension viscosity, η_c is proportional to the solvent viscosity, η_L, and most models quote a relative suspension viscosity, η_r;

$$\eta_r = \eta_c/\eta_L \tag{3.3}$$

3.1.2.1 Hard Sphere Suspensions

The rheology of the simplest system will be considered first, a suspension of hard spheres. Here, hard spheres are defined rigid spherical particles with no attraction or long range repulsion between the particles, other than infinite repulsion upon contact.[147] These systems can be considered as neutral systems, examples include glass beads (non-colloidal particles) or colloidal particles where the inter-particles forces are screened (e.g. crosslinked polymer particles).[148] For these systems hydrodynamic forces and Brownian motion dominate, and colloidal interactions can be considered negligible. Brownian motion is only significant when the particles are smaller than approximately 1 μm. These particles are non-aggregating colloidal particles, normally referred to as Brownian particles /spheres.[147] The particles in suspension cause a hydrodynamic disturbance to the flow causing an increase in the energy dissipated and in the viscosity of the system.

The following equation, derived by Einstein[149] (and later amended[150]), was first used to describe η_r of a dilute hard sphere suspension;

$$\eta_r = 1 + [\eta]\phi \tag{3.4}$$

Where ϕ is the volume fraction of the particles, and $[\eta]$ is the intrinsic viscosity of the particles. Particle shape determines $[\eta]$, and is normally 2.5 for hard sphere where a no slip condition between the particle surface and the solvent is assumed.[147]

For higher concentrations of hard sphere suspensions, numerous models have been derived to explain the dependence η_r with concentration. This is when particle crowding, with an increase in the probability of collisions between particles, causes a hydrodynamic interaction between particles. Equation 3.4 is no longer valid, and the following expression derived for mono-disperse suspensions is instead considered (the well known Krieger and Dougherty model[151]);

$$\eta_r = \left(1 - \frac{\phi}{\phi_m}\right)^{-[\eta]\phi_m} \tag{3.5}$$

Where ϕ_m is the maximum particle packing fraction. When the particle concentration approaches ϕ_m the viscosity of the system increases to infinity, as there is no longer a sufficient amount of fluid available to lubricate the particle motion. A

clear shear yield stress is observed at this concentration.[35] Theoretically ϕ_m for a monodisperse particle system is 0.74 for face centred cubic (FCC) packing, however ϕ_m in practice is close to 0.6 and for random close packing ∼0.64.[152] Beyond this concentration, the suspensions become solid when at rest but a flow can once again be induced by applying a finite stress, leading to significant particle ordering.

However before ϕ_m is reached, the system first goes through a phase transition at the freezing concentration ϕ_f=0.49 where crystals start to appear. Here, crystals refer to the formation of particle clusters /packing with a well-defined and homogenous inter-particle distance. This state exists with increasing particle concentration until the melting concentration is reached ϕ_M=0.545. A full transition into the crystal state (in the case of an FCC order) is observed at this concentration. Further increase in the particle concentration causes the system to reach the glassy state, with a glass concentration, ϕ_G=0.58. This is where long range particle motion is no longer observed. For a system where the particles are separated due to repulsive forces, the system is termed a repulsive glass.

The volume fraction (particle concentration) where the low shear viscosity increases to infinity for these systems is not yet known, although ϕ_m=0.58 is the accepted value at low shear stresses for repulsive glasses.[153]

The product of $[\eta]\phi_m$, from Equation 3.5, for most cases is usually around 2 and the expression can therefore be simplified to;

$$\eta_r = \left(1 - \frac{\phi}{\phi_m}\right)^{-2} \tag{3.6}$$

The $\dot{\gamma}$, particle, particle size distribution and particle deformability affect the hydrodynamic forces in the particle suspensions and therefore also affect the η. For a system where the size distribution cannot be considered to be monodisperse, as in most real systems, the ϕ_m value no longer holds true. The maximum packing fraction for these systems would then be for particles that are not monodisperse hard spheres, which can be termed as the effective maximum packing fraction $\phi_{m,eff}$. In order to calculate the relative viscosity for these systems, the $\phi_{m,eff}$ must be determined for each system, and Equation 3.6 must be rewritten as;

$$\eta_r = \left(1 - \frac{\phi}{\phi_{m,eff}}\right)^{-2} \tag{3.7}$$

At high particle concentrations the viscosity of hard sphere suspensions depends on the applied shear rate, Figue 1.9 At high shear rates the suspensions show an infinite shear viscosity, η_∞ where a limiting and constant value for viscosity is observed. At intermediate shear rates shear thinning behaviour is observed, where the viscosity decreases with shear rate. At low shear rates a constant zero shear viscosity is observed, η_0 i.e. Newtonian behaviour. The shear thinning behaviour observed is either due to the continuous phase, where the fluid is shear thinning or it is due to the alignment of particles to the flow direction. The well known Carreau equation models this behaviour quite well[154];

$$\eta_r = \eta_\infty + \frac{\eta_0 - \eta_\infty}{(1 + (\lambda_c \dot{\gamma})^2)^{\frac{N-1}{2}}} \tag{3.8}$$

Where λ_c is a time constant related to the suspended colloid relaxation time, and N is a dimensionless exponent, the so called flow index. The relative viscosity is usually observed to decrease with increasing shear rates for these systems. For monodisperse particles, this effect in equation 3.6, is expressed as an *approximate* increase in ϕ_m, from 0.63 at the zero shear limit to 0.73 at the infinite shear limit. The viscosity of such systems may be termed apparent η_r, as it is dependant on the $\dot{\gamma}$.

Shear thickening behaviour has also been reported for these systems at high shear rates, when the particle concentration is relatively high, $\phi > 0.4$.[153] This behaviour is observed when the shear rate is increased so much so that the viscosity levels off, after which if the shear rate is increased further and the critical shear rate overcome the viscosity then begins to increase. This can occur either gradually or abruptly depending on the system investigated. The high shear leads to changes in the suspension microstructure which causes the shear thickening behaviour. The high shear rate disrupts the particle ordering which then forms particle clumps that display this behaviour; these become more pronounced with increasing particle concentration.

The particle volume fraction, shape, size, size distribution, and particle-particle interactions have all been shown to affect the shear thickening behaviour of these non-aggregating solid particles.[155] Increasing particle concentration was shown to decrease the critical shear rate of the particle suspensions, with a rapid increase in the critical shear rate once the particle concentration is much below ϕ= 0.5.

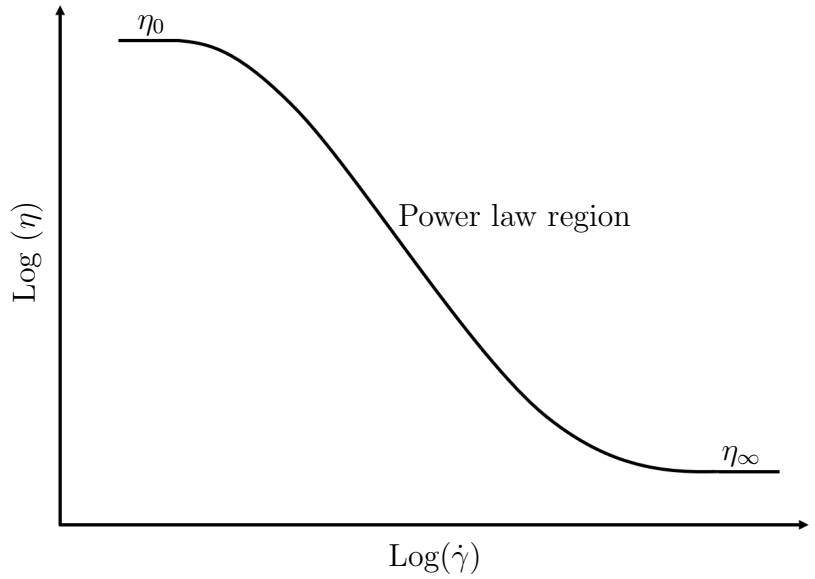

Figure 3.2: A graphical representation of a shear thinning suspension showing the three observed regions. The zero shear viscosity, η_0 at low shear, the infinite shear viscosity, η_∞ at high shear and the power law region at intermediate shears.

For this reason, it is much more difficult to attain this critical shear rate when the particle concentration is below $\phi = 0.5$ experimentally. Increasing the particle size causes the critical shear rate to decrease, however it increases with increasing polydispersity. This is observed because the maximum packing fraction increases for a more polydisperse system since smaller particles can occupy the spaces between the larger particles, allowing much higher solids to be achieved.[156] Smaller particles in a polydisperse system would reduce the overall viscosity as they would act as lubricants for larger particles. At dilute particle concentrations this has small effect on the viscosity, but at high concentrations this effect is significantly increased. The maximum packing fraction does also depend on the number of discrete size bands, and the ratio of the large particle diameter to the next sized smaller particle diameter.

3.1.2.2 Colloidal Suspensions

These are suspensions where the colloidal particles do not aggregate at a significant rate, despite density differences between disperse and continuous phases. In these

systems particles are kept apart from each other due to the dominating repulsive forces, and lead to an ordered crystalline liquid like structure or, at high enough particle concentrations, even quasi-crystal like structures. Extra energy is required for flow to occur in these suspensions, as the particles must be forced to move against other particles.[157] The net particle interaction potential, U_H (see Figure 1.8) may be theoretically predicted using the DLVO theory, as mentioned in chapter one. The structure and viscosity magnitude of colloidal dispersions is to a large extent controlled by particle-particle interactions, when under the action of an external force such as shear. For suspensions at extremely high shear, the viscosity response is a function of the hydrodynamic forces only. Compared to hard sphere suspensions, the presence of colloidal interaction forces will act to increase the suspension viscosity and in some cases will even lead to a yield stress, regardless of whether this is attractive or repulsive. The extent of this phenomena is determined by the particle concentration, overall interaction magnitude and the resulting micro-structure.

There are two methods commonly used to predict the viscosity of stable colloidal dispersions.[147] One of the methods involves separating the contribution of individual factors from each other (separation of contribution method), while the other takes the contribution of all the individual factors as one factor (effective volume fraction method).

Separation of Contribution Method

In the separation of contribution method, the relative viscosity of a particle suspension is taken as the sum of the contributions from both the colloidal force, η_r^{cf} and the hard sphere, η_r^{hs};

$$\eta_r = \eta_r^{hs} + \eta_r^{cf} \tag{3.9}$$

Equation 3.6 can be used to calculate η_r^{hs} as this is the relative viscosity of the equivalent hard sphere suspension. η_r^{cf} must be calculated experimentally, i.e. from the difference between the experimentally determined η_r and the theoretical η_r^{hs}. It is the relative viscosity increase due to interparticle interactions. Applying a shear to an electrostatically stabilised suspension distorts the EDL. This causes an increase in the viscosity due to the increased energy dissipation, called the primary electroviscous effect, *p.*[158]

For a dilute suspension p is used as a correction to Equation 3.4 and can be combined with Equation 3.9 to give;

$$\eta_r^{cf} = 2.5.p.\phi \tag{3.10}$$

p is a function of the ζ potential (the slip plane potential, see Figure 1.7), and the particle radius, r. A general expression for p, derived from the theoretical model proposed for concentrated dispersions and from investigating dilute suspensions, is proposed in terms of the activation energy or the energy barrier (primary maximum in Figure 1.8), U_{Max} (i.e. the maximum repulsive force between two particles)[159];

$$p = b\frac{U_{Max}}{k_B T} \tag{3.11}$$

b is defined as a dimensionless proportionality constant. U_{Max} is determined from the maximum of the $U(H)$ curve, Figure 1.8. For long term stability U_{Max} normally requires a value of 15-25 $k_B T$, at least.

The following expression has been derived to calculate η_r^{cf} for concentrated dispersions[160];

$$\eta_r^{cf} = c_1\phi.exp\frac{U_{Max}}{k_B T} - \frac{c_2 d^3 \sigma_p}{\phi k_B T} \tag{3.12}$$

Where d is the particle diameter, c_1 and c_2 are numerical constants (c_1 is assumed to be 1 for practical purposes), and σ_p is the particle stress. The apparent activation potential barrier is given by the exponent term, i.e. the activation energy of two neighbouring particles under shear. The mean activation energy when the particles are at rest is given by the first term of the exponent. The bias potential arising from the dispersion when under shear is given by the second term, and is the result of activation volume by particle stress. The inter-particle potential gives rise to the particle stress (elastic stress) and can be calculated using the following expression;

$$\sigma_p = \eta^{cf}\dot{\gamma} = \eta_r^{cf}\eta_L\dot{\gamma} \tag{3.13}$$

The activation volume is inversely proportional to the number of particles per unit volume, i.e. d^3/ϕ. Combining Equation 3.13 with Equation 3.12 then gives to the following expression, which must be solved numerically;

$$\eta_r^{cf} = c_1\phi.exp\left(\frac{U_{Max}}{k_BT} - \frac{c_2d^3\eta_L}{\phi k_BT}\eta_r^{cf}\dot{\gamma}\right) \tag{3.14}$$

According to Equation 3.12 a plot of $k_BTln(\eta^{cf}\phi)$ vs. σ_p, where U_{Max} is the y intercept and $-c_2d^3$ the slope, will show a linear decrease for each volume fraction (where c_1=1).[160] From this plot, the U_{Max} and c_2 can then be plugged into the above equation (3.14), and the equation solved for various $\dot{\gamma}$ values at each ϕ.[147] Then the contribution of inter-particle forces to the η_r can be determined from the plot of η_r^{cf} vs $\dot{\gamma}$.[147]

The validity has been shown experimentally for styrene-butadiene particles (approximately 100 nm in diameter) in water.[160] The volume fractions used to show this were 0.176, 0.234, 0.293 and 0.345 which then corresponded to U_{Max} values of 1.80, 3.06, 4.94, and 6.6 k_BT. This data, when used to solve Equation 3.14 at various $\dot{\gamma}$, shows that η_r^{cf} increases with ϕ and decreases with $\dot{\gamma}$.[147] However this shear thinning effect is only observed when $\phi > 0.25$ (approximately) and when hydrodynamic forces are more significant than the inter-particle forces at high $\dot{\gamma}$. This shear thinning behaviour is due to the ordering of particles upon flow.

If the $\dot{\gamma}$ is further increased a second plateau is observed, where the viscosity seemingly remains relatively constant, Figure 3.2. For sufficiently high volume fraction dispersions, at even higher $\dot{\gamma}$, the viscosity begins to increases rapidly when a critical $\dot{\gamma}$ is exceeded.[147] This shear thickening is similarly also observed for hard sphere suspensions, though for colloidal suspensions a different mechanism is proposed to be responsible for this behaviour.

This shear thickening behaviour here is due to shear induced disorder, for steric or electrostatically stabilised dispersions.[35,161] As the $\dot{\gamma}$ is increased the particles begin forming secondary ordered layers, which is observed as shear thinning behaviour. Once formed the viscosity no longer decreases, which is observed as the second Newtonian plateau. These ordered layers begin interacting if the $\dot{\gamma}$ is increased to the critical $\dot{\gamma}$. These interactions cause particles to be removed from the ordered layers, via hydrodynamic coupling which then leads to disorder, with increasing particle collisions, giving rise to shear thickening.

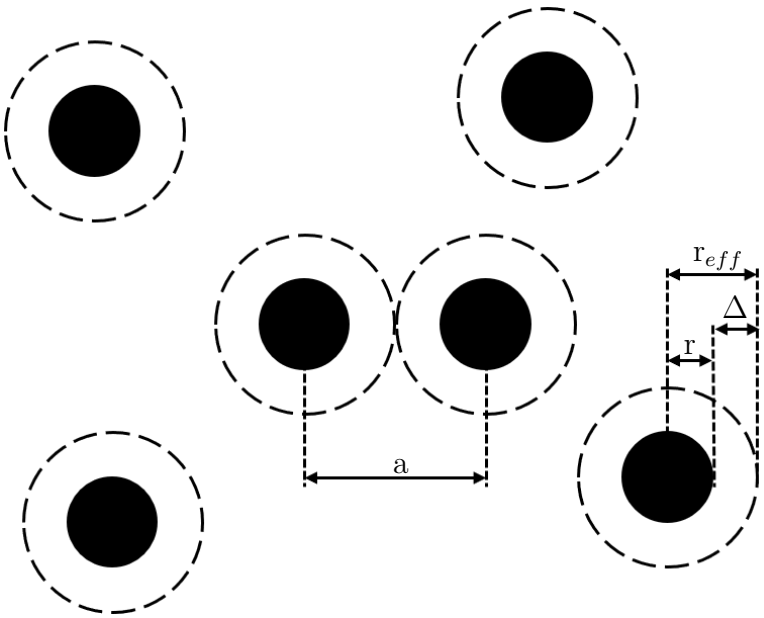

Figure 3.3: Schematic representation of a charge stabilised particle dispersion, where the dashed line represents the EDL. Note $\Delta = \kappa^{-1}$, but for the purposes of a model is termed Δ here.

Effective Volume Fraction method

The effective volume fraction method takes the contribution of all the individual factors as one factor, either the effective maximum packing fraction, $\phi_{m,eff}$ or the effective volume fraction, ϕ_{eff}. This method assumes that there is a certain distance, a that cannot be broached when particles approach each other, due to repulsive forces. This acts to increase the relative particle radius from r to r_{eff}, where $r_{eff} = a/2$ (see Figure 3.3).[153] Therefore these systems, where the particles interact with just a repulsive interaction, behave as equivalent hard spheres. Where the equivalent hard sphere radius, r_{hs} is equal to the effective particle radius, $r_{hs} = r_{eff}$, and the effective volume fraction of particles is calculated as;

$$\phi_{eff} = \phi \left(\frac{r_{eff}}{r} \right)^3 \tag{3.15}$$

As $r_{eff} > r$, the volume occupied by the particles is actually less than the volume occupied by the equivalent hard spheres, which means $\phi_{eff} > \phi$. Particles are considered as a core and surrounded by stabilising (exclusion) layers. Therefore

the particle radius, r is actually the particle core radius and the volume fraction, ϕ is actually the particle core volume fraction. Replacing ϕ by ϕ_{eff} in Equation 3.2, would then enable calculation of the viscosity for the colloidal dispersion equivalent hard sphere dispersion;

$$\eta_r = \left(1 - \frac{\phi_{eff}}{\phi_m}\right)^{-2} \tag{3.16}$$

Then combining Equation 3.16 with Equation 3.15 gives;

$$\eta_r = \left(1 - \frac{\phi}{\phi_m}\left(\frac{r_{eff}}{r}\right)^3\right)^{-2} \tag{3.17}$$

This expression when used to predict η_r, would show increasing viscosity, for a given particle volume fraction with the effective particle radius.

For a system where the particle core radius is much bigger than the extra volume around the particle that cannot be broached, i.e. $\Delta \ll a$ (see Figure 3.3 for definition), the following simple expressions can be used to calculate the effective particle radius and volume fraction;

$$a_{eff} = a\left(1 + \frac{\Delta}{a}\right) \tag{3.18}$$

$$\phi_{eff} = \phi\left(1 + \frac{\Delta}{a}\right)^3 \tag{3.19}$$

These expressions work well for electrostatically stabilised particles at high ionic strength and for sterically stabilised particles with short adsorbed or grafted chains in a good solvent.[148] These systems would display a steeply decaying interaction energy profile (Figure 1.8), where Δ is approximately equal to the EDL thickness, κ^{-1} for charge stabilised suspensions, or the polymer layer thickness for steric stabilised suspensions.[162]

For charge stabilised systems with a low ionic strength and sterically stabilised systems with long adsorbed or grafted chains, where $\Delta \gg a$, the interaction profile (Figure 1.8) would decrease slowly and it is difficult to determine the equivalent hard sphere radius. Therefore Equations 3.18 and 3.19 are no longer valid, and the observed data would deviate from Equations 3.16 and 3.17. This is due to the

deformation or overlap of the exclusion layers.[153] Conventionally, these particles are referred to as soft spheres, as they interact through soft potentials (EDL).

For these cases, Equation 3.7 must be used to determine $\phi_{m,eff}$. This can be obtained empirically from the plot of $\eta_r^{-1/2}$ vs. ϕ. As mentioned earlier, $\phi_{m,eff}$ varies with the particle size, size distribution and particle deformability. For these systems it is also affected by colloidal interactions and Brownian motion.[162] These systems also transition into an ordered/glassy state when $\phi_{eff} = \phi_G = 0.58$.[147] And this critical glass transition concentration is equivalent to the effective maximum packing fraction, i.e. $\phi_{G,eff} = \phi_{m,eff}$, where $\phi_{m,eff}$ is given by;

$$\phi_{m,eff} = \phi_m \left(\frac{r}{r_{eff}} \right)^3 \tag{3.20}$$

The flow behaviour of the suspension is strongly affected by particle crowding, as ϕ approaches $\phi_{m,eff}$); with an apparent stress observed when $\phi = \phi_{m,eff}$. Because $r_{eff} > r$, before the actual particle suspension concentration, $\phi = 0.58$, the equivalent hard spheres reach the glass transition, $\phi_{G,eff}$; which then implies $\phi_{m,eff} < \phi_m$. Combining Equations 3.15 and 3.20 gives the scaling relationship;

$$\frac{\phi_{eff}}{\phi} = \frac{\phi_m}{\phi_{m,eff}} \tag{3.21}$$

At this stage it might be worth redefining some of the symbols used for clarity. The volume fraction of a particle suspension is ϕ, ϕ_{eff} is the effective volume fraction of particles, the maximum effective volume fraction of particles is $\phi_{m,eff}$, and the maximum packing volume fraction for close packed monodisperse hard spheres is ϕ_m. So from Equation 3.21, when $\phi = \phi_{m,eff}$, then $\phi_{eff} = \phi_m$. From this, by combining Equation 3.21 into Equation 3.16, or Equation 3.20 into Equation 3.17 would then give Equation 3.7. This is the simplified Krieger-Dougherty equation, accounting for $\phi_{m,eff}$, defined earlier. This model is typically used to characterise both charge, and sterically stabilised particles.

The above described models are used later, to fit and analyse the viscosity profiles obtained from the particle dispersions discussed in the previous chapter.

3.2 Methods and Materials

The following section outlines the materials and methods used for the rheology and stability characterisation of p(MMA) nanoparticle dispersions, and p(MMA) nanoparticle dispersion with added non adsorbing free polymer, poly(styrene sulfonic acid) sodium salt (PSS).

3.2.1 Materials

Table 3.1: Materials used for particle dispersion preparation

Material	**Supplier**	**Purity /%**
Sodium chloride	Sigma-Aldrich	99.99
Ethylene glycol	Sigma-Aldrich	99.8

3.2.2 Methods

3.2.2.1 P(MMA) particles

The p(MMA) nanoparticles used throughout this chapter were prepared using the CTA mediated method discussed in the previous chapter. The particles were prepared as normal, and dialysed prior to use. Once dialysis was complete, i.e. the surface tension of the particle dispersions is close to 72.8 mN/m (at 20 °C), the dispersions are prepared and used immediately. For dispersions where the electrolyte concentration was varied, a solution of sodium chloride (prepared in MilliQ water at various concentration) was used to carefully adjust the concentration; i.e. for a dispersions, the stock p(MMA) particle concentration is first calculated, then added to a sample vial followed by remaining solvent (water), and NaCl to make up the desired concentration. All dispersions containing p(MMA) particle in this chapter, are from the same batch where d_H is 62 ± 1 nm, as determined by DLS at 21 °C and a 10 mM background [electrolyte], with a monodisperse size distribution, and a zeta potential of -49 ± 2 mV, at pH ∼7.

3.2.2.2 P(MMA) particles dispersed in 20:80 Ethylene glycol:water mixtures

Particle dispersions of p(MMA) in an ethylene glycol:water mixture at 20:80, were prepared by adding appropriate ethylene glycol (EG) and water to the freshly dialysed particle dispersions until the required concentration was attained. For example, to prepare a 10 mL dispersion at 2 vol.% from a 20 vol.% stock, 1 mL of the stock dispersion is added to 7 mL of Milli-Q water and 2 mL ethylene glycol.

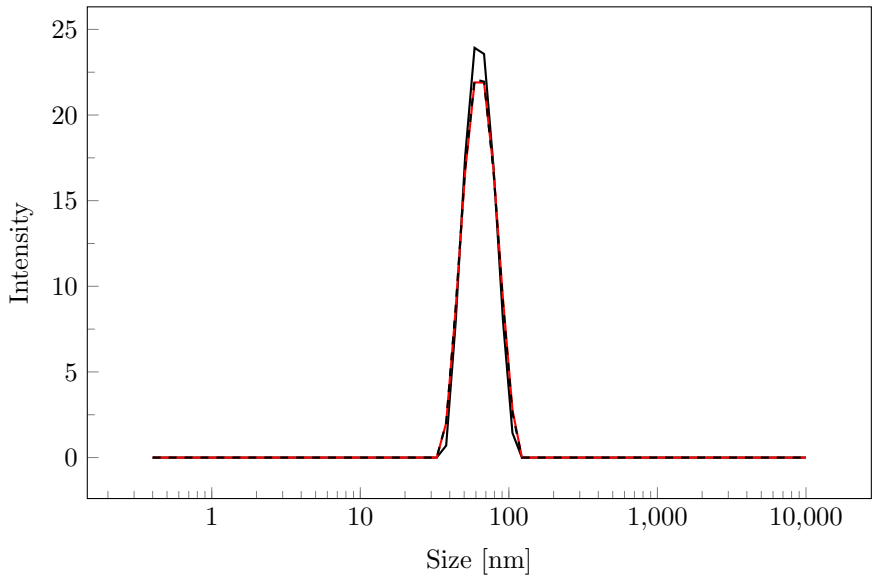

Figure 3.4: The particle size as measured via DLS, where each peak is an average of 10 individual runs. The average d_H from 3 measurements is 62, with PDI 0.04, with a 10 mM background electrolyte concentration at 21 °C

Surface tension

The particle dispersions in the water:ethylene glycol co-solvent were first prepared, mixed and allowed to stand for at least 24 hrs in order to reach equilibration conditions, before determining the surface tension. The surface tension of ethylene glycol:water mixtures is well known, Figure 3.5; there is even an equation to derive the surface tension for any given solvent composition.[163] The surface tension was determined for the particles used here, EG:water ratio is 20:80, and and was found to be 62.5 mN/m, which is close to the value predicted by calculations 64.3 mN/m. The discrepancy between the predicted and measured value is probably due to a

small residue of surfactant within the stock particle dispersion, complete surfactant removal via dialysis is very difficult.

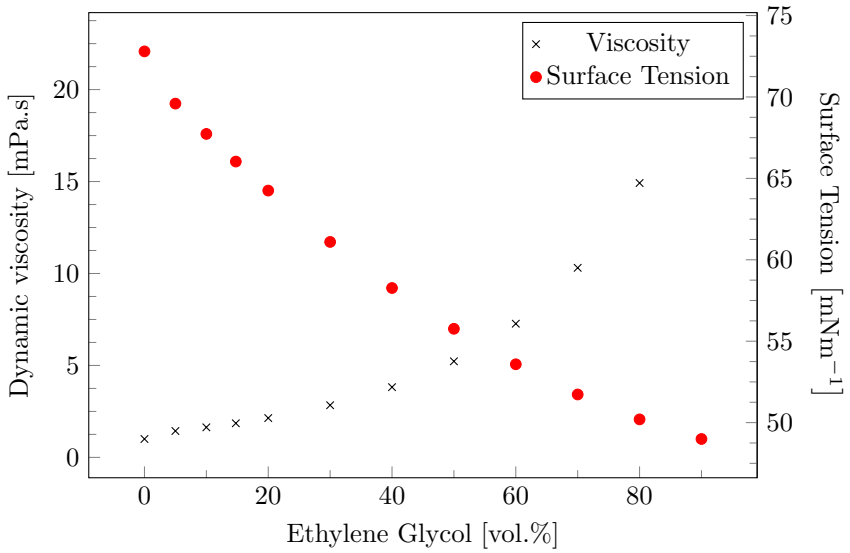

Figure 3.5: The change in viscosity and surface tension with increasing ethylene glycol volume w.r.t. water.[163]

3.2.3 Particle dispersion characterisation

The viscosity and stability of the prepared dispersions were analysed using an ARES-G2 rheometer, a RheoSense VROC rheometer, a LUMiSizer 611 (L.U.M. GmbH), and an Olympus BX51 Optical microscope. The techniques are individually examined below;

3.2.3.1 Rheology

The rheology measurements were carried using an ARES-G2 rheometer (TA Instruments) with a cone and plate geometry (1°, 50 mm diameter), at room temperature, 21 °C ± 0.05 °C. For an accurate measurement, a controlled variable is applied to a given substance and the response is measured. The ARES-G2 separates these two variables, i.e. for a cone and plate geometry, the strain is applied from the plate and the torque response is measured by the transducer connected to the cone. In other

words, the applied strain and the measured stress response are separated, leading to an improved accuracy in the collected data with few instrument artifacts.

For each sample measured, prior to the shear viscosity measurement, an initial measurement of viscosity with time was made at a fixed shear rate to determine if the dispersion has any thixotropic or rheopectic character.[145,146] Thixotropic materials are observed to have a decreasing viscosity with time, whereas rheopectic materials have an increasing viscosity with time. The dispersions used in this study were found to have a constant viscosity with time ($\dot{\gamma} = 5$ s^{-1}), and were concluded to be time independent fluids.

The particle dispersion prepared in this study were all found to exhibit very similar shear viscosity behaviour, postulated to be due to the relatively small size range ($\sim$ 50 - 65 nm). Therefore, data for the same batch of particles is discussed in this study, where d_H is 62 $\pm$ 1 nm.

A viscometer rheometer on a chip (VROC) rheometer was used for viscosity measurements at extremely high shear rates ($> 10^5$ s^{-1}).[164] The technique is based on a microfluidic device which precisely controls the flow behaviour, meaning only a small volume of sample is required for each measurement; approx. 1 mL to analyse a full $\dot{\gamma}$ range, but only a few μL to determine viscosity at a given $\dot{\gamma}$. In principle the viscosity is determined from the pressure drop, as the fluid is passed through a microfluidic device, at a given velocity.

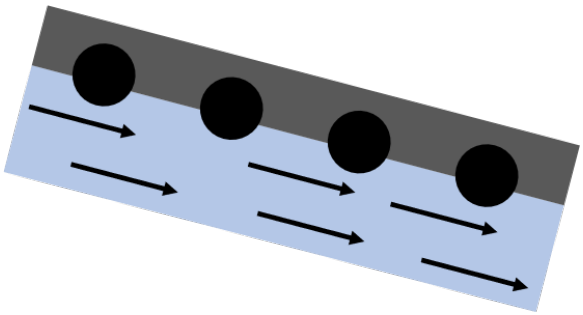

Figure 3.6: A schematic diagram of the VROC microfluidic device. The circles represent pressure sensors, the blue and grey rectangles represent the fluid and the wall respectively, and the arrows signify flow from within the channel.

The device itself consists of a rectangular flow channel, with pressure sensors aligned at known distances, Figure 3.6. The device is designed to mitigate any

perturbations while the fluid flows through the device. A measurement is only taken when a fully developed flow is observed, which is determined from the pressure readings; where the pressure as a function of the sensor position relationship (slope) should be linear when plotted.[164] η, σ and $\dot{\gamma}$ are calculated using the following expressions;

$$\dot{\gamma}_{app} = \frac{6Q}{wh^2} \tag{3.22}$$

$$\sigma = -slope\frac{wh}{(2w + 2h)} \tag{3.23}$$

$$\eta = \frac{\sigma}{(\dot{\gamma}_{app})} \tag{3.24}$$

Where Q is the flow rate and h & w represent the channel hight and width, respectively. The above expressions are fine for Newtonian fluids, however for non-Newtonian fluids the true $\dot{\gamma}$ must be determined using the following expression: applies the Weissenberg-Rabinowitsch correction, for flow in this device;

$$\dot{\gamma} = \frac{\dot{\gamma}_{app}}{3}\left(2 + \frac{dln\dot{\gamma}_{app}}{dln\sigma}\right) \tag{3.25}$$

Although this instrument does achieve extremely high shear rates (i.e. those unattainable on a standard bench-top rheometer), it does also have some inherent limitations. The maximum shear rates and therefore viscosity readings attainable are limited by the zero shear viscosity of the test fluid. In that, for a low viscosity fluid high shear rates can be attained, however for a highly viscous fluid the maximum attainable are lower than the previous case. This is due to the a limitation with the pressure that can be contained within such a device. For a highly viscous fluid this maximum pressure threshold will be broached at lower flow rates relative to low viscosity fluids.

Oscillatory Rheology

The oscillatory rheology of the particle dispersions was also determined using the ARES-G2, with a cone and plate geometry (1°, 50 mm diameter). All the measurements were carried out at room temperature (21 °C ± 0.05 °C). A viscoelastic measurement is made by applying a sinusoidal deformation to a sample and measuring the response.[145,146] The phase angle δ or phase shift is determined, and the complex (G^*), viscous (G'') and elastic G' modulus calculated. The viscoelastic

properties were determined by measuring G' and G'' as a function of the angular frequency ω.

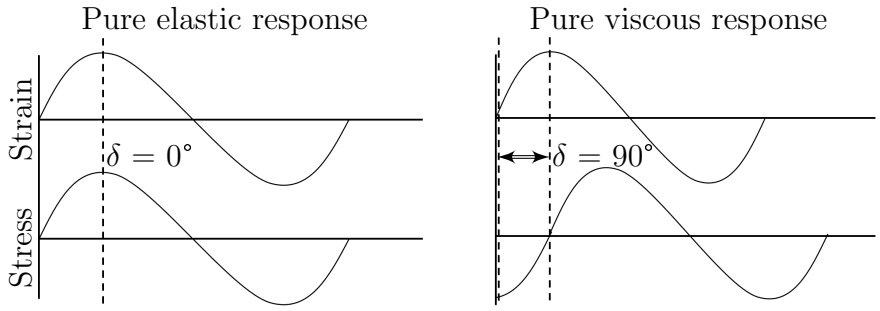

Figure 3.7: Schematic *representation* of the oscillatory response for a Hookean solid (pure elastic response), and a Newtonian liquid (pure viscous response), where δ represents phase angle.

Figure 3.7 is a representation of two extremes, for either a pure elastic response or a pure viscous response. A viscoelastic material has a phase angle shift in between these two cases (i.e. $0 < \delta < 90$), i.e. it possess both viscous and elastic character. The stress is referred to as the complex stress, σ^*. G^* is a measure of the material resistance to deformation and is calculated from the ratio of the complex stress response and applied strain. G' is the ability of the material to store energy, i.e. measure of the elasticity, and is also known as the storage modulus. G'' is the measure of the material ability to dissipate energy, and is also known as the loss modulus and characterises the viscous response.

$$G^* = G' + G'' \tag{3.26}$$

The following expressions are used to determine the two values;

$$G' = \frac{\sigma^*}{strain} cos\delta \tag{3.27}$$

$$G'' = \frac{\sigma^*}{strain} sin\delta \tag{3.28}$$

For oscillatory measurements the frequency response must be measured at an amplitude within the linear viscoelastic region. This region is found by first measuring the G^*, G' and G'' response as a function of the strain amplitude. Once the region is determined, the measurements are made as a function of the frequency at an amplitude within the linear region.

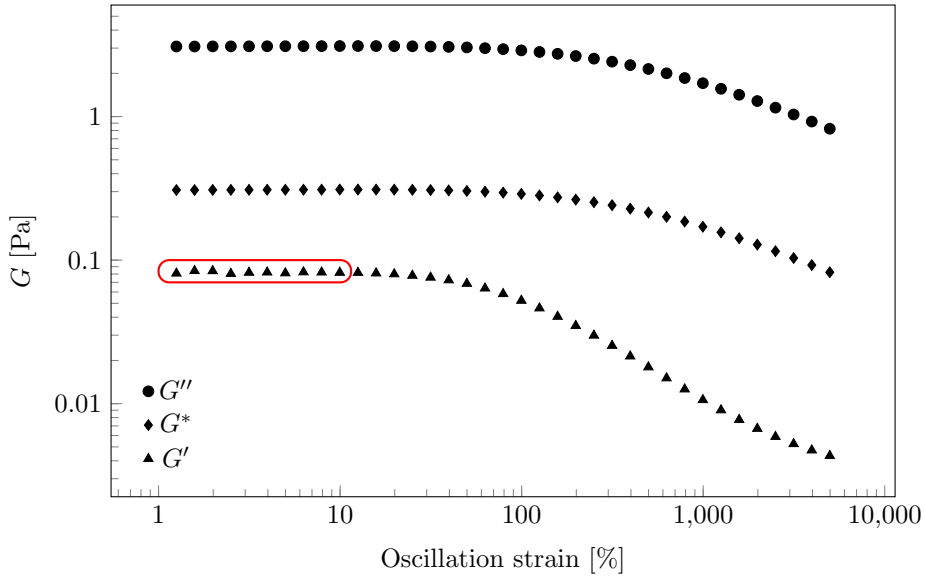

Figure 3.8: An example of the amplitude sweep made to determine the linear viscoelastic region (red box) for p(MMA) particles in water, at 18 vol.%.

3.2.3.2 Sedimentation - Lumisizer

The stability of dispersions used in this study was analysed using the centrifugal technique, LUMiSizer (L.U.M. GmbH). The stability is analysed by applying a centrifugal force to the sample in order to facilitate and accelerate destabilisation phenomena, including sedimentation and creaming. The instrument measures the transmitted light intensity to determine sample position, as a function of time. Each measurement therefore is a intensity transmission profile of the sample cell at a given time interval.

For each measurement, the sample cuvette is filled ($\sim$ 400 μL) and a centrifugal force is applied, 4000 rpm at 21 °C. A measurement is collected at 10 s intervals, and allowed to run until 900 profiles are collected. This is the protocol run for each of the particle dispersions used in this study.

For particles dispersed in pure water and EG:Water 20:80 co-solvent, no aggregation is observed, Figure 3.9.

The sedimentation height for this data is calculated from the change in sample position (intensity determined), over the maximum sample position change: the sedimentation height is typically measured over 20 mm sample height range, the

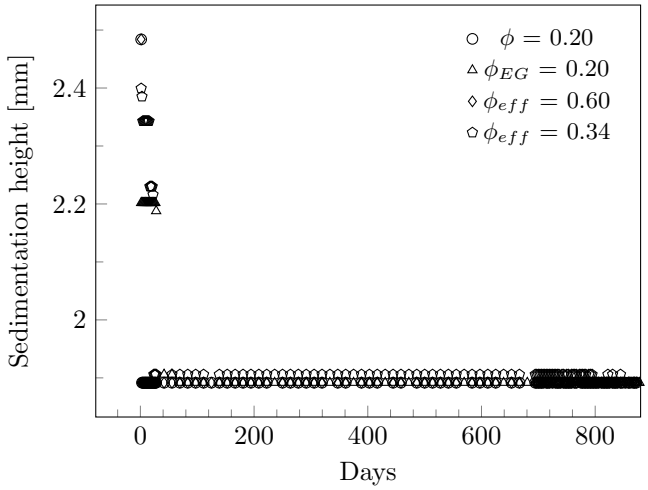

Figure 3.9: Sedimentation of the various particle dispersions tested in both pure water, and ethylene glycol:water co-solvent (20:80). The measurement is run at 4000 rpm for 2 hr at 21 °C

Y-axis range here is small to show no significant aggregation is observed. However, in the plot the sample position does not vary significantly. The stability index is a better tool to indicate the given dispersion stability.

The index is calculated as the % change in intensity across the measurement run, and which is then classified into a stability index for a given sample.[165] The instability index is a dimensionless number between 0-1, where 0 indicates complete stability and 1 indicates complete instability; although each dispersion is very stable overall, the y-axis range displayed here is small to better display the trends observed. From this plot it can be observed that the index value of all the tested samples is below 0.1, indicating good colloidal stability, with no observed aggregation over the equivalent time frame (> 800 days). This is a convenient method to show the overall stability of a given dispersion over the protocol length.

The stability was similarly determined for the particles dispersed in a pure water solvent, at $\phi = 0.2$, where the effect of added electrolyte was studied (and are later discussed in full), Figure 3.11.

No destabilising phenomena are observed for these dispersions, and the stability index similarly indicates good stability over the runtime of the measurement. However, in this series for ϕ_{eff} 0.50 & 0.60 small crystals were discovered in the

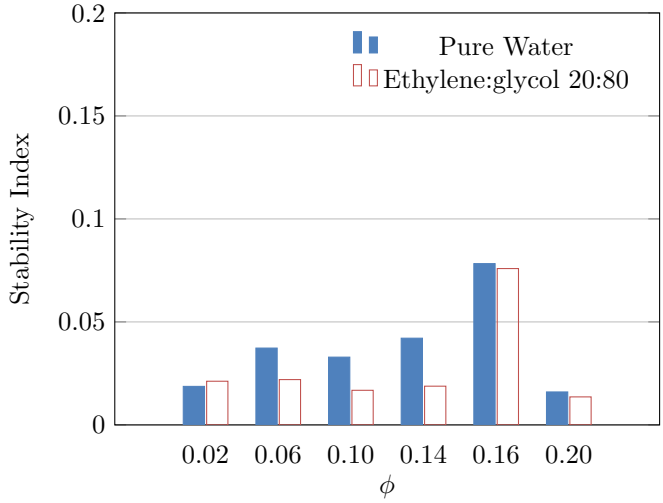

Figure 3.10: Stability index of the various particle dispersions tested in both a pure water, and ethylene glycol:water co-solvent (20:80). The measurement is run at 4000 rpm for 2 hr at 21 °C

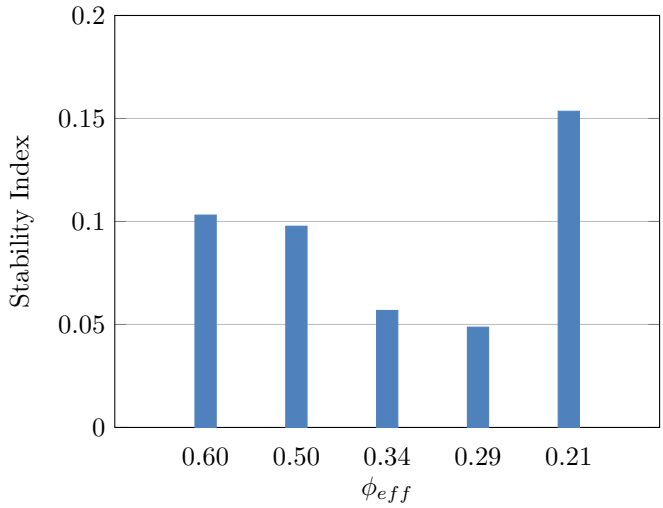

Figure 3.11: Stability index of the various particle dispersions tested in both pure water, and ethylene glycol:water co-solvent (20:80). The measurement is run at 4000 rpm for 2 hr at 21 °C.

dispersions. These are elaborated upon in the upcoming 'Impurities at high particle concentration' section. It is postulated, the size of these crystals, and the fact the dispersion is milky white means these cannot be observed within the LUMiSizer

instrument. The existence of these crystals is due to the high particle concentration within the dispersions, though most of the dispersion is still stable. This means that while no aggregation is observed there are still impurities formed within. Although these were found to be only observable using light microscopy.

The crystals are observed using a Olympus BX51 optical microscope, which has a Colourview 2 digital camera attached. The images were captured and the dimension calibrated with a stage graticule slide.

A further point to add, after the discovery of the existence of the crystal structures each particle dispersion upon preparation was observed for the presence of the crystal structure under the microscope. Only when the crystal structures are not observed for, at least a 2 month period is the dispersion declared crystal free. In the following study, crystals only exist in the ϕ_{eff} 0.50 & 0.60 dispersion, which again is discussed later in the results section.

Note, ϕ_{eff} 0.21 is classified as more unstable relative to the other dispersions in the series. This is most likely due to the increased electrolyte concentration used when the dispersion is prepared, which reduces the electrostatic repulsion potential in the system. Although it is only slightly less stable over the lifetime analysed.

3.3 Results and Discussion

The shear and oscillatory rheology was determined for the various particle dispersions used in this project, from low to extremely high shear rates in order to understand the behaviour of dispersions in an Inkjet printing system.

3.3.1 Particle Concentration

The initial dispersions tested were p(MMA) particles dispersed in a pure water solvent, i.e. as they are prepared and cleaned. The particles are dialysed in MilliQ water, with the resulting dispersions found to be extremely viscous and gel-like, and would in the first instance appear to be undergoing some destabilisation phenomena. However, this was not the case and this extremely viscous nature was found to be due to the effective volume fraction, ϕ_{eff} of the dispersions. This is further elaborated upon in the following 'Effective Particle concentration' section.

Of course, it is well known that the viscosity of a given dispersion increases with increasing particle concentration.[33,145,147] However, determining the root cause of the increase in viscosity, as well as the non-Newtonian effect is due to a number of factors including the ϕ, particle size, size distribution, inter-particle interactions and Brownian motion, as well as convective flow. Here, the particles are electrostatically stabilised, where the inter-particle interaction is repulsive at all but short distances and thus aggregation is not expected, where the size is 62 nm with monodisperse size distribution. The prepared p(MMA) dispersions were examined to determine the exhibited shear viscosity as a function of the particle concentration, Figure 3.12.

Figure 3.12 displays the shear viscosity data obtained for the particle concentrations (ϕ) examined (this series is termed ϕ^a here to aid differentiation later). The first thing to note from this plot is the range $\dot{\gamma}$ over which the viscosity data spans. The overall data for each curve is obtained from two independent instruments, the bench-top ARES-G2 rheometer (filled symbols) and the microfluidic VROC rheometer (open symbols). The data from both instruments are found to marry up nicely, further confirming the validity of the two datasets. Application of the VROC enables viscosity measurements to be carried out at extremely high shear rates. Although, it should be pointed out that maximum shear rates for each sample are not the same.

This is due to the sensitivity of the instrument, where the maximum shear rate attainable for a given fluid decreases with sample viscosity, see previous Rheology section (within the methods section).

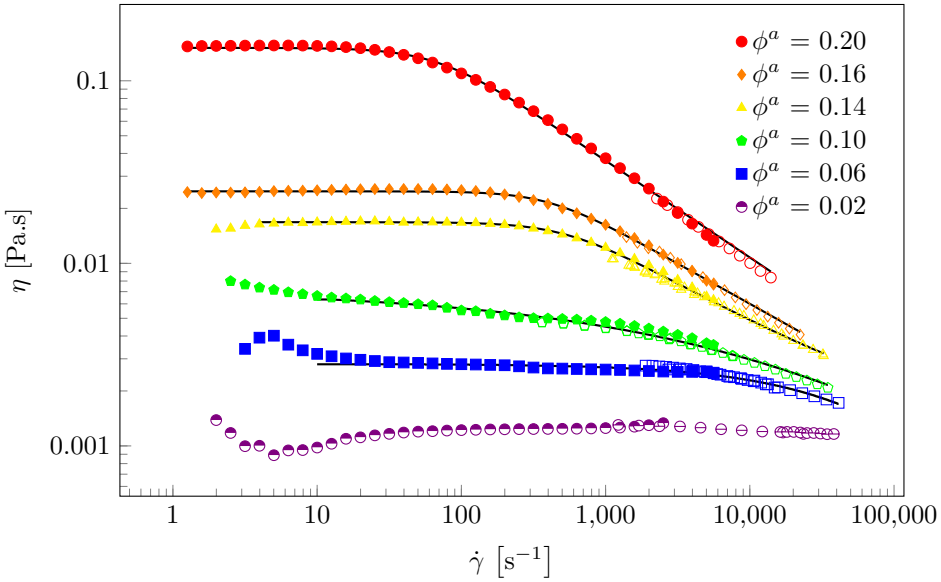

Figure 3.12: The viscosity of 62 nm p(MMA) particle dispersions at a range of ϕ^a. The filled symbols represent data obtain from the ARES-G2, and the open symbols data obtained from the VROC. The solid lines are from the Carraeu model fitting.

The viscosity is observed to span over two decades of magnitude, with an initial plateau region followed by a shear thinning regime for ϕ^a 0.14, 0.16 and 0.20. For ϕ^a 0.10, and 0.06 the initial plateau is not very clearly defined, which is thought to be due to instrument sensitivity rather than the dispersions themselves since they are concluded to be stable (See earlier Section 3.2.3.2).

For ϕ^a 0.02, the viscosity is found to be relatively constant over the shear rate range measured, excluding the initial few measurements, which are again, thought to be due to instrument sensitivity. At this dilute concentration the viscosity can be expected to follow the Einstein approximation for non-interacting hard spheres, equation 3.4. For dilute charged particles, the solvent flow convects ions from the EDL, causing a slight distortion which is counteracted by electrostatic forces. This leads to an increase in energy dissipation and manifests as a slight increase in the observed viscosity. The viscosity is linear, as particle collisions (from Brownian

motion, flow) at this concentration are unlikely, and the inter-particle separation distances are much larger than the repulsion interactions.

Of course it is relatively straight forward to understand that the inter-particle separation decreases with an increasing particle concentration. However, as the separation becomes smaller, the surface effects between particles become much more important, and understanding these separation distances, relative to particle size becomes much more difficult. The following expression remedies this and is used to determine the average inter-particle separation distance relative to d_H - where the assumption is $\phi_m \approx 0.63$[166];

$$\frac{h}{d_H} = \left(\frac{1}{3\pi\phi} + \frac{5}{6}\right) - 1 \tag{3.29}$$

From the plot of the above equation, Figure 3.13, the inter-particle separation decreases with ϕ at steady rate, until $\phi = 0.5$, where the separation decreases rapidly and particles become extremely crowded. This is as expected, however the plot provides an idea of the physical particle distances which enable one to appreciate the range of the inter-particle interactions with increasing ϕ. For dilute dispersions, where the average separation distance is relatively large, tied with the charge repulsion potential, implies that the probability of a particle coming within contact range of another particle is extremely low.

The viscosity is found to become increasingly non-linear, and higher as ϕ^a is increased, Figure 3.12. Although the electrostatic repulsion force for these particles is strong enough to prevent any coagulation, and thus particles coming into close contact with each other; the probability of inter-particle interactions becomes larger with increasing ϕ^a. As hydrodynamic interactions become more likely particles are forced to come within range of one another and concomitantly EDL overlap, and are subsequently kept apart by electrostatic repulsion. This results in an increase in the overall energy dissipation due to hydrodynamic interactions from EDL distortion.

The shear thinning behaviour observed here is indicative of a characteristic relaxation time, λ_c which is strongly dependant upon ϕ, proportional to Brownian diffusion time. These particle are therefore weakly viscoelastic, where λ_c is fundamentally due to Brownian diffusion. Brownian motion in the particle dispersion

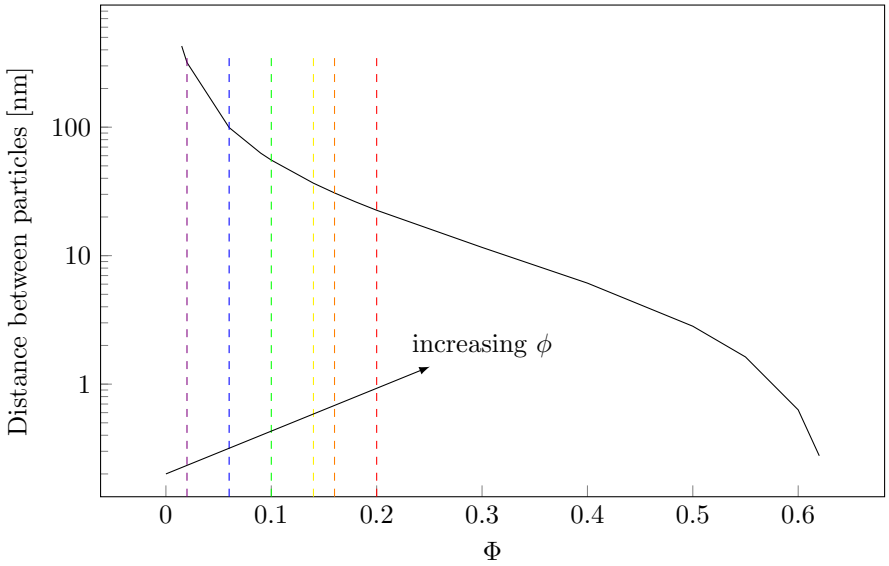

Figure 3.13: The average inter-particle separation as a function of the particle ϕ, determined for 62 nm particles. The dashed lines represent ϕ^a obtained from Figure 3.12

creates an effective force which leads to a diffusive particle motion which keeps particles well distributed at equilibrium.[145] When a given force acts on the system, this motion drives the particle structure back to the equilibrium state. The corresponding timescale of this motion is known as the characteristic relaxation time.

The shear thinning behaviour, i.e. the non-linear viscosity observed here is understood to be due to the shifting dispersion particle structure. At low shear the particle structure rearrangement due to flow is linear, and a plateau is observed in the shear viscosity. When the shear rate is increased, the structure cannot rearrange sufficiently to account for the increased shear and as this structure breaks down, the viscosity decreases and the shear thinning behaviour exhibited.

This is further confirmed when the oscillatory rheology of the particle dispersions is examined; elasticity is found to increase with particle concentration, Figure 3.14. The increasing elasticity is related to the particles disfavouring close contact with neighbouring particles. In that, as frequency increases, the particles are forced out of the equilibrium confirmation and thus exhibit an increase in the elasticity. Thereby, indicating a preference for the particles 'snapping' back into the the most energetically favourable configuration.

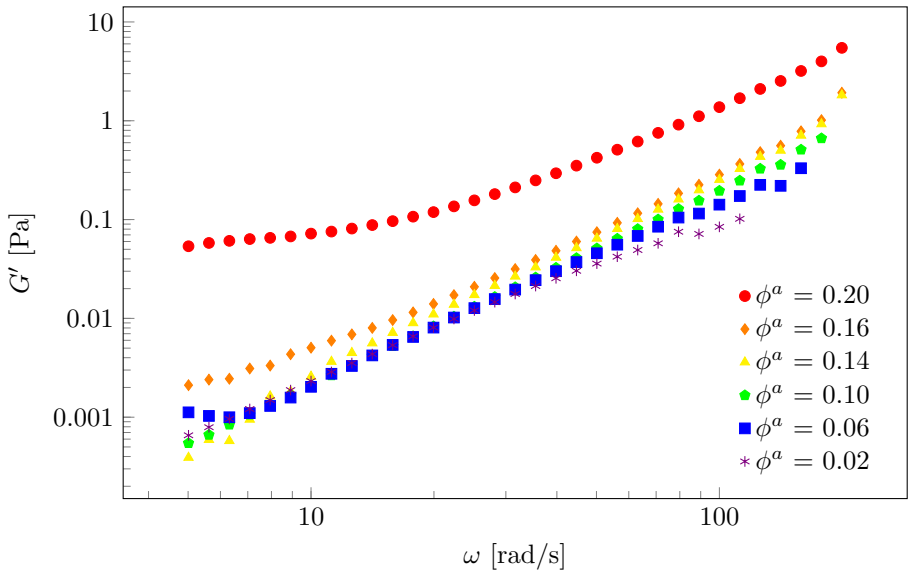

Figure 3.14: The measured elastic modulus, G' as a function of the angular frequency, ω at increasing ϕ^a.

Typically shear thinning of electrostatically stabilised dispersions is more extreme as the inter-particle repulsion increases, as is the case here, with increasing η_0 for each ϕ^a.[161] For repulsive particles the structuring is due to both Brownian motion and the inter-particle repulsion. The increasing ϕ^a also increases the order in the dispersion: from the DLVO theory it is apparent that as particles are brought closer together the repulsion potential increases. With increasing ϕ^a, where the separation distance is small, the particles strongly repulse their neighbours and therefore the resulting structure is more ordered, and held together with increasing strength.

This is where the particles are forced into closer than desirable contact, thus the inter-particle repulsion creates a structure where the particles repulse neighbours with equal force leading to increased order. Therefore, an increase in the overall viscosity of the system and the shear thinning character is observed, with ϕ^a; this is made apparent from the slope of the viscosity curves, shown in Table 3.2. As ϕ^a is increased, viscosity is observed to decrease with increasing sharpness (slope), thus increasing the observed non-linear viscosity.

According to the second law of thermodynamics this increasing order observation

implies that disorder decreases with ϕ^a, which is of course entropically unfavourable. The implications of the unfavourable change in entropy are discussed in the following, 'effective volume fraction' section.

Table 3.2: Shear thinning character for the various particle dispersions examined

ϕ^a	slope
0.10	-0.24
0.14	-0.39
0.16	-0.46
0.20	-0.56

ϕ_{EG}	slope
0.10	-0.18
0.14	-0.35
0.16	-0.43
0.20	-0.53

ϕ_{eff}	slope
0.29	-0.57
0.34	-0.57
0.50	-0.56
0.60	-0.66

Data for all systems used in this study is shown here and is included to aid overall comparison later. ϕ^a & ϕ_{EG} - particle concentration is varied, in pure water and ethylene glycol:water co-solvent 20:80, respectively and ϕ_{eff} - electrolyte concentration is varied at constant particle concentration

From the discussion above, the shear viscosity curves for these particle dispersions are expected to follow the Carreau model (Figure 3.2, equation 3.8); i.e. a zero shear viscosity region, η_0, shear thinning and an infinite viscosity region, η_∞. Here, η_∞ is never reached over the $\dot{\gamma}$ range measured.

The viscosity curves were fitted to the Carreau model, which is normally used to describe fluids that behave as Newtonian fluids at low $\dot{\gamma}$, and as power-law fluids at higher $\dot{\gamma}$. The model is found to fit the experimental data well, Figure 3.12, except for ϕ^a 0.02 and 0.06 where shear thinning is not particularly well defined. λ_c is also extracted from the model, Table 3.3.

As discussed above, λ_c is found to increase at higher ϕ^a; where this is the relaxation time for the system to return to its equilibrium particle distribution after a given force acts on the system. Longer λ_c are required at higher particle concentrations, as the particles need to rearrange into a configuration where the smallest inter-particle interaction is observed. For lower particle concentrations less time is required, as the average inter-particle separation is already quite large.

Table 3.3: The λ_c determined from the Carreau model shear viscosity fit

ϕ^a	λ_c /ms
0.10	0.02
0.14	1.83
0.16	2.47
0.20	14.54

ϕ_{EG}	λ_c /ms
0.10	0.47
0.14	1.03
0.16	1.83
0.20	15.07

ϕ_{eff}	λ_c /ms
0.29	4.28
0.34	7.19
0.50	18.22
0.60	328.07

Data for all systems used in this study is shown here and is included to aid overall comparison later. ϕ^a & ϕ_{EG} - particle concentration is varied, in pure water and ethylene glycol:water co-solvent 20:80, respectively and ϕ_{eff} - electrolyte concentration is varied at constant particle concentration

3.3.2 Ethylene glycol co-solvent

The shear viscosity of p(MMA) particles dispersed in an ethylene glycol:water solvent at a ratio of 20:80 was also determined. Ethylene glycol is typically added to Inkjet inks to improve upon the printing character of a given fluid; this is further expanded upon in the upcoming Inkjet printing chapter. The particle ϕ are the same as those used, when the particles are dispersed in a pure water solvent (ϕ^a), but the series is termed ϕ_{EG} to avoid confusion.

This particle system exhibits very similar viscosity profiles relative to when a pure water solvent is used, in the first instance. Although under closer inspection differences in the profiles can be seen. The shear thinning character is not as pronounced as for the pure water counterpart, Table 3.2. This is most likely because the repulsion interaction is slightly less effective in this co-solvent: ethylene glycol is much less polar than water. However, the relative permittivity of ethylene glycol:water 20:80 is 74.60 at 20 °C, relative to pure water, 80.37, at the same temperature.[167] Therefore the repulsive potential is not greatly affected, although is affected just enough to exhibit this slight change, Table 3.6.

At the same particle concentrations η_0 is slightly enhanced, relative to when a pure water solvent is used, Figure 3.17. Ethylene glycol is known to be both completely miscible with water, and to enhance the viscosity of the resulting solvent

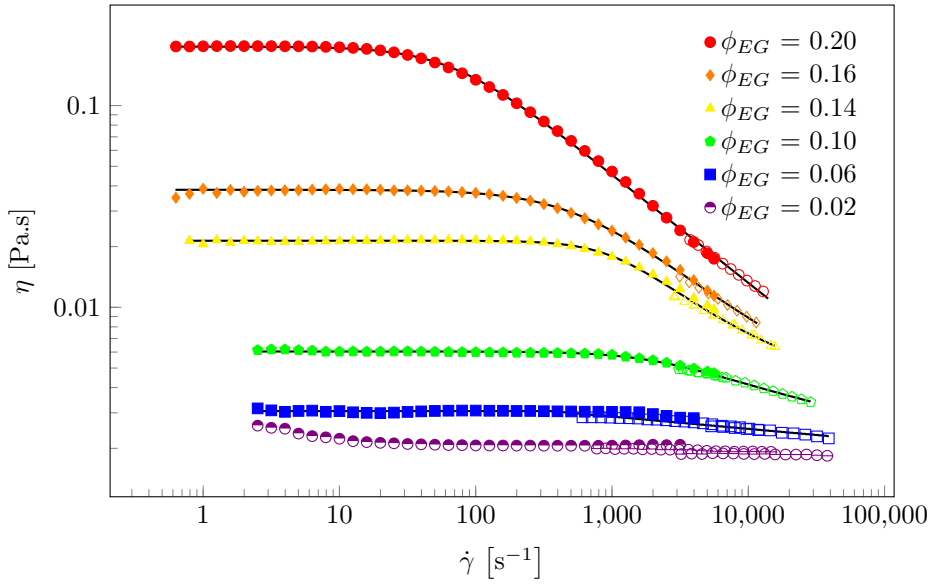

Figure 3.15: The viscosity of 62 nm p(MMA) particle dispersions at increasing ϕ_{EG}. The filled symbols represent data obtain from the ARES-G2, and the open symbols data obtained from the VROC. The solid lines are from the Carraeu model fitting.

mixture, Figure 3.5.[163] The viscosity of a 20:80 ethylene glycol:water mixture has a slightly higher viscosity relative to pure water, 2.1 & 1.0 mPa $\cdot$ s respectively.

Similarly to the previous case, where the particle are dispersed in pure water, the Carreau model fits the data well at all concentrations, except ϕ_{EG} 0.02 & 0.06 as again, a Newtonian flow is observed at this very dilute concentration. The λ_c, again is found to increase with particle concentration, Table 3.3. Small λ_c are required at low ϕ_{EG}, as the particles are not required to rearrange very much to obtain low energy configuration, as inter-particle distances are already quite large. Whereas, longer λ_c is required at higher ϕ_{EG} as the particle must rearrange into a configuration with the lowest repulsion interaction between each particle. This implies an increasing elasticity as the particle concentration in the fluid increases, which is again confirmed from the oscillatory measurements for these particle dispersions, Figure 3.16.

A theoretical approach for treating charge stabilised particles is to account for the EDL interaction as an excluded volume, the range of which is determined from particle size and κ^{-1}. That is the modified Krieger and Dougherty model, (eq 3.18,

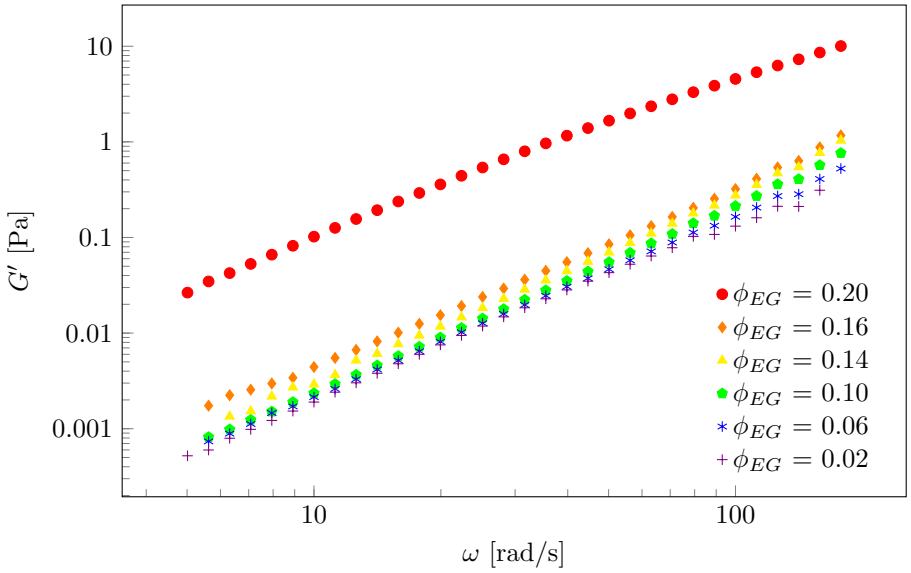

Figure 3.16: The measured elastic modulus, G' as a function of the angular frequency, ω at increasing ϕ_{EG}.

which is simplified into eq 3.7).

From Figure 3.17, the predicted η_0 for both the pure water, and ethylene glycol:water co-solvent systems is very similar up until $\phi \approx 0.16$, where the ethylene glycol co-solvent viscosity is predicted to increase significantly higher than pure water. A reasonably good correlation is obtained here for particles dispersed in the pure water solvent. For the ethylene glycol co-solvent, it appears the predicted η_0 at lower particle concentrations is a little low. This is most probably because the model does not account for the solvent viscosity sufficiently, and under estimates the significant effect of the EDL at lower particle concentrations.

The repulsion interaction arising from the electrostatic stabilisation in these dispersions is significantly affected by the ionic strength of the system, which varies with ϕ, and does indeed hold a significant influence over the η_0. However, as the effective volume fraction for each system is already accounted for by the model prediction as an excluded volume, determining the effective volume fraction will not affect this model fit: though the effective volume fractions do go a long way in explaining the increased η_0, and is theoretically determined in the following section.

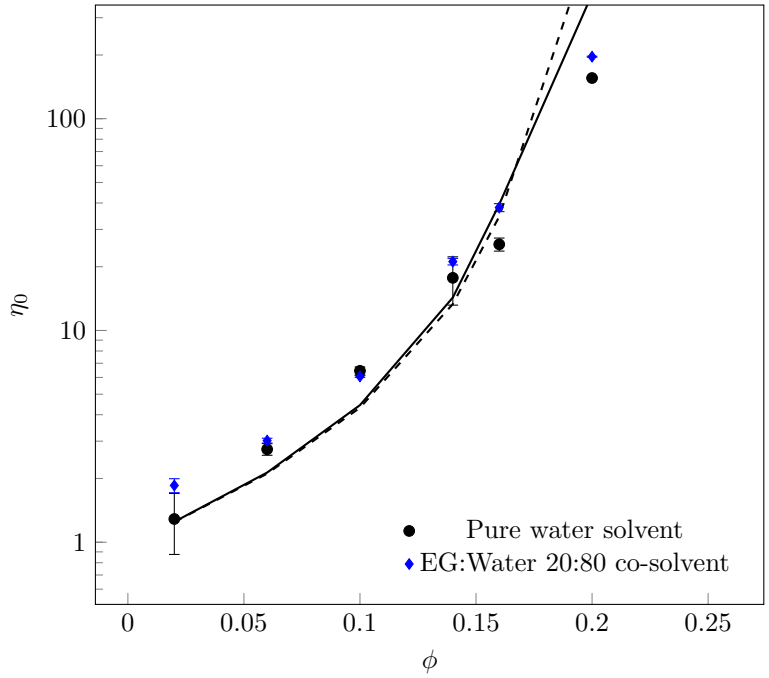

Figure 3.17: The change in η_0 with particle ϕ, for pure water, and the ethylene glycol:water 20:80 co-solvent. The predicted Krieger-Dougherty relationship is represented by a solid line for the pure water solvent, and a dashed line for the ethylene glycol:water co-solvent.

3.3.3 Effective particle volume fraction

The stock p(MMA) dispersions which upon initial examination appeared as though they were unstable and/or undergoing some destabilisation phenomena, mentioned earlier, are further examined here.

When the effect of surfactant and electrolyte removal (via dialysis) is considered according to the DLVO theory (see chapter one), it becomes apparent that since the Debye layer thickness, κ^{-1} is significantly affected by the electrolyte concentration, this highly viscous behaviour is not entirely unexpected. At extremely low electrolyte concentrations, κ^{-1} can be considered to be close to its maximum length according to equation 1.8; where long range inter particle interactions are expected, Figure 1.7.

Therefore, when considering the viscosity of these electrostatically stabilised dispersions, the effective volume fraction ϕ_{eff} must first be determined; i.e. the volume

occupied by each particle + κ^{-1}. In order to determine ϕ_{eff} here, the following expressions are used; where initially the volume of a single particle, V_c (p(MMA) particles) was first determined (for a spherical particle, which conveniently is the case here);

$$V_c = \frac{4}{3}\pi r^3 \tag{3.30}$$

Once V_c is known, the total volume of the dispersed phase, $V_{t,c}$ can then be determined;

$$V_{t,c} = \frac{m_c}{\rho_c} \tag{3.31}$$

Where m_c and ρ_c represent the mass and density of the dispersed phase respectively. The total number of dispersed particles, N_p can then be determined from;

$$N_p = \frac{V_{t,c}}{V_c} \tag{3.32}$$

The κ^{-1} was then determined using equation 1.8. From this it becomes apparent;

$$r_{eff} = r + (\kappa^{-1}/2) \tag{3.33}$$

Thus, once the r_{eff} is calculated, the effective volume occupied by a particle, $V_{eff,c}$ can be determined by replacing r with r_{eff} in equation 3.30, for the electrolyte concentration used to calculate the κ^{-1}. And as N_p in the dispersion is unaffected by κ^{-1}, the total effective volume occupied by the dispersed particles, $V_{efft,c}$ can then be determined from the rearranged equation 3.32, with the updated variables (where ϕ_{eff} is the ratio of $V_{efft,c}$ and the total dispersion volume);

$$V_{efft,c} = V_{eff,c}.N_p \tag{3.34}$$

A range of p(MMA) dispersions were prepared at various ϕ_{eff}, to further examine this hypothesis, Figure 3.18. Table 3.4 lists the prepared dispersions, and the calculated κ^{-1} for each sample. It must be stressed here that the actual volume fraction, ϕ is 0.2 for all the samples and it is the effective volume fraction, ϕ_{eff} that is being altered by increasing the electrolyte concentration.

Here, the particles are electrostatically stabilised, i.e. the inter-particle interaction is repulsive at all but short distances. As the ionic strength of the solvent

Table 3.4: The calculated κ^{-1} and the corresponding ϕ_{eff}, for 62 nm (d_H) p(MMA) particles

ϕ	[NaCl] /mM	κ^{-1}/nm	ϕ_{eff}
0.2	0.03	55.5	0.60
0.2	0.05	42.2	0.50
0.2	0.20	24.8	0.34
0.2	0.40	15.2	0.29
0.2	4.00	4.8	0.21

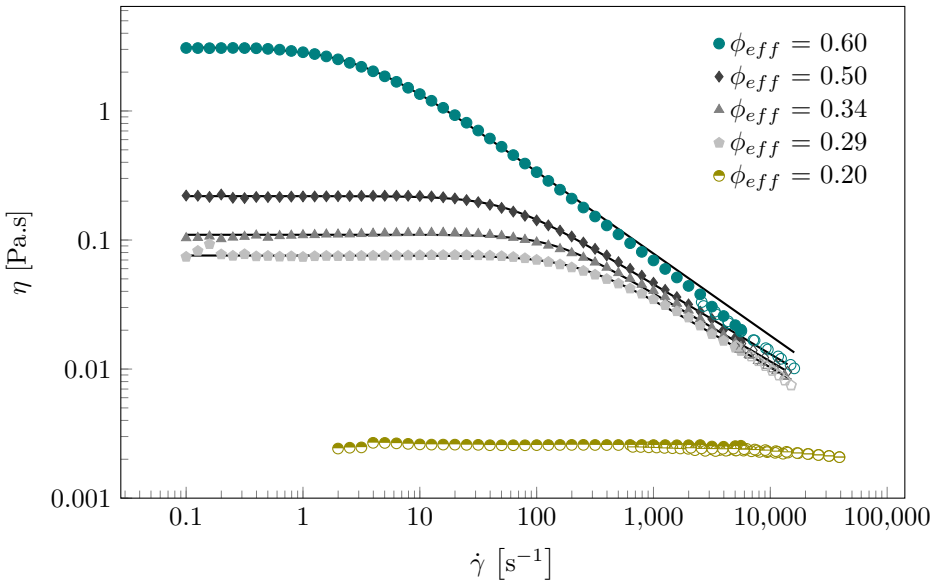

Figure 3.18: Viscosity of p(MMA) particle dispersions at various ϕ_{eff}, but constant ϕ (0.2), for 62 nm sized particles. The filled symbols represent data obtain from the ARES-G2, and the open symbols data obtained from the VROC. The solid lines are from the Carraeu model fitting.

is decreased the repulsive potential is increased, which is apparent from the calculated κ^{-1}. And as the ϕ_{eff} increases, the separation distances become smaller, and the inter-particle interactions become much more significant. This amplified inter-particle separation heightens the order within the system, and concomitantly the strength of the particle structure which must be broken by the applied shear,

hence the increasing viscosity.

The Carreau model fit is satisfactory for most of the particle concentrations tested. The model cannot be made to fit ϕ_{eff} 0.6 and 0.5, and deviates at high $\dot{\gamma}$. This is almost certainly due to impurities formed within the dispersions, when the particles become extremely ordered at small inter-particle separations, as is the case for these samples, Figure 3.19. The impurities formed, repulsive driven glasses/crystals, are discussed in due course. The extracted λ_c value again increase with particle concentration, providing further confirmation of the increased order within the dispersions at higher ϕ_{eff}, Table 3.3.

When the electrolyte concentration is increased, and the ϕ_{eff} is close to the actual ϕ (0.21 and 0.20 respectively) shear thinning is no longer observed, and there is a large decrease in the viscosity of the dispersion. This is due to the reduced inter-particle repulsion, where the repulsion is not strong enough to contribute towards the particle structuring. Therefore, when shear is applied to the system there is only the Brownian force contribution to the particle structure, which is easily rearranged with applied shear at this ϕ_{eff}.

Considering this marked effect on the shear viscosity when $\phi_{eff} = 0.21$ compared to the previously discussed particle dispersions (ϕ^a, in Section 3.3.1), where quite a different outcome is observed, (i.e. where the actual ϕ^a was varied to discern the viscosity contribution, in pure water); in order to fully appreciate the viscosity contribution due to effective particle volume fraction the former dispersions must be similarly compared in terms of the corresponding ϕ_{eff}.

Table 3.5: The calculated κ^{-1} and the corresponding ϕ_{eff}, for 62 nm (d_H) p(MMA) particles, at varying ϕ^a

ϕ^a	[NaCl] /mM	κ^{-1}/nm	ϕ^a_{eff}
0.20	0.3	17.6	0.31
0.16	0.3	17.6	0.25
0.14	0.3	17.6	0.23
0.10	0.3	17.6	0.17
0.06	0.3	17.6	0.10
0.02	0.3	17.6	0.04

The ϕ_{eff} calculated for the ϕ^a system are shown in the above table. The same concentration of electrolyte is used for each of the prepared dispersions, which means the κ^{-1} is the same for each ϕ^a considered. The need for this added electrolyte is to avoid formation of impurities, further expanded upon later in this section. Figure 3.19 displays the effective average inter-particle separation, updated from Figure 3.13.

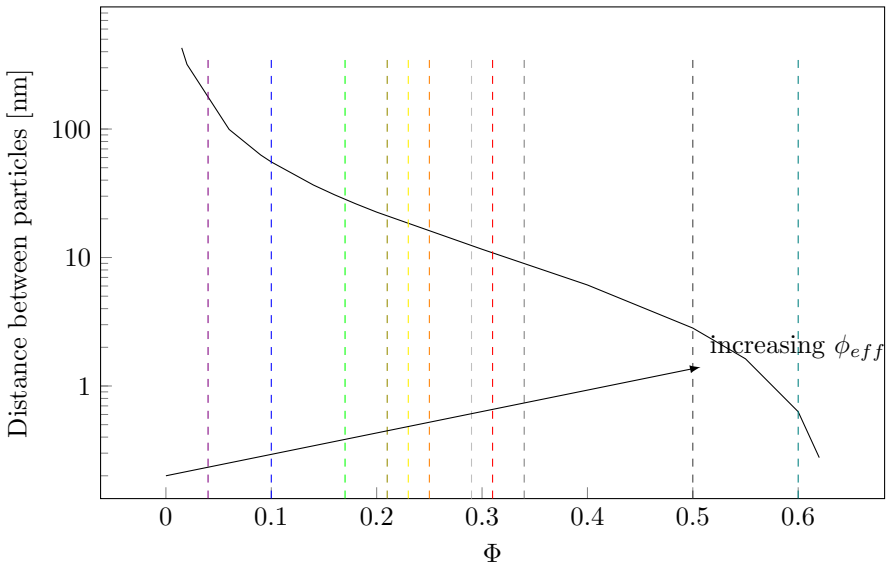

Figure 3.19: The average inter-particle separation as a function of the particle ϕ, determined for 62 nm particles. The dashed lines represent ϕ_{eff} from Figure 3.20

By combining Figures 3.12 & 3.18, with the corresponding ϕ_{eff}, the effective particle volume fraction viscosity contribution can be discerned, Figure 3.20. Note the discussion from the previous section still holds true, just the effective particle volume fraction is examined here.

Considering both the increasing volume occupied and thus the repulsive interaction with increasing ϕ_{eff}, the observed viscosity curves do correlate well with the predicted ϕ_{eff}: i.e. where the viscosity is found to increase with the magnitude of the electrostatic repulsion interaction. As the ϕ_{eff} increases, the particle structure within the solvent (order) increases, thus increasing the viscosity. Taking the slope of the power law region of the viscosity curves at each particle concentration, enables a comparison of the systems in question here, Table 3.2. The shear thinning

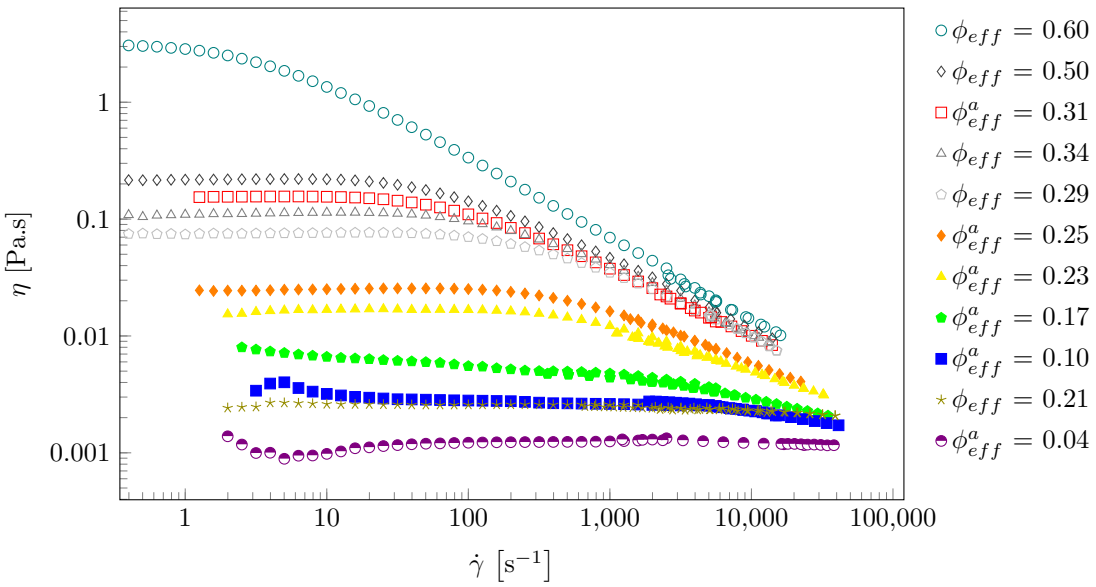

Figure 3.20: Viscosity of the p(MMA) particle dispersions at the full ϕ_{eff} range measured for 62 nm sized particles. Combined Figures 3.18 and 3.12, with coordinating colours to aid differentiation.

character is enhanced at higher ϕ_{eff}, as the repulsive potential holding the particle structure increases. Therefore, breaking this down at higher ϕ_{eff}, spans over a longer η range, thereby increasing the non-linear character of the dispersion.

In Figure 3.20, the viscosity decreases with ϕ_{eff} for all but two concentrations, ϕ_{eff} 0.31 and 0.20. For the particle dispersion ϕ_{eff} 0.31, the viscosity is found to be higher than for ϕ_{eff} 0.34. This is inconsistent with the dataset and is probably an outlier.

For ϕ_{eff} 0.20, the κ^{-1} is determined to be much less (4.8 nm) than for the dispersion with ϕ_{eff} 0.10 and 0.17, 17.6 nm. This means, although ϕ_{eff} is relatively larger, the repulsive potential is much higher for the dispersions with the *smaller* ϕ_{eff}. Thus despite the particles in the ϕ_{eff} 0.20 dispersion occupying a larger volume, the reduced repulsive potential implies the overall viscosity is reduced. The particles in this system can approach other particles at smaller distances relative to the particles in the dispersions with smaller ϕ_{eff} but larger κ^{-1}.

From this effect, it become apparent that when considering the shear viscosity as a function of ϕ_{eff}, either the particle concentration must be kept the same and

the electrolyte concentration systematically increased, or the effect from both the particle content as well ϕ_{eff} can be examined. Therefore, Figure 3.20 although is accurate, is effectively two different systems each examining slightly different effects. This is why the systems are initially examined separately, since two different effects are being examined.

This analysis highlights the importance of the EDL interaction, for electrostatically chargd particles, on the ensuing shear viscosity, and the need to determine the ϕ_{eff} when considering viscosity of charged particles. For this reason, the ϕ_{eff} is similarly calculated for the particle dispersed in the ethylene glycol:water co-solvent, termed $\phi_{EG,eff}$ here, Table 3.6. Similar $\phi_{EG,eff}$ are obtained relative to the ϕ^a system, in Section 3.3.1; this was mentioned earlier, but is calculated here in order to appreciate the magnitude of κ^{-1}, and the significant role it plays in determining the dispersion viscosity.

Table 3.6: The calculated κ^{-1} and the corresponding $\phi_{EG,eff}$, for 62 nm (d_H) p(MMA) particles, at varying ϕ_{EG} in an ethylene glycol:water 20:80 co-solvent

ϕ_{EG}	[NaCl] /mM	κ^{-1}/nm	$\phi_{EG,eff}$
0.20	0.3	17.2	0.31
0.16	0.3	17.2	0.25
0.14	0.3	17.2	0.22
0.10	0.3	17.2	0.17
0.06	0.3	17.2	0.10
0.02	0.3	17.2	0.03

3.3.3.1 Impurities at High Particle Concentrations

For the aforementioned systems where increasing particle order is deemed to be responsible for the dispersion shear viscosity, is at first glance at odds with the second law of thermodynamics; i.e. entropy, whereby disorder always irreversibly increases and the net entropy for a given system can never decrease over time.[168] In particular when ϕ_{eff} 0.60, the dispersion exhibits strong shear thinning behaviour, and follows the viscosity trend as laid out by previous dispersions. However, at high

$\dot{\gamma}$ it can be observed the Carreau model fit deviates and an ideal fit is not realised, 3.18. Also, the slope of the shear thinning region is larger than the other dispersions measured. Although, it could be argued that this should indeed be expected at high particle concentrations, the actual cause is more likely related to the formation of crystals (or repulsive driven glasses).[147]

Crystalline solids, or repulsive driven glasses are known to form at high particle concentrations $\phi \approx 0.58$.[145] These are closely packed particle clusters, the formation of which is actuality driven by entropy: where the entropy gained from the colloidal particle glass formation is greater than the disorder in the ensuing colloidal particle configuration. These were found to be impossible to re-disperse by either mechanical or sound (sonication) agitation, and very difficult to remove via centrifugation.

At high ϕ, when the dispersion is of high order the particles become crowded. This results in a fluid-crystal phase transition, which occurs between ϕ 0.49-0.54; below which the system is completely fluid. For electrostatically stabilised particles, with the presence of the EDL this effect is realised when the $\phi_{eff} \approx$ 0.49-0.54. However, because this is a soft interaction (EDL layers), the transition concentrations are normally expected to be slightly higher.[146] This was indeed found to be the case here, where crystal are only observed for ϕ_{eff} 0.60 and 0.50. Figure 3.21 shows the various crystals observed in these particle dispersions, over the course of 3-4 weeks from preparation.

The presence of these crystals is highly undesirable, particularly for the application in Inkjet printing, where the dispersions are to extruded from small nozzles (d = 50 μm). Once the root cause of the crystal formation was determined, particle dispersions at a range of electrolyte concentration were prepared and observed for crystal formation over the course of a 2 month period.

A 0.3 mM or highler [NaCl] was found to yield particle dispersions that are crystallite free for *at least* a 2 month period. Thus, each particle dispersion, hence forth was prepared with this baseline [NaCl]: all particle dispersion used for the rheology study were also prepared with this baseline [NaCl], except for the dispersions used to study the ϕ_{eff} effect (0.60, 0.50 and 0.34). These dispersions were prepared as needed in order to keep crystal concentration to a minimum, and each sample used within a week of preparation. A crystal formation vs time curve would perhaps be appropriate here, however this proved not to be possible. As the crystals could

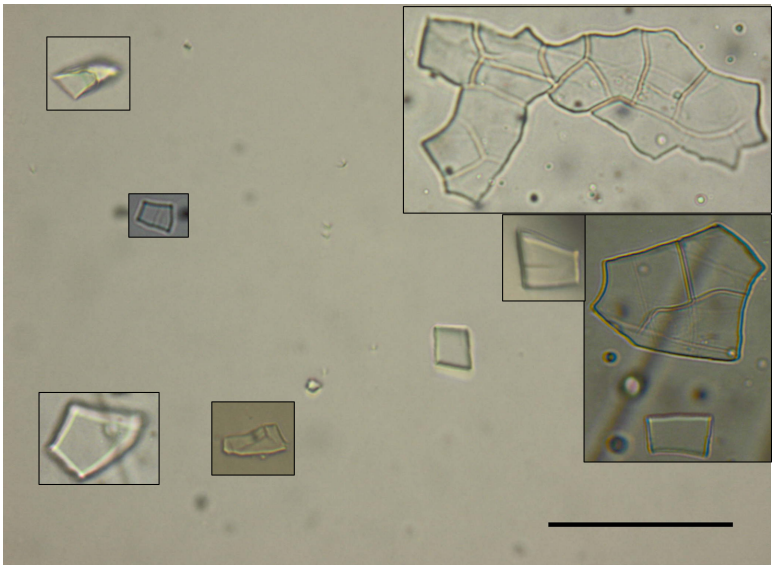

Figure 3.21: A compilation of light microscopy images showing crystal formation, observed for particle dispersions ϕ_{eff} 0.6 and 0.5. The scale bar represents 100 μm and is consistant across all images. A black box around each crystallite signifies a different image.

only be observed using light microscopy, and even then only for a relatively short period as the samples are prone to solvent evaporation. Additionally, it is difficult to predict whether these crystals sediment or cream, or if they are dispersed in these systems, due to the highly viscous nature of the parent dispersions. Therefore, aliquots are extracted from 3 areas ($\sim$ top, middle and bottom of sample vial) for each dispersion when examining for crystals.

3.4 Conclusions

The aim of the research in this project is to investigate how particle dispersions behave when used as inks for an Inkjet system. An initial constraint for fluids to be jetted in such a system is the zero shear viscosity, which is typically thought to be $\sim$ 20 mPa.s.[12] This chapter has outlined the rheological response of the various systems to be used for this purpose.

The rheology of the dispersions was thoroughly examined from a theoretical perspective to carefully characterise the different systems, as well as to gain an insight into the particle configuration as a function of the particle concentration, over the shear range examined.

The change in viscosity with increasing particle concentration in both water and ethylene glycol:water 20:80 co-solvent, is found to be as expected. The increase in the viscosity is shown to be due to the inter-particle repulsion, and the particle structure within the dispersions.

The importance of the electrolyte concentration was then examined and the need to determine the effective volume fraction understood, in order to fully realise the particle concentration effect for charged particle dispersions. The viscosity is shown to be tunable with the electrolyte concentration, from a highly viscous non-linear profile to a relatively low viscous Newtonian profile.

The particle dispersions were also examined for any aggregation, and were found to be very stable over a range of particle concentrations. However, crystal formation was observed for freshly dialysed particle dispersions, where the effective particle concentration is extremely high. At these concentrations, there is a net entropy gain from forming highly ordered colloidal crystals relative to the corresponding disorder in the colloidal particle configuration.[147]

These crystals were found to be irreversibly formed and are highly undesirable for Inkjet printing. Therefore, particle dispersions were then prepared at an effective volume fraction where crystal formation is not observed.

The information gleaned from these studies is then further analysed in the following chapter, where the elongational response of the dispersions is considered.

Chapter 4

Inkjet Printing Colloidal dispersions

4.1 Introduction

This section deals with the jetting behaviour of the previously prepared particle dispersions. The extensional viscosity of the particle dispersions is determined, and related to the observed jetting behaviour. The need to examine colloidal dispersion jetting behaviour for the application of the inkjet technique in industry is highlighted earlier (Chapter 1). Here, a brief overview of jetting complex fluids is given and some of the previous work in this area discussed. Techniques used to determine the extensional viscosity are briefly discussed, before the results obtained in this study are examined.

4.1.1 Jetting complex fluids

Complex fluids are defined here as functional fluids, including colloidal particle dispersions and polymer solutions. These complex fluids are required to be printed for many applications in materials science, including printed electronics and biomaterials.[12–14] These fluids are typically found to exhibit non-Newtonian rheological behaviour, as seen in the previous chapter.[12] As discussed earlier, most inks for graphics printing contain pigment particles. For printing applications other than

graphics printing, i.e. electronics, textile manufacture, particles provide the functional component in the ink.[12]

The jetting behaviour is affected from the presence of particles in these inks, and although these inks are used widely, relatively little is known about how particles affect jetting. Much more attention has been focused on polymer solutions, and Newtonian fluids.[12]

The jetting behaviour of high molecular weight polymer suspensions is suggested to be from the interplay between the extensional rate, U_J/N_D (where U_J is the jet speed, and N_D is the nozzle diameter) and the finite extensibility, L (related to the polymer weight and solvent viscosity).[169] For polymer suspensions, three regimes where the jet slows down have been suggested[169];

(1) The polymers remain in their equilibrium conformation corresponding to the Newtonian low shear rate viscosity,

(2) The polymers, in a viscoelastic fluid, are first extended then relax to equilibrium conformation,

(3) The polymers are fully extended and the Newtonian low shear viscosity is less than the extensional viscosity due to the fluid they are dispersed in.

The effect due to high extensional viscosity is reduced ($\sim$ a factor of L) by the filament thinning action before the drop breaks off from the nozzle. The third regime predicts that DOD printing can be used to jet high polymer concentrated suspensions, on the basis that the fluid displays a viscoelastic response with a relaxation.

The flow behaviour is known to be greatly affected by the introduction of particles and polymers.[12,33,145,147,170] Simple low shear rate viscosities ($< 10^2$ s^{-1}) cannot be used to evaluate fluids for DOD printing, and characterise jetting performance (the piezoelectric drive pulses repeatedly at a typical frequency of 10^4 s^{-1}).[171]

4.1.1.1 Fluid Properties for Inkjet printing

The surface tension, viscosity and inertia are the most significant fluid properties that affect the inkjet printing process, and are dominant during jetting and drop generation.[12,168] Surface tension is from the cohesive forces of the fluid, and drives the fluid to form the most energetically (smallest surface energy) favourable fluid shape. Both the surface tension and Rayleigh-Plateau (capillary) instability are

actually responsible for jetting behaviour in inkjet printing; the nozzle ejects ink in a cylindrical shape, which then necks inwards due to surface tension, and thus breaks up into spherical drops.

The viscosity and inertia oppose this fluid contraction into drops. Inertia is the resistance to change from, a given body's current state, i.e. from rest or motion.[172] For a fluid jet this momentum change, M_o is $M_o \propto \rho.dV$. Where dV is rate of change in fluid velocity.

Viscosity is the measure of the fluid resistance to deformation. The viscosity of a given fluid varies from the type of deformation applied, i.e. from shear ($\dot{\gamma}$) or extension ($\dot{\varepsilon}$). The shear viscosity (termed η_S herein) has been examined in the previous chapter. The fluid viscosity arising from an extensional deformation (termed η_E) for Newtonian fluids is typically, $Tr = \eta_E/\eta_S = 3$ and is known as the Trouton ratio.[173] The $\dot{\varepsilon}$ and η_E relationship become non-linear, with much larger Trouton ratios observed for non-Newtonian fluids, specifically fluids incorporating polymers.[174,175]

There are a number of important dimensionless numbers used to describe the behaviour of liquid drops. The Reynolds number (Re) and the Weber number (We), both describe the importance of aforementioned three significant properties as such;

$$Re = \frac{\rho L U}{\mu} \tag{4.1}$$

where ρ is the fluid density, L is the characteristic length (in this case the jet radius), U the characteristic velocity (drop speed) and μ the viscosity.

The inertial and viscous forces ratio is described by the Reynolds number, in this case with a jet. The Weber number describes the inertial force and surface tension (g) ratio as;

$$We = \frac{\rho L U^2}{g} \tag{4.2}$$

Typically, the Ohnesorge number characterises the drop formation, and expresses the viscosity and surface tension ratio, without a velocity scale, as;

$$Oh = \frac{\sqrt{We}}{Re} = \frac{\mu}{\sqrt{\rho g L}} \tag{4.3}$$

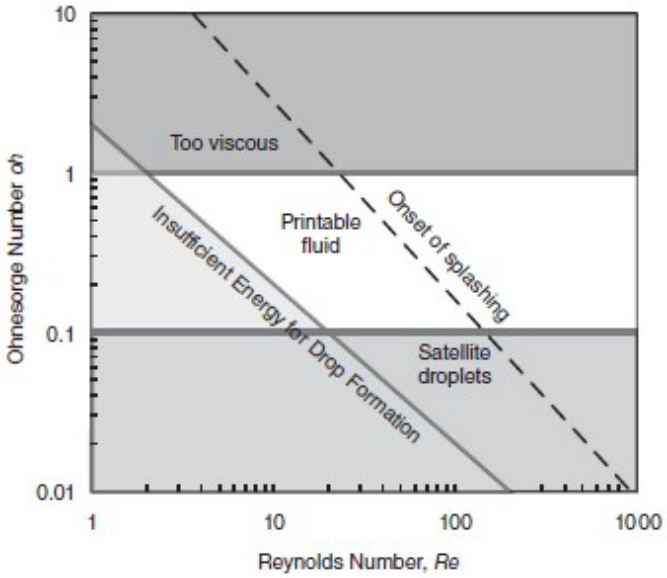

Figure 4.1: Phase diagram showing the optimum drop on demand region, from the Ohnesorge and Reynolds numbers relationship. Reprinted from ref (12).

The ability for a given fluid to print, i.e. printability can be determined from phase diagrams constructed using these dimensionless numbers, Figure 4.1.[172] These diagrams map the desirable fluid properties for drop generation as well as the properties where drops cannot be generated. The optimum viscosity range for drop generation lie in the range $0.1 < Oh < 1$ for Newtonian fluids, where no satellites are observed.[2,176]

At higher Ohnesorge numbers the viscosity prevents the fluid detachment from the nozzle. For the opposing case, where the Ohnesorge number is too small, satellite drops are observed due to the dominating surface tension.[172] The fluid properties which vary with the nozzle size and jetting velocity thus, control the observed jetting behaviour.

During jetting, for DOD printing satellite drops are usually observed, which follow each ejected fast moving drop.[177] These satellites are easily misdirected and can reduce the resolution of the print. When printing circuits (electronics) they could also cause bridging between two conducting tracks and thus cause the device to fail. Satellite drops are therefore, very undesirable and must be avoided where possible.

4.1.1.2 Reduction of Satellite drops

Various methods to reduce the formation of satellites have been suggested, including low jetting speeds, surfactants and high fluid viscosity.[177] Using low jetting speeds is not really feasible as the applications of the technology would then become limited. Addition of surfactants would enhance the wetting and conductivity of the fluid, however these improvements could also be counteracted by the dynamic surface tension. Increasing the viscosity of the fluid would reduce the formation of satellites, as break off time would increase however this would again lower jetting speeds.

Aqueous suspensions of PEDOT:PS have been used to successively print transparent conductors in printed electronics, with or without the aid of surfactants.[178] PEDOT:PS is an ionomer, a polymer mixture of sodium polystyrene sulfonate and poly(3,4-ethylenedioxythiophene) which together form a macromolecular salt. This has been proven to be due to the strong shear thinning behaviour exhibited by these suspensions.[177] In the printing nozzle these suspensions show low viscosities over a wide range of jetting speeds. However once the jet has formed and the shear rate now relatively low, the suspensions recover a higher viscosity very quickly, ~ 10 μs. This recovery causes a delay in the formation of satellites over a 0.8 mm standoff distance to the substrate. The satellites are then sufficiently suppressed, and thus do not cause any undesirable effects to the print quality.

4.1.2 Extensional rheometry

As mentioned earlier evaluating fluids for DOD printing can not be done using simple shear viscosity measurements, particularly with the low deformation rates obtained by typical bench top rheometers. The jetting process is inherently a extensional flow, at high deformation rates ($> 10^6$ s^{-1}). In order to gain an understanding of a given fluids jetting behaviour, the response to both shear and extensional flow must first be determined.

The extensional rheology of polymer solutions is well understood, with many approaches used to examine the behaviour, including filament stretching, flows through a contraction etc.[179–183] As such several models have been developed from the understanding of both the shear and extensional deformation.[184]

In order to extend the range of materials currently jet-able, there is clear need for a better understanding of the shear extensional response for colloidal particle dispersions. Despite this clear requirement, most of the work in this area focusses on exclusively understanding the shear flow rheology response.[185–187] This is perhaps due to the experimental difficulty in achieving a purely extensional flow. These deformations stretch fluids apart exponentially rather than linearly, and can be considered more severe than shear deformations.[188]

Albeit, there have recently been some studies considering the extensional rheology of particle suspensions, although these mainly focussing on shear thickening systems.[189,190] However, the systems under consideration here exhibit shear thinning behaviour, for which there has not been much work focussing on the extensional deformation response.

Extensional viscosity is an elusive quantity to determine, and is extremely difficult to measure.[191,192] A pure extensional flow is described as shear and vorticity free, where the deformation rate tensor, D that has only non-zero elements in its diagonal.[191] In practice it is very difficult to apply a purely extensional strain to a mobile fluid. There is always an elements of shear contribution present, from surfaces or interfaces which must then be accounted for.

Another issue with determining the extensional deformation is the dependence on both the applied strain and accumulated strain. The non-affine transfer of the strain from the deformed fluid to the suspended microstructure further exacerbates the issue, where the affinity is also strain rate dependant.[193,194] Techniques which apply a strain for a small time and therefore, a small microstructural strain within the fluid, generally report a transient extensional viscosity.

For steady state extensional viscosity, the strain must be applied to the system until the microstructure within the fluid is strained to saturation. This is satisfied by a persistent extensional flow, which is readily observed at a stagnation point. This is where the residence time is arbitrary.[173,175]

Rheology measurements are affected by various instabilities. For extensional flow, complex fluids are often observed to display viscoelastic instabilities, particularly significant in this case as the deformation is greater than for shear flows.[191]

Another issue to consider is the initial fluid condition, where the fluid must attain a consistent initial condition for a reliable measurement, over a range of

applied deformation rates. This is a particularly significant issue when determining the extensional deformation from flows through a contraction. The fluid in these measurements is flowed through a contraction, where the extensional deformation is applied, thereby raising questions about the flow deformation history.[173]

It becomes apparent from these considerations that the extensional viscosity measurements of the fluid by different methods could vary significantly.[192] It almost seems like a thankless task, measuring the extensional viscosity, although the problem is still very much examined and addressed. Even if a true extensional viscosity cannot be obtained, by measuring the deformation with a technique configuration that models the application well still provides valuable data, as the fluid response can still be characterised.

4.1.2.1 Extensional rheometry using a microfluidic cross-slot

Stagnation point flows, where a continuous flow incorporating a stagnation point where a persistent extensional flow can be applied with an arbitrary residence time, are a well established method for determining the extensional viscosity.[173,175] These flows readily achieve steady state deformation conditions. The strain rate at a stagnation point is finite with a zero local flow velocity. The fluid flowing past the stagnation point region is still affected by the velocity gradient for finite time and therefore is subjected to a limited strain which could still be large but is dependant on the flow path.

Typically, cross-slot devices are used to examine stagnation point flows, Figure 4.2.[173,175,195] In these devices the fluid enters through two opposing inlets and exits from directly opposing outlets. From a symmetric channel position, the stagnation point forms at the centre of the cross. Fluid flowed through this device is stretched along the outlet axis, with shear and vorticity free flow at appropriate Re numbers.

In these devices, the flow is planar and can therefore be observed using fluorescence imaging, as well as enabling velocimetry and birefringence measurement. Stable flows can be attained at higher rates, as both the inlets and outlets are typically bound to a pump. The flow rate, and thereby the stain rate is therefore easily controlled using the pump. The extensional viscosity of the fluids flowed through the

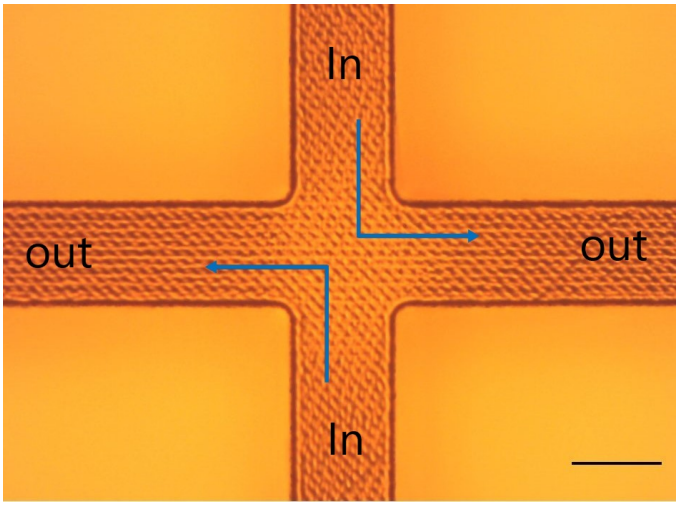

Figure 4.2: An optical micrograph of the cross-slot used in this study. The arrows indicate the fluid flow through the device, with a stagnation point formed in the geometric centre of the device (x = y = z = 0), scale bar is 100 μm

device is either assessed using the stress-optical rule or from measuring the pressure drop. The relative simplistic design of the device means it can readily be prepared at the micron scale.

Typically these devices are prepared with high aspect ratio $\sim$ 10, defined as $\alpha = d/w$, where d and w represent the depth and width of the channels, respectively.

The strain rate in these devices are dependant upon w, $\dot{\varepsilon} \approx 2U/w$, and similarly the Reynolds number determined with characteristic length w, i.e. in Eq 4.1, where $L = w$.[196–198] Where U is the flow velocity. From this relationship it is apparent that very high deformation rates can be obtained by reducing the size of the length scale and imposing large flow rates. Microfluidic cross-slot devices can therefore examine the extensional viscosity of fluids with both, low shear viscosity and small relaxation times.

The z plane in these devices is defined as the depth, normal to the xy plane. Therefore, the geometric centre of the device, the reference origin (x=y=z=0), is where the stagnation point occurs. The cross-slot devices approximate ideal planar extension, is defined by D with the components $D_{xx} = \delta v_x/\delta x = \dot{\varepsilon}$ and $D_{yy} = \delta v_y/\delta x = -\dot{\varepsilon}$, with the remaining components = 0.

From experimental studies for this type of device (where $\alpha = 5$), it is known that

the ideal hyperbolic streamlines (describing flow) are perturbed by the four cross-slot corners, with ideal flow approximated closer to the stagnation point.[173] Fluid dynamic simulations have shown that around the stagnation point the extension rate varies $< 5\%$, within a $w/16$ radius.[199] Flow velocity measurements, within a cross-slot device with smaller α (0.53), in the midplane have been found to show planar extensional flow with reasonably good agreement with expectations, over a wider radius $\sim w/4$, around the stagnation point.

It is important to note here that the flow only approximates to 2D, even for high α where the channel depth is large. The flow velocity (thus, the strain rate) through the channel depth will be subject to variation due to the no-slip boundary conditions at both the top and bottom surfaces. It has been shown previously that Dean vortices can form in the outlet channels with 3D instability flow onset, at moderate Reynolds numbers ($10 \lesssim \mathrm{Re} \lesssim 100$ for α - 0.53).[200–202] Therefore, in order to maintain a stable and symmetric flow profile the Reynolds number should be kept to a minimum to best approximate a 2D planar flow.

Extensional viscosity can be determined using a cross-slot device by determining the pressure drop across the device.[202] Typically, the pressure drop is determined from a given imposed flow rate, U where both the shear contribution (ΔP_s) and the total pressure drop (ΔP_t) is determined; ΔP_t contribution is obtained from flow through all 4 channels, and the ΔP_s contribution determined from flow around one corner (2 channels). The extensional contribution, ΔP_E can then be determined, and related to the tensile stress difference, $\Delta\tau$;

$$\Delta\tau(U) \propto \Delta P_E(U) = \Delta P_t(U) - \Delta P_s(U) \tag{4.4}$$

The strain dependant extensional viscosity can then be calculated (where $\dot{\varepsilon} \approx 2U/(w/2)$) from[203];

$$\eta_E(\dot{\varepsilon}) = \frac{\Delta\tau(\dot{\varepsilon})}{\dot{\varepsilon}} \tag{4.5}$$

This relatively straight forward determination of η_E makes this approach much more attractive compared to other geometries which rely on stagnation points or transient extensional flows, where several assumptions and/or approximations are required to calculate η_E with no shear contributions.[173,181,204,205]

4.1.3 Summary

The aim of the consortium this project is part of, is to revolutionise the inkjet printing technique so it become ubiquitous in manufacturing, where the clear advantages obtained are very desirable. However, fluids used for manufacturing purposes are complex in nature, and typically include colloidal particles in their formulation.[12,172] It has been shown, that even though there is a clear requirement for better understanding the jetting behaviour of colloidal particle dispersions, not many authors have investigated this systems in terms of inkjet printing. Most of the work in this area focusses on the extensional/jetting behaviour of polymer solutions, or particle and polymer mixtures.

Therefore in order to remedy this, the jetting behaviour of model small colloidal particle dispersions is investigated here. A microfluidic cross-slot device is also used to determine the extensional viscosity, which is then related to the observed jetting behaviour. There are not many examples in the literature where the extensional viscosity of a model colloidal particle dispersion has been determined and examined, as it has been here, particularly for the extremely high extensional rates obtained here.[206]

4.2 Methods and Materials

The following section outlines the methods used to determine the extensional rheology and jetting behaviour of p(MMA) nanoparticle dispersions.

The dispersions used throughout this study were prepared as described in Chapter 3 (Section 3.2). All dispersions containing p(MMA) particles in this chapter, are from the same batch where d_H is 62 ± 1 nm, as determined by DLS at 21 °C and a 10 mM background [electrolyte], with a monodisperse size distribution, and a zeta potential of -49 ± 2 mV, at pH ∼7. The shear viscosity of these dispersions was determined and discussed in the previous chapter.

4.2.1 Methods

4.2.1.1 Microfluidic cross-slot rheometry

The microfluidic cross-slot was prepared, and used to examine the extensional viscosity at the Okinawa Institute of Science and Technology, within the Prof Amy Shen's microfluidic group.[207] The microfluidic cross-slot device used here was designed and prepared with the aid of Dr Simon Haward and Kazumi Toda-Peters.

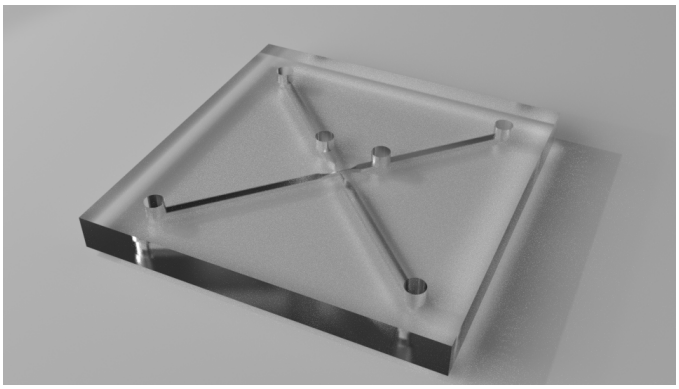

Figure 4.3: A 3D rendered drawing of the microfluidic cross-slot chip used to build the device used in this study. This drawing was created by Kazumi Toda-Peters (OIST) for this project.

Figure 4.3 shows the 3D rendered image of the cross-slot device used in this study.[208] The device was prepared by selective laser induced etching in fused silica

glass (Optostar, Japan) using a LightFab 3D Printer (LightFab GmbH). This is precise technique, with a precision of ± 1 μm in x and y direction and ± 2 μm in the z direction.

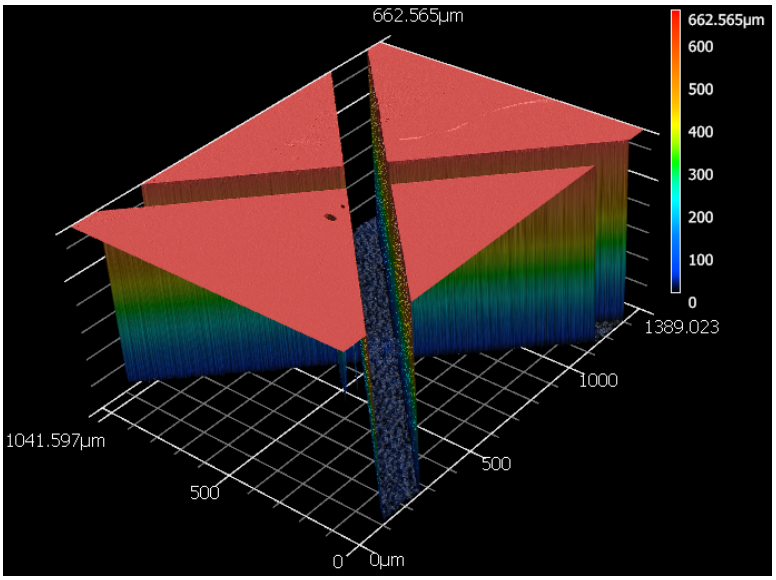

Figure 4.4: The internl cross-slot dimensions, where the channel depth is 645 μm and width is 122 μm.

The "chip" (Figure 4.3) was then attached to a glass slide using a UV cured epoxy. The inlets were attached using a soft epoxy to hold them in place, followed by a stronger bonding epoxy to keep them in place. The final device is shown in Figure 4.5. The internal channel dimensions were determined using laser profilometry with a Laser Confocal Microscope (Keyence), Figure 4.4. The channels depth and width were determined to be 645 μm and 122 μm, respectively. This has been shown previously, to provide a good approximation of 2D flow, from the relatively high α - 0.53.[200–202] This α is chosen as extremely high $\dot{\varepsilon}$ can be attained, which are in the comparable range to those exhibited when jetting.

Fluids samples tested with the device are flowed through at controlled total volume flow rates (Q), using a Harvard PHDUltra syringe pump to drive the fluid into (inlets) the device, and another pump driving the fluid out (outlets) of the device. The superficial flow velocity (U) can then be defined as;

$$U = Q/wd \tag{4.6}$$

The imposed flow rate controls the homogeneous extensional strain rate ($\dot{\varepsilon}$) on the flow axis, and is determined here with the use of micro-particle image velocimetry.

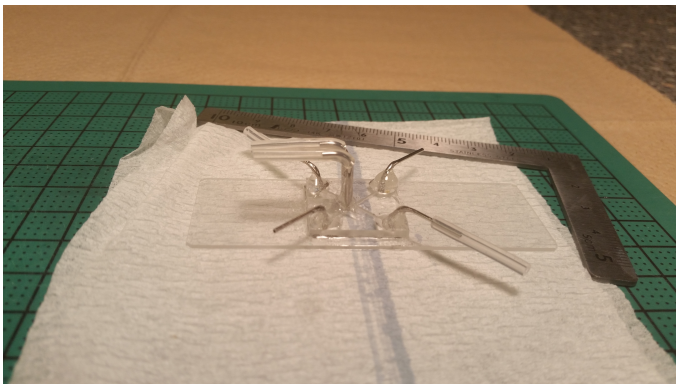

Figure 4.5: The microfluidic cross-slot device used to determine the extensional viscosity, where the channel hight/depth is 645 μm and width is 122 μm.

The flow within the device is measured quantitatively on the fluid sample, where fluorescent particles (excitation 520 nm and emission 580 nm, 0.02 wt.%) are added to enable flow visualisation. The addition of these fluorescent particles does not affect the shear viscosity significantly, but for the sake of continuity the dispersions used to determine the shear viscosity in the previous chapter all contained the same amount of fluorescent tracer particles.

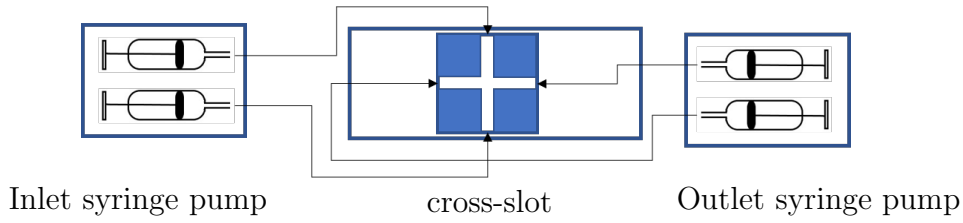

Figure 4.6: A schematic of the microfluidic cross-slot pump arrangement used to determine the extensional rheology.

A 4 x 0.13 NA objective is focussed on the device mid-plane, and the fluid illuminated using a double pulsed Nd:YAG laser (5 ns). A G-2A epifluorescent

filter is used to filter out the laser light, and the fluorescent emissions detected by a CCD array. A frame straddling CCD camera (TSI Instruments, PIV-Cam, 14 megapixels) captures the image pairs. The time separation between the image pairs is determined from the flow rate, where it should yield images with average particle displacements of $\sim$ 4 pixels. This displacement is found to be most appropriate for PIV analysis. 4 image pairs are captured approximately, every second.

The standard cross correlation PIV algorithm is used to analysis the captured images. The algorithm is incorporated within the TSI insight software, and has an interrogation area of 32 x 32 pixels and with an Nyquist criterion for analysis. The outflow velocity profile, v_x is determined along y = 0 axis and is extracted using TECPLOT 10 software (Amtec Eng. Inc.). The resulting vector fields are used to determine the $\dot{\varepsilon}$.

Pressure drop measurements were carried out using a 5 PSI pressure transducer (Honeywell), and the change in pressure recorded using a LabView code. The cross-slot device was cleaned by twice flowing through ethanol, followed by ultra pure water prior to each measurement run.

The particle dispersions prepared in this study were all found to exhibit very similar extensional viscosity behaviour, postulated to be due to the relatively small size range ($\sim$ 50 - 65 nm). Therefore, data for the same batch of particles is discussed in this study, where d_H is 62 $\pm$ 1 nm.

4.2.1.2 Inkjet printing

The jetting experiments discussed here, were carried out at the Inkjet Research Centre, University of Cambridge. The jetting rig set-up used has been used to examine several different systems.[26,169,172,177,209,210]

A 40 μm MicroFab (MF)inkjet nozzle was used to jet the particle dispersions examined in this study. The nozzle was purged with isopropyl alcohol, ultra pure water and isopropyl alcohol again between each dispersion to avoid any cross contamination. The waveform used by the MF JetDrive III controller for each dispersion was kept constant for all the experiments to ensure a fair jetting behaviour comparison for a given drive voltage. The drive voltages used to examine the dispersions here were 20 V and 30 V.

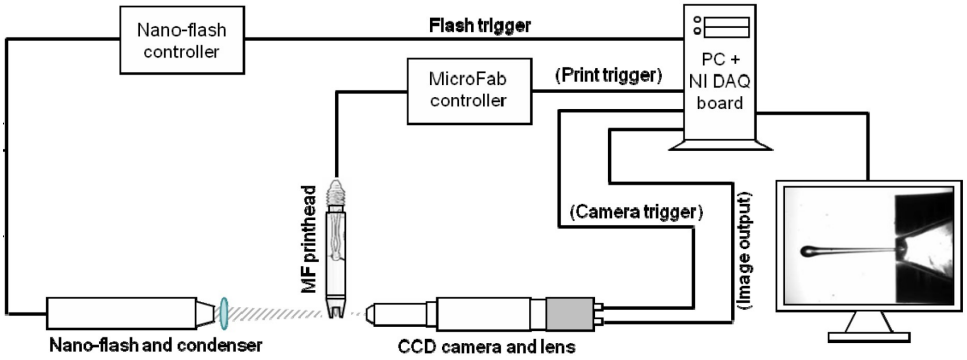

Figure 4.7: A schematic of the printing set up used to examine the jetting behaviour in this study. Taken from ref (26).

A schematic of the jetting set up used to examine the jetting behaviour is shown in Figure 4.7.[210] The jetted fluid behaviour was captured in a series of images using shadowgraph imaging, the total number defined by the user, with the ultra high speed Shimadzu HPV-1 camera. The jet in flight was illuminated using an Adept Electronics long duration spark flash lamp (20 ns). The captured images are calibrated by imaging a wire of known diameter in the jet focal plane.

The extracted images are analysed using IrfanView and ImageJ software, where each image field of view is $\sim$ 1.0 mm analogous to the real inkjet printing techniques.[26]

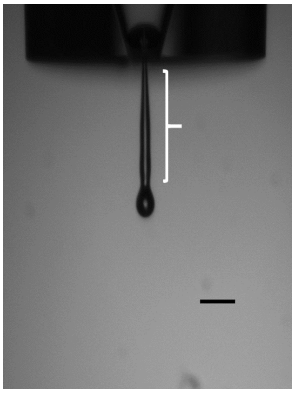

Figure 4.8: A typically obtained jetting image, specifically for $\phi_{EG,eff}$ 0.10 particle (62 nm) dispersion, from a 40 μm nozzle. Where the white super imposed comment bar defines the ligament length quoted in this study. The scale bar represent 50 μm.

4.3 Results and Discussion

4.3.1 Extensional viscosity

The extensional viscosity was determined for the various particle dispersions used in this project, from low to extremely high extensional rates in order to understand the behaviour of dispersions in an Inkjet printing system.

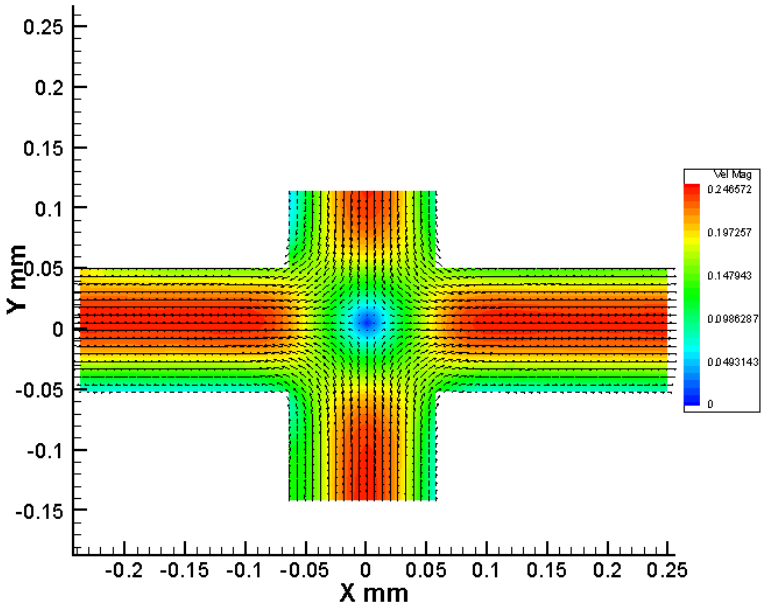

Figure 4.9: The flow velocity vector field measured using μPIV for the $\phi_{EG,eff}$ 0.17 particle (62 nm) dispersion, at $U = 0.2$ m s^{-1} (Re = 3).

Figure 4.9 shows a velocity vector field for the $\phi_{EG,eff}$ 0.17 particle dispersion, at $U = 0.2$ m s^{-1} (where Re = 3). The flow velocity at the centre of the microfluidic device can be observed to be close to 0, and the fluid stretched in the x direction as it flows out. The plot was obtained from TECHPLOT software, and can be observed to be slightly misaligned along y-axis, this is simply due to the software and how this image was extracted. The y = 0 position is actually defined as exact the middle of the outflow channel, this is where the velocity profile is extracted from: where the profile is v_x as a function of x, Figure 4.10.

v_x varies linearly with x, Figure 4.10, for any given flow rate (below Re = 10), with a constant velocity gradient equal to the extension rate, $\dot{\varepsilon} = \delta v_x / \delta x$ on the x

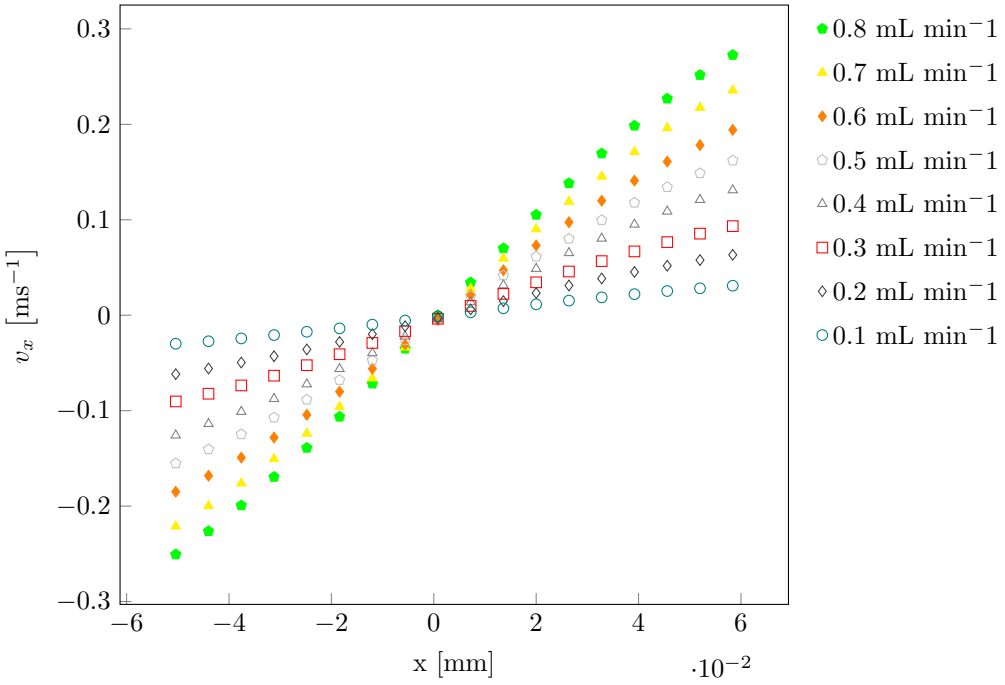

Figure 4.10: The measured outflow velocity v_x as a function of x, measured at y = 0, for the $\phi_{EG,eff}$ 0.17 particle (62 nm) dispersion (where Re $\leq$ 10)

axis.

These flow measurements were made over a range of applied flow rates for the various particle dispersions examined both, in water and the ethylene glycol:water 20:80 co-solvent. The maximum flow rates (and therefore the extensional strain) imposed upon the fluids were limited to Re = 10. Above these Re numbers, flow instabilities, from Dean vortices, were observed to arise.[200–202]

Reynolds number characterises the inertial contributions to the flow and is depend upon both the imposed flow rate and the fluid viscosity, defined for this geometry as;

$$Re = \frac{\rho U w}{\mu(\dot{\gamma})} \tag{4.7}$$

The shear rate dependant viscosity is evaluated from the viscosity data discussed in the previous chapter. It was found earlier, that the particle dispersion viscosity increases with the effective particle concentration, for the particle dispersion used in this research. Therefore, from eq 4.7, as the dispersion viscosity increases at a

given shear rate, the consequent Reynolds numbers decrease, i.e. larger flow rates can be imposed upon higher viscosity fluids before instabilities arise.

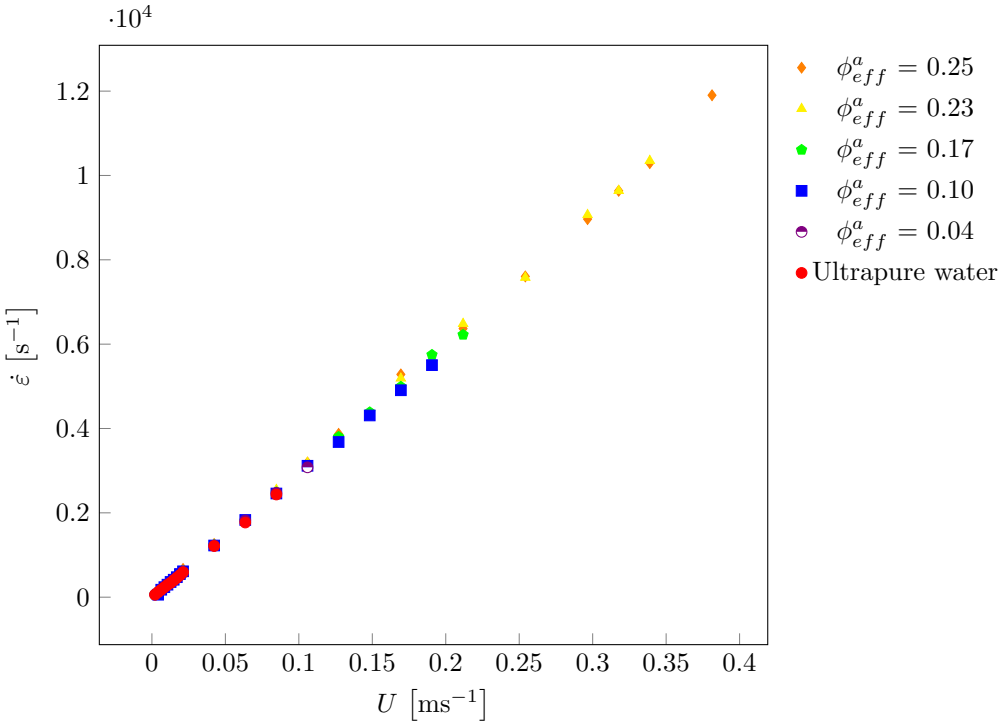

Figure 4.11: Extension rate as a function of the superficial flow velocity, for 62 nm p(MMA) particle dispersions at a range of ϕ^a_{eff}, determined at 21°C.

Both of the particle dispersion series, termed ϕ^a_{eff} (for particles dispersed in water) and $\phi_{EG,eff}$ (for particles dispersed in the ethylene glycol:water 20:80 co-solvent) in the previous chapter, were examined using the microfluidic cross-slot device. Figure 4.11 shows the extension rate as a function of the superficial flow velocity, determined for most of the ϕ^a_{eff} series concentrations examined thus far except for ϕ^a_{eff} 0.31.

At this concentration, the particle dispersion was found to be very difficult to examine. When flowing through the device, the dispersion caused the tubing connections to fail, with leaks observed during the measurements. It was postulated to be due to the device inlets being unable to cope with increased pressures due to the highly viscous nature of the fluid. The same concentration for the particle dispersed in the ethylene glycol:water 20:80 co-solvent, was successfully characterised using

this technique. Although the ethylene glycol:water co-solvent series was examined first, so perhaps the failure of the previous dispersion was due to gradual wear on the inlet, which then failed.

From Figure 4.11 it can be observed that the ϕ^a_{eff} series dispersions all show a linear dependence of the $\dot{\varepsilon}$ on the imposed superficial flow rate. This implies the dispersions all closely match the expectations for a Newtonian fluid. A similar linear dependence upon the imposed flow rate is observed for the $\phi_{EG,eff}$ series dispersions, Figure 4.12.

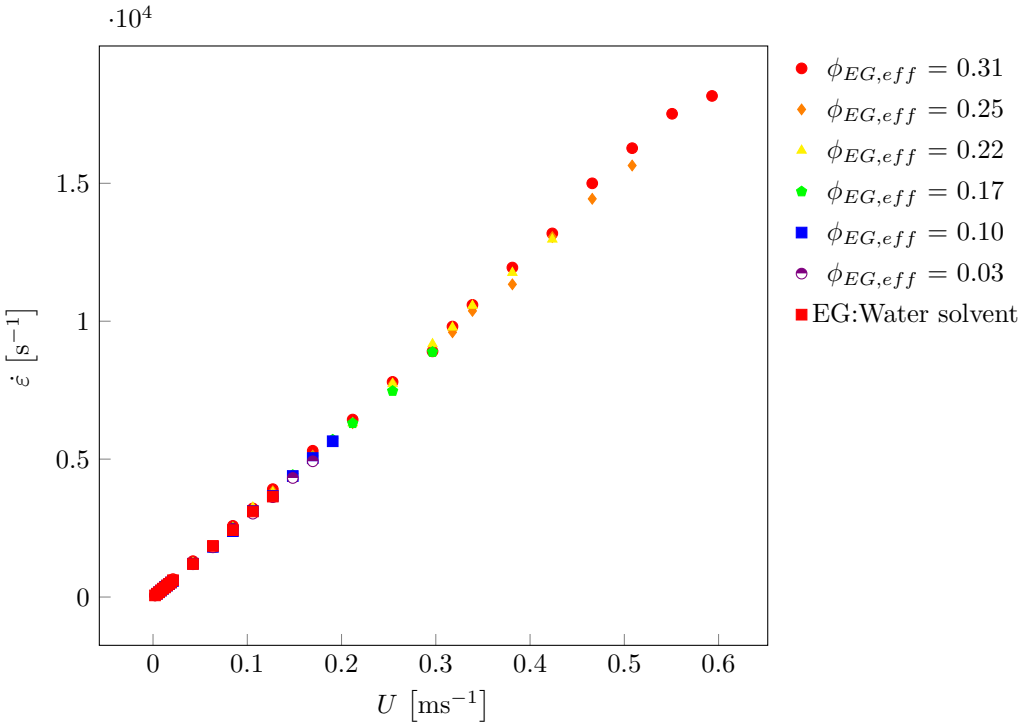

Figure 4.12: Extension rate as a function of the superficial flow velocity, for 62 nm p(MMA) particle dispersions at increasing ϕ_{EG}, determined at 21°C.

The extensional viscosity of these particle dispersions can then be determined from the pressure drop measured across the device. ΔP_t is measured when a sample is flowed through all 4 channels, and ΔP_s (the shear contribution) is determined from flowing the sample around one corner only i.e. flowed through only two channels (from Figure 4.2, where the samples is flowed through only one inlet and outlet).

The pressure drop for both the ϕ^a_{eff} and $\phi_{EG,eff}$ series was determined at various flow rates (at Re $\leq$ 10), and the subsequent η_E determined using eq 4.5. For ϕ^a_{eff} series, the particle dispersions are found to exhibit a extension thinning extensional viscosity, Figure 4.13. The dispersion viscosity at a given $\dot{\varepsilon}$ decreases with particle concentration, similar to the relationship observed when the dispersions are sheared, Figure 3.12. For ϕ^a_{eff} 0.10 the η_E seems to plateau above $\sim$ 2500 s^{-1}. This is unexpected, and possibly due to some error in the measurements used to determine the data set, most probably from the pressure drop measurements where the pressures are small or perhaps from some blockage within the tubing used to pump the dispersion into the device.

For relatively inelastic shear thinning fluids, the η_E is known to follow the shear viscosity response, once the two deformations and viscosities are accounted for using the relevant factors.[211,212] The particle dispersions used in this study are not particularly elastic, Figure 3.16 & 3.14 and can be expected to exhibit extension thinning behaviour.

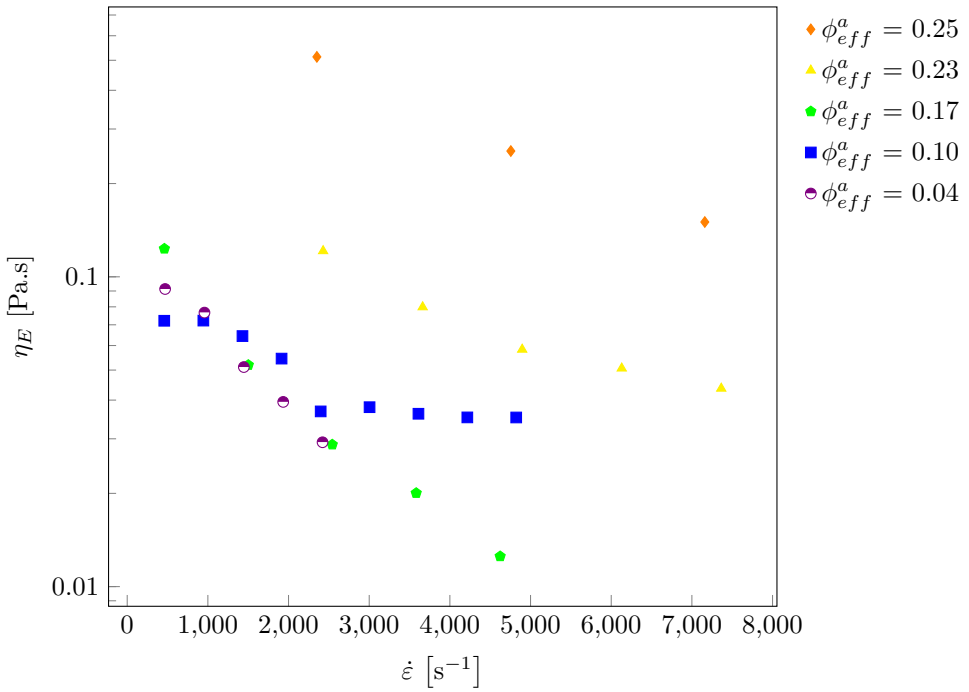

Figure 4.13: The extensional viscosity of 62 nm p(MMA) particle dispersions at a range of ϕ^a_{eff}, determined at 21°C.

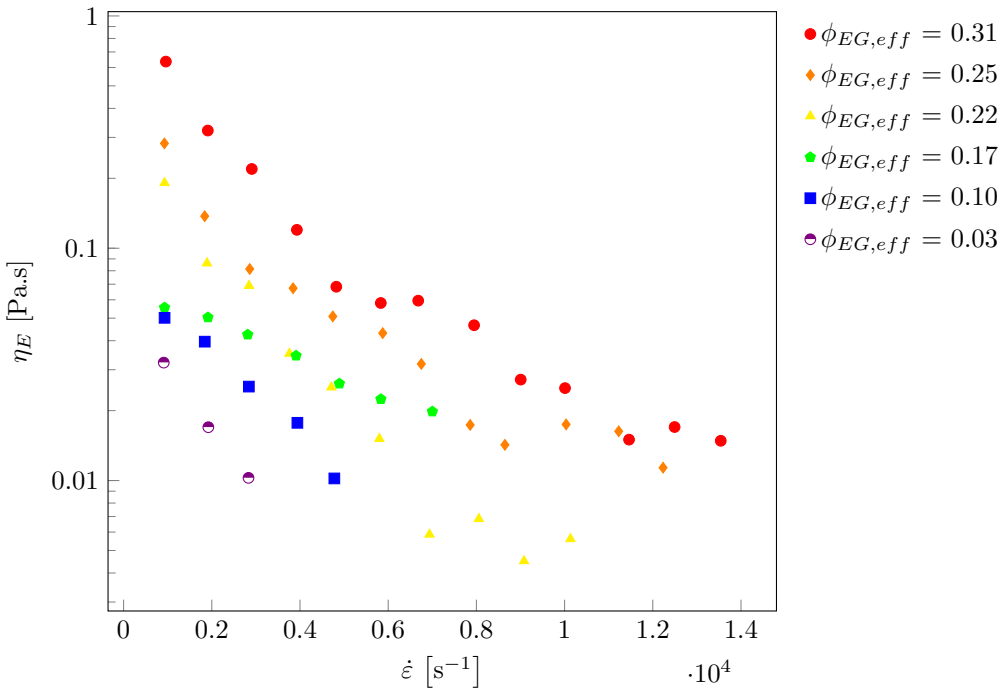

Figure 4.14: The extensional viscosity of 62 nm p(MMA) particle dispersions at increasing ϕ_{EG}, determined at 21°C.

The extensional viscosity for the whole of the $\phi_{EG,eff}$ series of particle dispersions is found to better adhere to the expected extensional thinning response. The viscosity is a little noisy, though overall decreases with the $\phi_{EG,eff}$, similar to the shear viscosity response for these dispersions.

The extensional thinning behaviour is due to the particle micro structure within the dispersions, similarly to that discussed for the shear viscosity response. Where, the viscosity increases with the particle concentration (for both $\phi_{EG,eff}$ and ϕ^a_{eff} systems), as the inter-particle distances become smaller, Figure 3.19. And, with the decrease in inter-particle distances there is an increased order within the system, where the particles are thought to form more ordered structures. The applied deformation, $\dot{\varepsilon}$ in this case, causes the structure within the dispersions to breakdown and is observed as a thinning response.

The extremely high $\dot{\varepsilon}$ range attained for these measurements, are significantly large relative to investigations previously using this techniques.[173] However, the instabilities arising at higher Re, where the extensional rate would be in the order

comparable to the inkjet printing technique ($\sim 10^6$ s^{-1}), mean this is the maximum range attainable using this device. Note, these instabilities lead to vortices, and an unsymmetrical flow profiles such that reproducible velocity profiles can no longer be attained.

4.3.2 Jetting behaviour

The jetting behaviour was determined using a 40 μm MicroFab nozzle, for the various particle concentrations from both the ϕ^a_{eff} and $\phi_{EG,eff}$ colloidal dispersion series.

Several phenomena observed during jetting are examined here, as a function of the particle concentration. These include the ejected drop speed, defined here as the drop velocity over 1 mm length scale. Break off time, which is defined as time at which the jet ligament detaches from the nozzle meniscus. Finally the number of satellite drops for a given jet is calculated at the point where drop speed is measured, i.e. when the main drop has travelled 1 mm.

The jetting behaviour was examined for both the ϕ^a_{eff} and $\phi_{EG,eff}$ series of particle dispersions. It must be mentioned here, the ϕ^a_{eff} series particle dispersions were particularly difficult to examine using this set up. Indeed for $\phi^a_{eff} > 0.17$, the dispersions were found to dry within the nozzle either during the measurement or immediately as the nozzle is loaded.

The $\phi_{EG,eff}$ was found to be more amenable for jetting experiments, most likely due to the slight decrease in the surface tension.[210] However, the surface tension in these dispersions is only sightly reduced (62.5 mN/m), relative to the surface tension for the ϕ^a_{eff} series (72.8 mN/m). It can be observed however, that it is reduced sufficiently to decrease the formation of satellite drops at a 20V drive voltage compared to when jetted at a 30V drive voltage, Figure 4.15.

However any satellite drop formation is highly undesirable and must be kept to a minimum for good jetting behaviour. These drops are easily misdirected by aerodynamic and electrostatic forces, thereby reducing the quality of the final print.[209] Here, at the lower drive voltage of the two used, where the drop speed is $\sim$ 6-7 ms^{s-1}, is when these dispersions are found to produce the least amount of satellite drops. It was previously shown that shear thinning fluids can rapidly recover a higher viscosity once jetted, and thereby delay satellite formation up to a 0.8 mm

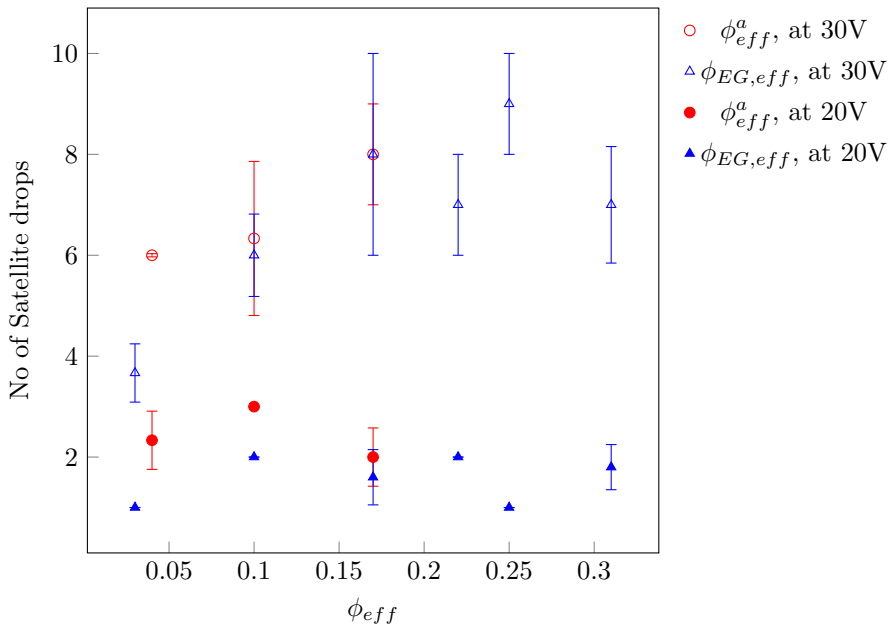

Figure 4.15: Formation of satellites for particle dispersions in both pure water and an ethylene glycol:water 20:80 co-solvent, determined using a 40 μm nozzle, at both a 20V and 30V drive voltage.

jet distance.[169] However, although the dispersions used here have been shown to be strongly shear thinning, formation of satellite drops is still observed. This is most probably due to fluid being unable to recover a high viscosity in time to avoid satellite drop formation.

Increased particle concentrations are known to increase the drive voltage required to jet the dispersion due to the increased viscosity.[210] However, the dispersions used in these study are found to be readily jetted at relatively low drive voltages, with no significant difference observed with increasing ϕ_{eff}. This is most probably due to the shear thinning nature of this dispersions. Both the extensional and shear viscosities of the particle dispersions used in these studies are observed to thin over the applied deformation rate (Figures 4.13, 4.14, 3.12, 3.15).

Thus, at the exceedingly large extension rate applied upon jetting ($\sim 10^6$ s^{-1}) these dispersions almost certainly attain an extremely low Newtonian viscosity profile where they are readily jet-able using a relatively low drive voltage. It is most likely that the dispersions attain the solvent viscosity profiles (i.e water and

EG:water 20:80 co-solvent) at these deformation rates The ejected drop speed was similarly observed to be relatively unaffected with increasing ϕ_{eff}, for the $\phi_{EG,eff}$ dispersion series, jetted at both 20V and 30V drive voltage, Figure 4.16.

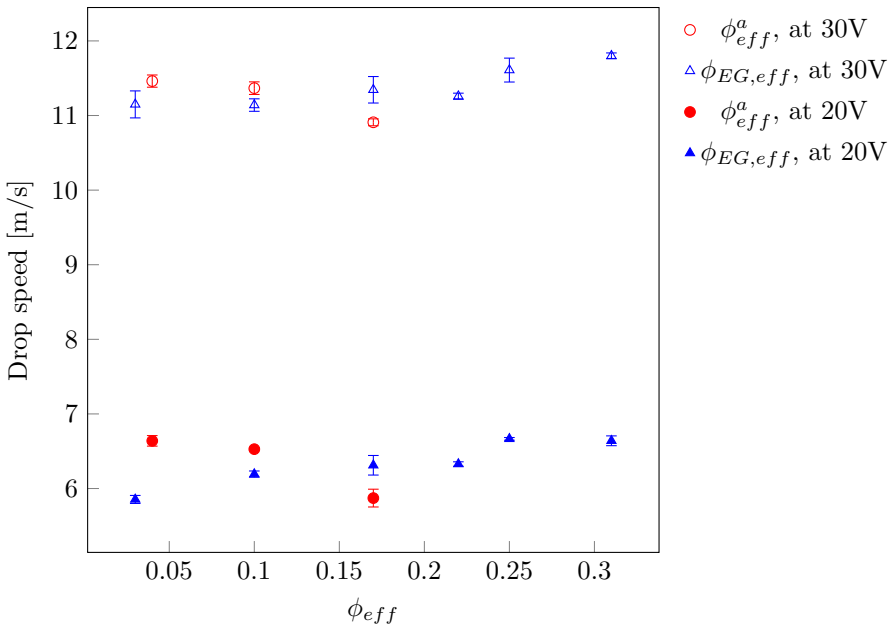

Figure 4.16: Change in drop velocity for particle dispersions in both pure water and an ethylene glycol:water 20:80 co-solvent, determined using a 40 μm nozzle, at both a 20V and 30V drive voltage.

For the ϕ^a_{eff} dispersion series, drop speed can be seen to be decreasing with increasing ϕ_{eff} at both drive voltages tested here, Figure 4.16. However, the slight trend observed is ≤ 0.5 m/s, and cannot be considered as a significant effect. However, a slight trend can be observed in the break off time, Figure 4.17. It is observed to increase with the ϕ_{eff}. It is only for this particle series that the increasing viscosity with ϕ_{eff} is observed to affect the jetting behaviour.

For the $\phi_{EG,eff}$ dispersion series, again no significant difference is observed in the jet break up time with increasing particle concentration at both the drive voltages examined.

Overall, the lack of any significant effects on the observed jetting behaviour is somewhat surprising. From the ϕ_{eff} viscosity contribution, the jetting was expected to, at the very least require a higher drive voltage. However, it seems these colloidal

dispersions can be readily jetted, and exhibit a relatively Newtonian response to the applied deformation in the nozzle.

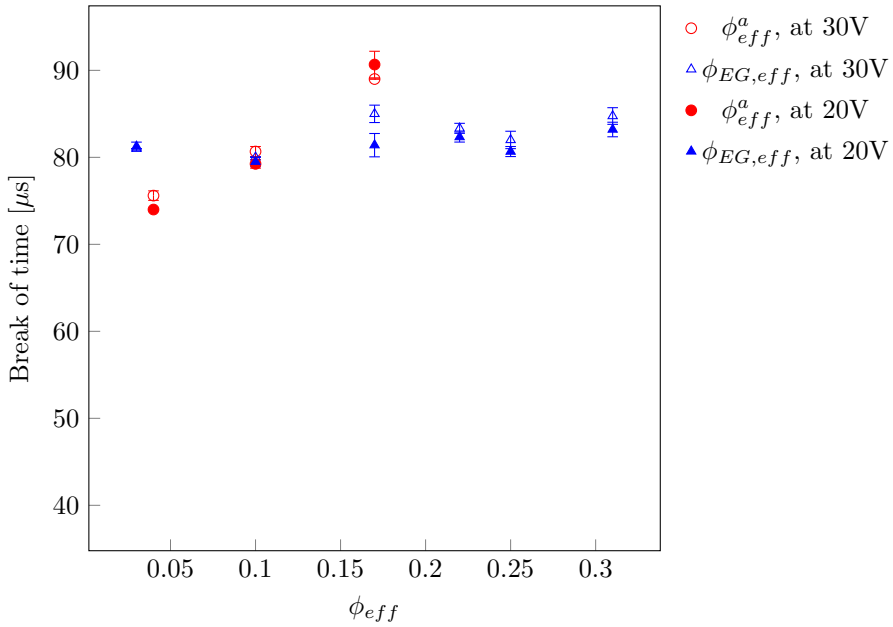

Figure 4.17: The jet break up time for particle dispersions in both pure water and an ethylene glycol:water 20:80 co-solvent, determined using a 40 μm nozzle, at both a 20V and 30V drive voltage.

The extensional viscosity determined using the microfluidic cross-slot device, similarly predicts that at the extremely high deformation rates when jetting ($\sim 10^6$ s^{-1}) mean all of the particle dispersions likely attain very low viscosities, most probably on the order of the parent solvent viscosity. This is true for all the particle concentrations examined, and is further confirmed by the similarity in the jetting behaviour for all the dispersions tested.

4.4 Conclusions

The extensional viscosity of the particle dispersions used throughout this project was determined using a microfluidic cross-slot device. Measurements such as these for colloidal particle dispersions are rarely found in the literature, and to the authors knowledge is the first reported experimental dataset for colloidal particle extensional viscosity.

The particle dispersions are observed to show a extension thinning extensional viscosity, similar to the shear viscosities observed for the colloidal particles in the previous chapter. Where a higher viscosity is found for larger effective volume fraction of particles, for the dispersions in both a pure water solvent and in the ethylene glycol:water 20:80 co-solvent. The two viscosities are related, in that they are both due to the breakdown of the particle micro structure within the dispersion. A slight discrepancy was found for the effective volume fraction 0.10 dispersion, in the pure water solvent, where the extensional viscosity is observed to plateau above $\sim$ 2500 s^{-1}. This could not be explained, and is postulated to be most probably due to an error in the measurement (possibly from the pressure drop measurements, where the pressure drops for this dispersion were small and could perhaps have been affected by a blockage with the tubing connectors).

The particle dispersions were then used to examine the jetting behaviour as a function of the particle concentration. No significant effect due to dispersion viscosity or the particle content within the dispersion was observed. This is most likely thought to be due to the dispersions most probably behaving as Newtonian fluids at the extremely high deformation rates applied in the nozzle. In that, at these deformation rates the particle structure within the fluid breaks down and the dispersions attain and exhibit the solvent viscosity.

This was indeed apparent from the extensional viscosity determined using the microfluidic cross-slot device, where a extensional thinning response is observed. Although the device cannot attain deformation rates in the order expected when jetting, the trend in the viscosity data indicates an overall extensional thinning response. This therefore is a good indication that the particle dispersions most likely thin to extremely small viscosities, and most probably attain viscosities close to the parent solvent viscosity.

The microfluidic cross-slot was found to be an extremely useful tool to quickly examine a given fluid extensional viscosity response, which is a good indicator of the fluid behaviour upon jetting. It can be used to examine a range of fluids quickly, prior to testing fluids using an inkjet printing set-up. This is a valuable tool to avoid complications when testing complex fluids suitable for inkjet printing, and provides a good overview of what can be expected, without any issues arising from blockages or fluids drying in the nozzles. The device must be further tested with other fluids/dispersions to further confirm this claim, but it is postulated here that the device would indeed be a useful tool for this purpose.

Chapter 5

Conclusions and Future directions

5.1 Project Summary and Conclusions

This project has explored how particle dispersions affect the inkjet printing process, from preparing a model particle system to investigate this to the rheological profiles of a range of particle dispersions.

The importance of preparing high solids content latex particles was highlighted, and a novel approach to the problem discussed.

The chain transfer mediated emulsion polymerisation process was tuned to prepare a range of p(MMA) nanoparticles, from 40 - 70 nm, with a high solids content, 40 wt.%. Although the CTA used does not create a 'living' polymer system, as is typically the case when using a CTA, it is still found to significantly improve the final particle size, and size distribution. A small CTA concentration range is found to be sufficient to subtly, but significantly enhance the particle nucleation efficiency during the polymerisation process. This enhanced nucleation efficiency is thus responsible for the monodispersity, and a reduction in particle size, at these high solids concentrations. Use of a higher CTA concentration leads to loss of monodispersity, as well as increased coagulate formation and polydispersity.

Other component concentrations with the synthesis system are also tuned to prepare smaller particle sizes, though the surfactant concentration is only reduced to the minimum concentration at which stable particle with the desired properties are still prepared. The presence of surfactant greatly affects the surface tension of the

resulting dispersion, and is considered a deleterious for most application, including for Inkjet printing. Thus, it is postulated that if the surfactant concentration is increased a reduction in particle size will be observed.

The stability of the particle dispersion was also examined as a function of the pH, where over the pH range tested, the particles were found to respond with similar zeta potential values and no significant decrease in overall stability observed. This was due to the presence of surfactant molecules on the particle surface. Where, through dialysis most of the surfactant is removed from the bulk of the dispersion but not the particle surface. This was due to the surfactant used, SDS, which binds tightly on the particle surface, where the particles exhibit a positive surface potential from the initiator employed during synthesis. From surface tension measurements, it is found that after dialysis SDS no longer affects the surface tension of the particle dispersion, thus implying surfactant present within the dispersion is exclusively located on the particle surface.

The shear viscosity of a range of particle concentrations in both a pure water, and ethylene glycol:water, 20:80, co-solvent was examined. The viscosity and non-linearity were both found to increase with the particle concentration, and are well described by the Carreau model. The inter-particle repulsion was shown to become more significant with increasing concentration, which forced particle into close contact, and thus lead to an increase in viscosity. Another effect of increasing particle concentration, is the formation of a particle configuration within the dispersion, where the long range repulsion interaction drives particles to an inter-particle distance where the smallest potential is felt. This leads to an overall ordering within the particle dispersion, which is required to rearrange when shear is applied to the dispersion. At a high enough shear, the structure can no longer be held and breaks down, and is observed as a decrease in the viscosity with increasing shear (shear thinning). These dispersions were also examined for any sedimentation, and were found to be very stable, with little sedimentation observed. A reasonably good zero shear viscosity fit is obtained, with predicted viscosity from the Krieger-Dougherty model.

The prepared samples, when dialysed were found to be extremely viscous, and almost gel-lie in appearance. This was due to the increase in the effective volume fraction, due to electrolyte and surfactant removal from dialysis. Where the effective

particle size is much larger from the extended electric double layer when electrolyte is removed form the system. The effective volume fraction was then varied and the corresponding viscosity curves further providing evidence of this - with a decrease in suspension viscosity observed with decreasing effective volume fraction.

The freshly dialyses particle dispersions were found to contain crystal structures, that are highly undesirable. These were found to be due to the increased order within these dispersions, where formation of the crystals leads to an net gain in the entropy of the system relative to the corresponding particle dispersion configuration. The formation of these crystals was countered with addition of a small amount of electrolyte, by reducing the electric double layer until this effect is no longer observed.

The extensional viscosity of the particle dispersions was examined using a cross-slot device. The extensional viscosity of colloidal dispersions such as the ones used in this project has not been previously reported, using this technique nor at the deformation rates examined. Here an elongation thinning (hence non-Newtonian) extensional viscosity was observed due, similarly to the shear viscosity observations, to a breakdown in the particle network.

The particle dispersions were then examined for their jetting behaviour, as function of the effective particle concentration, for both dispersion series examined in this project (particles dispersed in pure water, and ethylene glycol:water co-solvent). A surprising result was observed here, where no apparent jetting dependence on the effective particle concentration was observed. It is postulated here that this observation has not been previously shown, as colloidal dispersions such as the ones used here are rarely used to examine the jetting behaviour.

5.2 Future Directions

There are numerous avenues which could be followed to build upon the work from this research project. For example, it would of fundamental interest to expand upon the synthesis process outlined in Chapter 2. This could be further examined in terms of the monomers used for synthesis, to create a range of latex nanoparticles that could be prepared using this route. It could conceivably argued that styrene

should behave similarly to methyl methacrylate, and similar results should be expected when preparing particles using this route. It would be of particular interest to examine whether poly(N-isopropylacrylamide) and poly(dimethylaminoethyl methacrylate) particle could be prepared using this route, as the resulting particles could be further tailored to exhibit a pH or thermal response. From changing the monomer, the CTA type would also have to be varied to suit each monomer, and similarly a CTA concentration study for each particular monomer determined.

For further study of the different polymer particles proposed above, it would be of experimental interest to prepare these in an EG:water co-solvent, as in this manner model particle dispersions can be prepared easily in the solvent most suitable for examining jetting, as well for inkjet printing. This could further be expanded upon to examine the jetting behaviour in the various other solvents known to be suitable for inkjet printing, including diethyl phthalate.[172]

Directly moving forward from this project, it would be of interest to further investigate the maximum jet-able particle concentrations. This could be achieved by tuning the particle preparation method further, to produce small particles at even higher concentrations. The other route to even higher particle concentrations, as mentioned above would be to prepare the particle directly within the EG:water co-solvent, for this series of particles.

Other systems to further investigate include colloidal particles and free polymer mixtures. These systems would provide an invaluable insight into whether the addition of free polymer could enhance the jetting behaviour to reduce formation of satellite drops. The addition of free polymer to particle laden fluids has already been proven to effectively suppress the coffee ring effect usually observed when drying a drop of particle laden fluid.[213] This is when the free polymer concentration increases, upon solvent evaporation/drop drying, to the concentration required to induce depletion flocculation, where the effect can be used to trap particles prior to ring stain formation, and therefore avoid the coffee ring stain. Thus, it would be of topical interest to determine if the addition of free polymer to particle laden fluids similarly improves the jetting behaviour.

Appendix A

Appendix

A.1 Supplementary Information

Conventional Emulsion Polymerisation - Kinetics

Emulsion polymerisation is a form of free radical addition polymerisation. In principle these reactions are comprised of three steps, initiation, propagation and termination.[46–49] During the initiation stage, free radicals are generated from an initiator, which react with the unsaturated monomer initiating polymerisation. The species formed from this is also a radical, i.e. an active monomer which then further reacts with other monomers thus propagating into a growing polymer chain. These chains are terminated by free electron coupling which destroys the radical and the activity of the propagating chain.

The initiation step has two stages, free radical production and monomer initiation. Commonly initiators produce free radicals either by thermal dissociation (homolysis due to heat) or by redox reactions (electron transfer). Thermal dissociation initiators are normally used for emulsion polymerisation.

$$I \xrightarrow{k_d} 2R^{\cdot} \tag{A.1}$$

Shown above is the homolytic cleavage of the initiator, I producing 2 free radicals, $R^{\cdot}$ with the rate constant, k_d for initiator dissociation. The rate of dissociation, R_d is given by,

$$R_d = 2fk_d[I] \tag{A.2}$$

Where f is the initiator efficiency, which is the fraction of the free radicals, $R^{\cdot}$ that successfully reacted with a monomer, and $[I]$ is initiator concentration. The factor 2 comes from the 2 free radicals produced from each initiator molecule. f is normally $\sim$ 0.3-0.8 due to wasted reactions and varies with initiator type and concentration. The second stage of the initiation step monomer(M) initiation for chain growth occurs as shown below;

$$R^{\cdot} + M \xrightarrow{k_i} RM^{\cdot} \tag{A.3}$$

Where k_i is the initiation rate constant and $RM^{\cdot}$ is the active centre. The monomer initiation stage is much faster than the initiator dissociation stage, therefore the initiator dissociation stage is the rate determining step for the initiation step. This implies that the rate of initiation, R_i is equal to the rate of dissociation, R_d;

$$R_i = 2fk_d[I] = R_d \tag{A.4}$$

The propagation step is where the active centre is grown into a polymer chain;

$$RM^{\cdot} + nM \xrightarrow{k_p} P^{\cdot}_{n+1} \tag{A.5}$$

Where n monomer units are added to the active centre, $[RM]^{\cdot}$ to create a polymer chain, P_{n+1} with a propagation rate contestant, k_p. The monomer available for polymerisation is consumed in the initiation and propagation steps. Therefore the rate of polymerisation, R_p is the rate of monomer consumption and is given by;

$$R_p = -\frac{d[M]}{dt} = k_i[R^{\cdot}][M] + k_p[M^{\cdot}][M] \tag{A.6}$$

Where M is the monomer concentration, $[R^{\cdot}]$ is the concentration of primary free radicals, and $[M^{\cdot}]$ is the concentration of all activated monomer units (or oligomers) with any chain length. The amount of monomer consumed in the initiation step is negligible compared to that used in the propagation, and the rate of polymerisation can then be simplified to;

$$R_p = k_p[M^{\cdot}][M] \tag{A.7}$$

The termination step is where the propagating polymer chain is terminated either by recombination or disproportionation, both of which involve the propagating chain reacting with either another propagating chain or a free radical.

Recombination is the coupling of two propagating chains to form a single chain, with recombination termination rate constant, k_{tr};

$$P_n^{\cdot} + P_m^{\cdot} \xrightarrow{k_{tr}} P_{n+m} \tag{A.8}$$

Disproportionation, though it rarely occurs, is when a propagating chain extracts a proton from another propagating chain forming both a saturated and an unsaturated chain, with a disproportionation termination rate constant, k_{td};

$$P_n^{\cdot} + P_m^{\cdot} \xrightarrow{k_{td}} P_n + P_m \tag{A.9}$$

The overall termination rate constant is then given by;

$$k_t = k_{tr} + k_{td} \tag{A.10}$$

Termination can also occur by other means, including addition of an inhibitor or retarder which terminate a propagating chain and forms another radical. This new radical is unable to or has little ability to grow a propagating chain. Another reaction affecting termination, where a proton is extracted from a substance present in the reaction mixture such as an impurity, additives, a polymer, monomer, solvent etc. to give a new radical which may or may not act similarly to the primary radicals and form an active centre followed by a propagating polymer chain or may not form anything; this is known as a chain transfer reaction, where specific molecules designed to form new active centres are called chain transfer agents (CTA). These are designed to terminate a propagating chain and form a new radical. This radical then acts similarly to the primary radical and forms an active centre followed by a propagating polymer chain (impact on kinetics, and mechanism of the use of such molecules is discussed in more detail in section 2.1.4);

$$P_n^{\cdot} + ZK \rightarrow P_nK + Z^{\cdot} \tag{A.11}$$

Where ZK is a chain transfer agent. The new radical could affect the rate of polymerisation if the reactivity is not similar to the primary radicals. Usually the propagating chain is terminated by proton extraction from the CTA, which then creates a new reactive radical, $Z^{\cdot}$.

Kinetically free radical polymerisations operate under steady state conditions, during the propagation stage. This is where rate of initiation is equal to the rate of termination, which implies an overall constant concentration of the active centres (the propagating polymer chains, $M^{\cdot}$);

$$R_i = R_t = \frac{d[R^{\cdot}]}{dt} = 2k_t[M^{\cdot}]^2 \tag{A.12}$$

However in practice, the steady state conditions are only achieved after an initial induction period ($\sim$ few seconds), which then means the above expression can be rearranged to;

$$[M^{\cdot}] = \left(\frac{R_i}{2k_t}\right)^{1/2} \tag{A.13}$$

Which can then be used to obtain a general expression for the rate of polymerisation, by combining equations A.7 & A.13;

$$R_p = k_p[M]\left(\frac{R_i}{2k_t}\right)^{1/2} \tag{A.14}$$

The derived expression implies that the rate of polymerisation depends on the square root of the initiation rate, which can again be rearranged, with the expression derived for the rate of initiation (equation A.4), to show the rate of polymerisation depends on the square root of the initiator concentration;

$$R_p = k_p[M]\left(\frac{fk_d[I]}{k_t}\right)^{1/2} \tag{A.15}$$

Conventional Emulsion Polymerisation - Main components

Emulsifier

Emulsifiers play a crucial role in emulsion polymerisation, and have been covered earlier, Section 1.4. They are required for a number of functions, including the ability to generate micelles and reducing the interfacial tension between the hydrophobic phase (monomer) and aqueous phase. These then allow the monomer to be dispersed, with agitation into the aqueous phase. Emulsifiers also stabilise the large monomer droplets, which act as a monomer reservoir during polymerisation. The latex particles are stabilised by the emulsifier both during growth and in the final particle dispersion.

Initiator

Emulsion polymerisation is a free radical reaction, and therefore requires the free radicals available to enable the reaction to proceed, Section 2.1.2. The initiator is the source of these radicals, and forms them either by thermal dissociation or a redox reaction. Persulfate based initiators are an example of a thermal dissociating water soluble initiator and produce radicals in the following manner[67];

$$S_2O_8^{-2} \xrightarrow[\text{heat}]{} SO_4^{\cdot -1} + SO_4^{\cdot -1} \tag{A.16}$$

Organic peroxides are also thermal dissociating initiators, however these are oil soluble initiators.[214] They behave similarly to persulfate initiators;

$$H_2O_2 \xrightarrow[\text{heat}]{} OH^{\cdot} + OH^{\cdot} \tag{A.17}$$

$AIBN$ is a commonly used oil soluble initiator.[60] It dissociates thermally as such;

$$RN = NR_x \xrightarrow[\text{heat}]{} R^{\cdot} + R_x^{\cdot} + N_2 \tag{A.18}$$

Another interesting type of initiator available for such a purpose is one that acts as both an initiator and a stabiliser.[215] These have been proven to work well during polymerisation without the use of any additional stabiliser.

Reaction medium

Water is the most common solvent used where possible for most reactions, including for emulsion polymerisation. It is the best solvent for such a purpose as it is relatively inert, has low viscosity, is cheap and very environmentally friendly. Other solvents commonly used for emulsion polymerisation are usually mixtures of water and a volatile solvent.

Monomer

A wide variety of monomers are polymerised to create their subsequent polymers, including styrene, methyl methacrylate, acrylate ester, etc.[51,57,65–69,74] The chemical and physical properties of a monomer can have a marked effect of the polymerisation process. See section 1.3.1 (Section 1.3.1) for further information.

Emulsion polymerisation types

The routes mentioned in Sections 2.1.2-2.1.4 can be further broken down to clarify the method used to obtain the final polymer; batch, semi-continuous or continuous polymerisation. These are based on how the particle growth stage, and the completion stage are affected[216];

Batch synthesis process; this method is the simplest one available when preparing polymers.[65–70] It is a one pot synthesis method, where all the ingredients are added to the reaction vessel, under agitation. This is then heated to the required temperature, under continuous agitation, and the polymerisation begins once the initiator is added/system reaches the initiator dissociation temperature. The polymerisation is then allowed to proceed until the desired conversion is achieved. The variables affecting this method are the type/speed of agitation, reaction vessel design, and the temperature (outside of the ingredients of course). The polymerisation behaviour here behaves as discussed earlier in the emulsion polymerisation section (Section 2.1.2), with 3 clearly defined stages observable. This method is typically used in academia, rather than industry, to discern the effect of certain ingredients, and the mechanism & kinetics on the final polymer.

Semi-continuous synthesis process; this method is, generally the method of choice for industrial applications and is also employed in academia when required.[107,217–226]

It can be broken down into 3 steps, the seeding, feeding and finishing steps. The seeding step is where a given amount of monomer, emulsifier, solvent and initiator are added and the polymerisation allowed to proceed for a given time (seeding time), to produce the nucleating particle centres. The feeding step begins once these have formed, and more monomer, emulsifier and solvent are fed into the reaction vessel. Two feeds are employed, where one contains monomer/emulsified monomer and the other, the emulsifier feed (surfactant/s, solvent). The difference between the two is the total emulsifier concentration; initiator can either be all added during the initial seeding step or fed continuously with the emulsifier feed. These feeds can be added at any given time or at any given rate, thereby significantly affecting the reaction mechanism & kinetics. Generally a monomer flooded or monomer starved strategy is used. For the former, monomer is added to the reaction a a higher rate than the maximum polymerisation rate possible in the reaction. Therefore the monomer then forms monomer droplets, and act as monomer reservoirs thereby validating the kinetics and mechanism discussed in the particle growth stage discussed earlier (Section 2.1.2). For the second strategy, monomer starved, the mechanism and kinetics for the completion stage are valid; where the added monomer migrates directly to the growing particles, enabling the particles to attain their maximum size. This is followed by the finishing step, where the reaction is left to polymerise for a given time following once the feeding step is complete. This ensure very little un-reacted monomer in the final dispersion. This technique has been used effectively in the past to prepare particle suspensions with a high solids content, while maintaining a small particle size.

Continuous synthesis process; this method is designed for production of significantly large volumes of polymer with a highly uniform final product.[54,55,216,227] The method involves continuously feeding in the initial polymerisation ingredients while simultaneously removing product, thus at any given the total volume undergoing polymerisation in the system is constant. Usually one of two reaction vessel types are used for such reactions, a tubular or tank reactor. Of the two, the later is often more favourable, as overall, it is the more efficient route. Tubular reactors require extremely long lengths of tubing for the reaction mixture to flow through; the reaction mixture is fed into the tubes and the product collected once the mixture undergoes heating and polymerisation. However, this type of reaction vessel is not

favoured as it has poor mixing, it very difficult to clean, and of course if there are any blockages it brings the synthesis to a stop. On the other hand when using a tank reactor, the initial ingredients are fed into a continuously stirring tank, and the final product removed simultaneously. The reaction mixture is stirred at such a rate that the mixture is homogeneous at any point. Depending on the properties required of the product, there may be just a single reactor or several leading into each other; where the first may be used to prepare the initial emulsion which is then fed into a following tank for the polymerisation step, then into another tank to either reach completion or for collection. Polymerisations in these systems are controlled by the residence time, i.e. the total time the reaction mixture remain in the system. In that conversion, number of particles, particle size and the polydispersity all depend on the residence time.

References

[1] *I4T Project*, https://www.ifm.eng.cam.ac.uk/research/irc/i4t/about/.

[2] B. Derby, *Annual Review of Materials Research*, 2010, **40**, 395–414.

[3] C. Williams, *Physics World*, 2006, **19**, 24–29.

[4] P. Calvert, *Chemistry of Materials*, 2001, **13**, 3299–3305.

[5] R. D. Boehm, P. R. Miller, J. Daniels, S. Stafslien and R. J. Narayan, *Materials Today*, 2014, **17**, 247–252.

[6] C. Ainsley, N. Reis and B. Derby, *Journal of Materials Science*, 2002, **37**, 3155–3161.

[7] T. Wang, R. Patel and B. Derby, *Soft Matter*, 2008, **4**, 2513–2518.

[8] J. Bharathan and Y. Yang, *Applied Physics Letters*, 1998, **72**, 2660–2662.

[9] B.-J. de Gans and U. S. Schubert, *Langmuir*, 2004, **20**, 7789–7793.

[10] J. Moon, J. E. Grau, V. Knezevic, M. J. Cima and E. M. Sachs, *Journal of the American Ceramic Society*, 2004, **85**, 755–762.

[11] K. A. M. Seerden, N. Reis, J. R. G. Evans, P. S. Grant, J. W. Halloran and B. Derby, *Journal of the American Ceramic Society*, 2001, **84**, 2514–2520.

[12] I. M. Hutchings and G. D. Martin, *Inkjet technology for digital fabrication*, J Wiley, 2012, p. 390.

[13] B. Derby, *Journal of Materials Chemistry*, 2008, **18**, 5717.

[14] J. R. Castrejon-Pita, W. R. S. Baxter, J. Morgan, S. Temple, G. D. Martin and I. M. Hutchings, *Atomization and Sprays*, 2013, **23**, 541–565.

[15] A. Pekarovicova, H. Bhide, P. D. Fleming and J. Pekarovic, *Journal of Coatings Technology*, 2003, **75**, 65–72.

[16] S. El-Sherbiny, *Surface Coatings International Part B: Coatings Transactions*, 2003, **86**, 263–271.

[17] A. Borhan, S. B. Pence and A. H. Sporer, *Journal of Imaging Technology*, 1990, **16**, 65–69.

[18] H. Noguchi and M. Shimomura, *RadTech Report*, 2001, **15**, 22–25.

[19] A. Hudd, in *The Chemistry of Inkjet Inks*, ed. S. Magdassi, WORLD SCIENTIFIC, Singapore, 1st edn., 2009, pp. 3–18.

[20] T. Lamminmaki, J. Kettle and P. Gane, *Colloids and Surfaces A: Physicochemical and Engineering Aspects*, 2011, **380**, 79–88.

[21] S. Sousa, J. A. Gamelas, A. de Oliveira Mendes, P. T. Fiadeiro and A. Ramos, *Materials Chemistry and Physics*, 2013, **139**, 877–884.

[22] H. K. Uma and S. K. Menon, *Procedia Engineering*, 2013, **51**, 436–442.

[23] H. Koo, M. Chen, P. Pan, L. Chou, F. Wu, S. Chang and T. Kawai, *Displays*, 2006, **27**, 124–129.

[24] D. J. Shaw, in *Introduction to Colloid and Surface Chemistry*, Elsevier, 4th edn., 1966, p. 306.

[25] P. K. Prasad, A. V. Reddy, P. Rajesh, P. Ponnambalam and K. Prakasan, *Journal of Materials Processing Technology*, 2006, **176**, 222–229.

[26] S. D. Hoath, D. C. Vadillo, O. G. Harlen, C. McIlroy, N. F. Morrison, W.-K. Hsiao, T. R. Tuladhar, S. Jung, G. D. Martin and I. M. Hutchings, *Journal of Non-Newtonian Fluid Mechanics*, 2014, **205**, 1–10.

[27] K. Holmberg, B. Jönsson, B. Kronberg and B. Lindman, *Surfactants and polymers in aqueous solution.*, John Wiley & Sons, Great Britain, 2nd edn., 2003, p. 562.

[28] B. Kronberg, K. Holmberg and B. Lindman, *Surface chemistry of surfactants and polymers*, John Wiley & Sons, 2014, p. 496.

[29] Z. Miao, J. Yang, L. Wang, Y. Liu, L. Zhang, X. Li and L. Peng, *Materials Letters*, 2008, **62**, 3450–3452.

[30] G. Ran, Y. Zhang, Q. Song, Y. Wang and D. Cao, *Colloids and Surfaces B: Biointerfaces*, 2009, **68**, 106–110.

[31] A. M. Cardoso, H. Faneca, J. A. Almeida, A. A. Pais, E. F. Marques, M. C. P. de Lima and A. S. Jurado, *Biochimica et Biophysica Acta (BBA) - Biomembranes*, 2011, **1808**, 341–351.

[32] M. J. Rosen and J. T. Kunjappu, *Surfactants and Interfacial Phenomena, Fourth Edition*, Milton J. Rosen, 4th edn., 2012, p. 580.

[33] H. N. W. Lekkerkerker and R. Tuinier, *Colloids and the depletion interaction*, Springer, Dordrecht, Netherlands, 2011, p. 234.

[34] Y. Liang, N. Hilal, P. Langston and V. Starov, *Advances in Colloid and Interface Science*, 2007, **134-135**, 151–166.

[35] Z. Zhou, P. J. Scales and D. V. Boger, *Chemical Engineering Science*, 2001, **56**, 2901–2920.

[36] J. K. Oh, R. Drumright, D. J. Siegwart and K. Matyjaszewski, *Progress in Polymer Science*, 2008, **33**, 448–477.

[37] M. Kuruppuarachchi, H. Savoie, A. Lowry, C. Alonso and R. W. Boyle, *Molecular Pharmaceutics*, 2011, **8**, 920–931.

[38] S.-C. Luo, E. M. Ali, N. C. Tansil, H.-h. Yu, S. Gao, E. A. B. Kantchev and J. Y. Ying, *Langmuir*, 2008, **24**, 8071–8077.

[39] H. A. Clark, M. Hoyer, M. A. Philbert and R. Kopelman, *Analytical Chemistry*, 1999, **71**, 4831–4836.

[40] L. L. de Arbina and J. Asua, *Polymer*, 1992, **33**, 4832–4837.

[41] M. do Amaral, S. van Es and J. M. Asua, *Journal of Applied Polymer Science*, 2005, **97**, 733–744.

[42] F. Ylmaz, *Polymer Science*, InTech, 2013, p. 246.

[43] F. Hofmann and K. Delbruck, *Free Radical Suspension Polymerization*, 1909, `Gr.Pat. ,250690,.`

[44] T. Lindner, *Us1732975 a*, 1929.

[45] C. Chern, *Progress in Polymer Science*, 2006, **31**, 443–486.

[46] W. D. Harkins, *The Journal of Chemical Physics*, 1945, **13**, 381–382.

[47] W. V. Smith and R. H. Ewart, *The Journal of Chemical Physics*, 1948, **16**, 592–599.

[48] H. B. Yamak, *Book Chapter*, 2013, 1–38.

[49] M. C. Smith and G. D. Parfitt, *Trans. Faraday Soc.*, 1969, **65**, 1138–1145.

[50] J. Qiu, B. Charleux and K. Matyjaszewski, *Progress in Polymer Science*, 2001, **26**, 2083–2134.

[51] C. Babac, G. Guven, G. David, B. C. Simionescu and E. Piskin, *European Polymer Journal*, 2004, **40**, 1947–1952.

[52] A. Lapresta-Fernandez, P. J. Cywinski, A. J. Moro and G. J. Mohr, *Analytical and bioanalytical chemistry*, 2009, **395**, 1821–1830.

[53] J. Deng, B. Chen, X. Luo and W. Yang, *Macromolecules*, 2009, **42**, 933–938.

[54] R. M. Fitch, *Polymer colloids : A Comprehensive Introduction*, Academic Press, USA, 2nd edn., 1997, p. 346.

[55] P. A. Lovell and M. S. El-Aasser, *Emulsion polymerization and emulsion polymers*, Wiley, England, 1st edn., 1997, p. 826.

[56] D. Hunkeler, F. Candau, C. Pichot, A. E. Hemielec, T. Y. Xie, J. Barton, V. Vaskova, J. Guillot, M. V. Dimonie and K. H. Reichert, in *Theories and Mechanism of Phase Transitions, Heterophase Polymerizations, Homopolymerization, Addition Polymerization*, Springer-Verlag, Berlin/Heidelberg, 1994, ch. 2, pp. 115–133.

[57] J. R. Leiza, E. D. Sudol and M. S. El-Aasser, *Journal of Applied Polymer Science*, 1997, **64**, 1797–1809.

[58] Z. Zhang, X. Ji and P. Wang, *Colloids and Surfaces A: Physicochemical and Engineering Aspects*, 2014, **441**, 510–516.

[59] J. Reimers and F. J. Schork, *Journal of Applied Polymer Science*, 1996, **59**, 1833–1841.

[60] B. Kriwet, E. Walter and T. Kissel, *Journal of Controlled Release*, 1998, **56**, 149–158.

[61] A. Ethirajan, U. Ziener and K. Landfester, *Chemistry of Materials*, 2009, **21**, 2218–2225.

[62] X. Jiang, J. Dausend, M. Hafner, A. Musyanovych, C. Ro?cker, K. Landfester, V. Mailander and G. U. Nienhaus, *Biomacromolecules*, 2010, **11**, 748–753.

[63] J. Ugelstad, M. S. El-Aasser and J. W. Vanderhoff, *Journal of Polymer Science: Polymer Letters Edition*, 1973, **11**, 503–513.

[64] J. M. Asua, *Progress in Polymer Science*, 2002, **27**, 1283–1346.

[65] A. Munoz-Bonilla, A. M. van Herk and J. P. A. Heuts, *Macromolecules*, 2010, **43**, 2721–2731.

[66] J. C. Garay-Jimenez, D. Gergeres, A. Young, D. V. Lim and E. Turos, *Nanomedicine: Nanotechnology, Biology and Medicine*, 2009, **5**, 443–451.

[67] X. Hu, J. Zhang and W. Yang, *Polymer*, 2009, **50**, 141–147.

[68] J. D. S. Nunes and J. M. Asua, *Langmuir*, 2013, **29**, 3895–3902.

[69] S.-J. Yoon, H. Chun, M.-S. Lee and N. Kim, *Synthetic Metals*, 2009, **159**, 518–522.

[70] J. Gao and C. Wu, *Langmuir*, 2005, **21**, 782–5.

[71] S.-W. Pang, H.-Y. Park, Y.-S. Jang, W.-S. Kim and J.-H. Kim, *Colloids and Surfaces B: Biointerfaces*, 2002, **26**, 213–222.

[72] C. Chern, T. Chen and Y. Liou, *Polymer*, 1998, **39**, 3767–3777.

[73] X. Cui, S. Zhong and H. Wang, *Polymer*, 2007, **48**, 7241–7248.

[74] S. Akgöl, N. Öztürk and A. Denizli, *Journal of Applied Polymer Science*, 2010, **115**, 1608–1615.

[75] R. P. Moraes, R. A. Hutchinson and T. F. L. McKenna, *Journal of Polymer Science Part A: Polymer Chemistry*, 2010, **48**, 48–54.

[76] W. Ming, F. N. Jones and S. Fu, *Polymer Bulletin*, 1998, **40**, 749–756.

[77] S. Sajjadi, *Langmuir*, 2006, **23**, 1018–1024.

[78] N. M. B. Smeets, R. P. Moraes, J. A. Wood and T. F. L. McKenna, *Langmuir*, 2011, **27**, 575–581.

[79] S. H. Park, H. H. Song, J. H. Han, J. M. Park, E. J. Lee, S. M. Park, K. J. Kang, J. H. Lee, S. S. Hwang, S. C. Rho, S. O. JHeong, H. J. Chung and K. S. Shinn, *Invest Radiol*, 1994, **29**, 54–58.

[80] T. Tanrisever, O. Okay and I. e. Snmezo?lu, *Journal of Applied Polymer Science*, 1996, **61**, 485–493.

[81] Z. An, W. Tang, C. J. Hawker and G. D. Stucky, *Journal of the American Chemical Society*, 2006, **128**, 15054–15055.

[82] S. T. Camli, F. Buyukserin, O. Balci and G. G. Budak, *Journal of colloid and interface science*, 2010, **344**, 528–532.

[83] A. M. Telford, B. T. T. Pham, C. Neto and B. S. Hawkett, *Journal of Polymer Science Part A: Polymer Chemistry*, 2013, **51**, 3997–4002.

[84] X. Wang and Z. Zhang, *Radiation Physics and Chemistry*, 2006, **75**, 1001–1005.

[85] C. J. Hawker, A. W. Bosman and E. Harth, *Chemical Reviews*, 2001, **101**, 3661–3688.

[86] B. B. Wayland, G. Poszmik, S. L. Mukerjee and M. Fryd, *Journal of the American Chemical Society*, 1994, **116**, 7943–7944.

[87] M. K. Georges, R. P. N. Veregin, P. M. Kazmaier and G. K. Hamer, *Macromolecules*, 1993, **26**, 2987–2988.

[88] M. Kato, M. Kamigaito, M. Sawamoto and T. Higashimura, *Macromolecules*, 1995, **28**, 1721–1723.

[89] J. Chiefari, Y. K. B. Chong, F. Ercole, J. Krstina, J. Jeffery, T. P. T. Le, R. T. A. Mayadunne, G. F. Meijs, C. L. Moad, G. Moad, E. Rizzardo and S. H. Thang, *Macromolecules*, 1998, **31**, 5559–5562.

[90] G. Moad, E. Rizzardo and S. H. Thang, *Australian Journal of Chemistry*, 2009, **62**, 1402–1472.

[91] G. Moad, J. Chiefari, B. Y. B. Y. Chong, J. Krstina, R. T. T. Mayadunne, A. Postma, E. Rizzardo and S. H. Thang, *Polymer International*, 2000, **49**, 993–1001.

[92] J. Rieger, F. Stoffelbach, C. Bui, D. Alaimo, C. Jerome and B. Charleux, *Macromolecules*, 2008, **41**, 4065–4068.

[93] S. W. Prescott, M. J. Ballard, E. Rizzardo and R. G. Gilbert, *Australian Journal of Chemistry*, 2002, **55**, 415–424.

[94] A. Butté, G. Storti and M. Morbidelli, *Macromolecules*, 2001, **34**, 5885–5896.

[95] S. W. Prescott, M. J. Ballard, E. Rizzardo and R. G. Gilbert, *Macromolecules*, 2002, **35**, 5417–5425.

[96] B. T. T. Pham, D. Nguyen, C. J. Ferguson, B. S. Hawkett, A. K. Serelis and C. H. Such, *Macromolecules*, 2003, **36**, 8907–8909.

[97] C. J. Ferguson, R. J. Hughes, D. Nguyen, B. T. T. Pham, R. G. Gilbert, A. K. Serelis, C. H. Such and B. S. Hawkett, *Macromolecules*, 2005, **38**, 2191–2204.

[98] S. E. Shim, Y. Shin, H. Lee, H. Jung, Y. H. Chang and S. Choe, *Journal of Industrial and Engineering Chemistry*, 2003, **9**, 619–628.

[99] J. M. Asua, *Polymeric Dispersions: Principles and Applications*, Springer Netherlands, Dordrecht, 1997.

[100] A. Guyot, F. Chu, M. Schneider, C. Graillat and T. F. McKenna, *Progress in Polymer Science*, 2002, **27**, 1573–1615.

[101] I. d. F. Mariz, I. S. Millichamp, J. C. de la Cal and J. R. Leiza, *Progress in Organic Coatings*, 2010, **68**, 225–233.

[102] I. d. F. A. Mariz, J. C. de la Cal and J. R. Leiza, *Macromolecular Reaction Engineering*, 2011, **5**, 361–372.

[103] S. Boutti, C. Graillat and T. F. McKenna, *Macromolecular Symposia*, 2004, **206**, 383–398.

[104] M. Schneider, J. Claverie, C. Graillat and T. F. McKenna, *Journal of Applied Polymer Science*, 2002, **84**, 1878–1896.

[105] Z.-Q. Ai, Q.-L. Zhou, C.-S. Xie and H.-T. Zhang, *Journal of Applied Polymer Science*, 2007, **103**, 1815–1825.

[106] M. Schneider, C. Graillat, A. Guyot and T. F. McKenna, *Journal of Applied Polymer Science*, 2002, **84**, 1916–1934.

[107] S. Sajjadi, *Journal of Polymer Science Part A: Polymer Chemistry*, 2001, **39**, 3940–3952.

[108] R. Ledezma, M. Esther Treviño, L. E. Elizalde, L. A. Pérez-Carrillo, E. Mendizábal, J. E. Puig and R. G. López, *Journal of Polymer Science Part A: Polymer Chemistry*, 2007, **45**, 1463–1473.

[109] C. Norakankorn, Q. Pan, G. L. Rempel and S. Kiatkamjornwong, *Macromolecular Rapid Communications*, 2007, **28**, 1029–1033.

[110] G. He, Q. Pan and G. L. Rempel, *Industrial and Engineering Chemistry Research*, 2007, **46**, 1682–1689.

[111] G. He, Q. Pan and G. L. Rempel, *Journal of Applied Polymer Science*, 2007, **105**, 2129–2137.

[112] H. Wang, Q. Pan and G. L. Rempel, *European Polymer Journal*, 2011, **47**, 973–980.

[113] J. Aguilar, M. Rabelero, S. M. Nuño-Donlucas, E. Mendizábal, A. Martínez-Richa, R. G. López, M. Arellano and J. E. Puig, *Journal of Applied Polymer Science*, 2011, **119**, 1827–1834.

[114] J. D. S. Nunes and J. M. Asua, *Langmuir*, 2012, **28**, 7333–7342.

[115] M. G. Pérez-García, M. Rabelero, S. M. Nuño-Donlucas, E. Mendizábal, A. Martínez-Richa, R. G. López, M. Arellano and J. E. Puig, *Journal of Macromolecular Science, Part A*, 2012, **49**, 539–546.

[116] A. Mader, A. Schirò, M. Brischetto and B. Pizzo, *Progress in Organic Coatings*, 2011, **71**, 123–135.

[117] A. Bellamine, E. Degrandi, M. Gerst, R. Stark, C. Beyers and C. Creton, *Macromolecular Materials and Engineering*, 2011, **296**, 31–41.

[118] D. England, N. Tambe and J. Texter, *ACS Macro Letters*, 2012, **1**, 310–314.

[119] S. Nimesh, R. Manchanda, R. Kumar, A. Saxena, P. Chaudhary, V. Yadav, S. Mozumdar and R. Chandra, *International Journal of Pharmaceutics*, 2006, **323**, 146–152.

[120] C. Larpent, S. Amigoni-Gerbier and A.-P. De Sousa Delgado, *Comptes Rendus Chimie*, 2003, **6**, 1275–1283.

[121] W. Zheng, F. Gao and H. Gu, *Journal of Magnetism and Magnetic Materials*, 2005, **293**, 199–205.

[122] M. Antonietti, Y. Shen, T. Nakanishi, M. Manuelian, R. Campbell, L. Gwee, Y. A. Elabd, N. Tambe, R. Crombez and J. Texter, *ACS Applied Materials & Interfaces*, 2010, **2**, 649–653.

[123] C. Cannizzo, C. R. Mayer, F. Sécheresse and C. Larpent, *Advanced Materials*, 2005, **17**, 2888–2892.

[124] S. H. Sonawane, B. M. Teo, A. Brotchie, F. Grieser and M. Ashokkumar, *Industrial & Engineering Chemistry Research*, 2010, **49**, 2200–2205.

[125] D. C. Steytler, A. Gurgel, R. Ohly, M. Jung and R. K. Heenan, *Langmuir*, 2004, **20**, 3509–3512.

[126] T. P. Davis, D. M. Haddleton and S. N. Richards, *Journal of Macromolecular Science, Part C: Polymer Reviews*, 1994, **34**, 243–324.

[127] T. Davis, D. Kukulj, D. Haddleton and D. Maloney, *Trends in Polymer Science*, 1995, **3**, 365–373.

[128] J. P. A. Heuts and N. M. B. Smeets, *Polymer Chemistry*, 2011, **2**, 2407–2423.

[129] J. P. A. Heuts, G. E. Roberts and J. D. Biasutti, *Australian Journal of Chemistry*, 2002, **55**, 381–398.

[130] A. A. Gridnev* and S. D. Ittel*, *Chemical Reviews*, 2001, **101**, 3611–3660.

[131] *Milli-Q® Reference Water Purification Systems (accessed 10/03/2018)*, `http://www.merckmillipore.com/GB/en/product/Milli-Q-Reference-Water-Purification-System,MM{_}NF-C79625`.

[132] Malvern Instruments, *Dynamic Light Scattering: An Introduction in 30 Minutes*, https://www.malvernpanalytical.com/en/learn/knowledge-center/technical-notes/TN101104DynamicLightScatteringIntroduction.

[133] R. Finsy, *Advances in Colloid and Interface Science*, 1994, **52**, 79–143.

[134] R. Pecora, *Dynamic Light Scattering : Applications of Photon Correlation Spectroscopy*, Plenum Press, New York, 1985, p. 420.

[135] M. Rhodes and Wiley InterScience (Online service), *Introduction to Particle Technology*, Wiley, Chichester, UK, 2008.

[136] R. J. Hunter, *Colloids and Surfaces A: Physicochemical and Engineering Aspects*, 1998, **141**, 37–66.

[137] J. Lyklema, *Fundamentals of interface and colloid science. Particulate colloids*, Elsevier Ltd, 2005.

[138] Malvern Panalytical, *Measure zeta potential to improve formulation stability*, https://www.malvernpanalytical.com/en/products/measurement-type/zeta-potential.

[139] J. Kuo, *Electron microscopy : methods and protocols.*, Humana Press, 2007, p. 608.

[140] L. Reimer, *Scanning electron microscopy : physics of image formation and microanalysis*, Springer, 1998, p. 527.

[141] R. N. Ibbett, *NMR spectroscopy of polymers*, Blackie Academic & Professional, 1993, p. 362.

[142] BiolinSientific, *Optical Tensiometers*, https://www.biolinscientific.com/attension/optical-tensiometers/theta-lite.

[143] J. Bao and A. Zhang, *Journal of Applied Polymer Science*, 2004, **93**, 2815–2820.

[144] S. L. Kettlewell, A. Schmid, S. Fujii, D. Dupin and S. P. Armes, *Langmuir*, 2007, **23**, 11381–11386.

[145] J. Mewis and N. J. Wagner, *Colloidal suspension rheology*, Cambridge University Press, 2012, p. 393.

[146] M. A. Rao, *Rheology of fluid and semisolid foods : principles and applications*, Springer US, 2007, p. 481.

[147] D. B. Genovese, *Advances in Colloid and Interface Science*, 2012, **171-172**, 1–16.

[148] T. Tadros, *Advances in Colloid and Interface Science*, 1996, **68**, 97–200.

[149] A. Einstein, *Annalen der Physik*, 1906, **324**, 289–306.

[150] A. Einstein, *Annalen der Physik*, 1911, **34**, 591–592.

[151] I. M. Krieger and T. J. Dougherty, *Transactions of the Society of Rheology*, 1959, **3**, 137–152.

[152] K. Qin and A. A. Zaman, *Journal of Colloid and Interface Science*, 2003, **266**, 461–467.

[153] D. Quemada and C. Berli, *Advances in Colloid and Interface Science*, 2002, **98**, 51–85.

[154] C. W. Macosko, *Rheology : principles, measurements, and applications*, Wiley-VCH, 1994, p. 568.

[155] H. A. Barnes, *Journal of Rheology*, 1989, **33**, 329–366.

[156] A. B. Metzner, *Journal of Rheology*, 1985, **29**, 739–775.

[157] C. Berli, J. Deiber and M. Añón, *Food Hydrocolloids*, 1999, **13**, 507–515.

[158] F. Rubio-Hernandez, F. Carrique and E. Ruiz-Reina, *Advances in Colloid and Interface Science*, 2004, **107**, 51–60.

[159] D. B. Genovese, J. E. Lozano and M. A. Rao, *Journal of Food Science*, 2007, **72**, R11–R20.

[160] A. Ogawa, H. Yamada, S. Matsuda, K. Okajima and M. Doi, *Journal of Rheology*, 1997, **41**, 769–785.

[161] J. M. Brader, *Journal of Physics: Condensed Matter*, 2010, **22**, 363101.

[162] P. Coussot and C. Ancey, *Physical Review E*, 1999, **59**, 4445–4457.

[163] *MEGlobal Ethylene Glycol product guide (accessed 10/03/2018)*, `http://www.meglobal.biz/media/product{_}guides/MEGlobal{_}MEG.pdf`.

[164] RheoSense, *m-VROC Viscometer*, `http://www.rheosense.com/products/viscometers/m-vroc/overview`.

[165] LUM GmbH, *LUMiSizer®*, `http://www.lumisizer.com/`.

[166] H. A. Barnes, *Rheology Reviews*, 2003, 1–36.

[167] M. Zahn, Y. Ohki, D. B. Fenneman, R. J. Gripshover and V. H. Gehman, *Proceedings of the IEEE*, 1986, **74**, 1–55.

[168] P. W. Atkins and J. De Paula, *Atkins' Physical chemistry*, Oxford University Press, 2010, p. 972.

[169] S. D. Hoath, O. G. Harlen and I. M. Hutchings, *Journal of Rheology*, 2012, **56**, 1109–1127.

[170] P. P. Bhat, S. Appathurai, M. T. Harris, M. Pasquali, G. H. Mckinley and O. A. Basaran, *Nature Physics*, 2010, **6**, 625–631.

[171] T. Tuladhar and M. Mackley, *Journal of Non-Newtonian Fluid Mechanics*, 2008, **148**, 97–108.

[172] *Fundamentals of inkjet printing: the science of inkjet and droplets*, ed. S. D. Hoath, Wiley-VCH Verlag GmbH & Co. KGaA, Weinheim, Germany, 2016.

[173] S. J. Haward, *Biomicrofluidics*, 2016, **10**, 043401.

[174] F. Del Giudice, S. J. Haward and A. Q. Shen, *Journal of Rheology*, 2017, **61**, 327–337.

[175] S. J. Haward, A. Jaishankar, M. S. N. Oliveira, M. A. Alves and G. H. McKinley, *Biomicrofluidics*, 2013, **7**, 044108.

[176] G. H. McKinley and M. Renardy, *Physics of Fluids*, 2011, **23**, 127101.

[177] S. D. Hoath, S. Jung, W.-K. Hsiao and I. M. Hutchings, *Organic Electronics*, 2012, **13**, 3259–3262.

[178] Z. Xiong and C. Liu, *Organic Electronics*, 2012, **13**, 1532–1540.

[179] T. Sridhar, V. Tirtaatmadja, D. Nguyen and R. Gupta, *Journal of Non-Newtonian Fluid Mechanics*, 1991, **40**, 271–280.

[180] G. H. McKinley and T. Sridhar, *Annual Review of Fluid Mechanics*, 2002, **34**, 375–415.

[181] D. Binding and K. Walters, *Journal of Non-Newtonian Fluid Mechanics*, 1988, **30**, 233–250.

[182] A. E. Everage and R. L. Ballman, *Nature*, 1978, **273**, 213–215.

[183] M. R. Mackley, R. T. J. Marshall and J. B. A. F. Smeulders, *Journal of Rheology*, 1995, **39**, 1293–1309.

[184] A. Tripathi, K. C. Tam and G. H. McKinley, *Macromolecules*, 2006, **39**, 1981–1999.

[185] B. Guy, M. Hermes and W. Poon, *Physical Review Letters*, 2015, **115**, 088304.

[186] M. Trulsson, B. Andreotti and P. Claudin, *Physical Review Letters*, 2012, **109**, 118305.

[187] F. Boyer, É. Guazzelli and O. Pouliquen, *Physical Review Letters*, 2011, **107**, 188301.

[188] J. M. Brader, M. E. Cates and M. Fuchs, *Physical Review Letters*, 2008, **101**, 138301.

[189] M. Chellamuthu, E. M. Arndt and J. P. Rothstein, *Soft Matter*, 2009, **5**, 2117.

[190] E. E. Bischoff White, M. Chellamuthu and J. P. Rothstein, *Rheologica Acta*, 2010, **49**, 119–129.

[191] C. J. Petrie, *Journal of Non-Newtonian Fluid Mechanics*, 2006, **137**, 15–23.

[192] A. A. Collyer, *Techniques in Rheological Measurement*, Springer Netherlands, New York, 1993, p. 360.

[193] D. E. Smith and S. Chu, *Science (New York, N.Y.)*, 1998, **281**, 1335–40.

[194] T. T. Perkins, D. E. Smith and S. Chu, *Science (New York, N.Y.)*, 1997, **276**, 2016–21.

[195] K. D. Coventry and M. R. Mackley, *Journal of Rheology*, 2008, **52**, 401–415.

[196] D. Auhl, D. M. Hoyle, D. Hassell, T. D. Lord, O. G. Harlen, M. R. Mackley and T. C. B. McLeish, *Journal of Rheology*, 2011, **55**, 875–900.

[197] J. Soulages, T. Schweizer, D. Venerus, M. Kröger and H. Öttinger, *Journal of Non-Newtonian Fluid Mechanics*, 2008, **154**, 52–64.

[198] A. Abedijaberi, J. Soulages, M. Kröger and B. Khomami, *Rheologica Acta*, 2009, **48**, 97–108.

[199] R. Dylla-Spears, J. E. Townsend, L. Jen-Jacobson, L. L. Sohn and S. J. Muller, *Lab on a Chip*, 2010, **10**, 1543.

[200] J. A. Pathak and S. D. Hudson, *Macromolecules*, 2006, **39**, 8782–8792.

[201] N. Ait Mouheb, D. Malsch, A. Montillet, C. Solliec and T. Henkel, *Chemical Engineering Science*, 2012, **68**, 278–289.

[202] S. J. Haward, R. J. Poole, M. A. Alves, P. J. Oliveira, N. Goldenfeld and A. Q. Shen, *Physical Review E*, 2016, **93**, 031101.

[203] S. J. Haward, M. S. N. Oliveira, M. A. Alves and G. H. McKinley, *Physical Review Letters*, 2012, **109**, 128301.

[204] Z. Li, X.-F. Yuan, S. J. Haward, J. A. Odell and S. Yeates, *Journal of Non-Newtonian Fluid Mechanics*, 2011, **166**, 951–963.

[205] A. S. Lubansky and M. T. Matthews, *Journal of Rheology*, 2015, **59**, 835–864.

[206] O. Cheal and C. Ness, *Journal of Rheology*, 2018, **62**, 501–512.

[207] *Micro/ Bio/ Nanofluidics Unit (Amy Shen)*, `https://groups.oist.jp/mbnu`.

[208] *Three-dimensional rendering of the microfluidic platform used in this research to study polymer solution*, https://www.oist.jp/news-center/photos/three-dimensional-rendering-microfluidic-platform-used-research-study-polymer.

[209] S. Hoath, I. Hutchings, G. Martin, T. Tuladhar, M. Mackley and D. Vadillo, *Journal of Imaging Science and Technology*, 2009, **53**, 050304–050308.

[210] S. D. Hoath, J. R. Castrejón-Pita, W.-K. Hsiao, S. Jung, G. D. Martin, I. M. Hutchings, T. R. Tuladhar, D. C. Vadillo, S. a. Butler, M. R. Mackley, C. McIlroy, N. F. Morrison, O. G. Harlen and H. N. G. Yow, *Journal of Imaging Science and Technology*, 2013, **57**, 1–10.

[211] H. Barnes and G. Roberts, *Journal of Non-Newtonian Fluid Mechanics*, 1992, **44**, 113–126.

[212] J. Greener and J. R. G. Evans, *Journal of Rheology*, 1998, **42**, 697.

[213] E. L. Talbot, H. N. Yow, L. Yang, A. Berson, S. R. Biggs and C. D. Bain, *ACS Applied Materials & Interfaces*, 2015, **7**, 3782–3790.

[214] U. S. Nandi and S. R. Palit, *Journal of Polymer Science*, 1955, **17**, 65–78.

[215] A. Guyot, K. Tauer, J. Asua, S. Van Es, C. Gauthier, A. Hellgren, D. Sherrington, A. Montoya-Goni, M. Sjoberg, O. Sindt, F. Vidal, M. Unzue, H. Schoonbrood, E. Shipper and P. Lacroix-Desmazes, *Acta Polymerica*, 1999, **50**, 57–66.

[216] D. C. Blackley, *Polymer latices science and technology*, Chapman & Hall, London, 2nd edn., 1997, p. 616.

[217] D. Donescu, K. Goa, J. Languri and A. Ciupioiu, *Journal of Macromolecular Science: Part A - Chemistry*, 1985, **22**, 941–954.

[218] D. Donescu, K. Goa, A. Ciupioiu and I. Languri, *Journal of Macromolecular Science: Part A - Chemistry*, 1985, **22**, 931–940.

[219] J. Šupárek, P. Bradna, L. Mrkvičková, F. Lednický and O. Quadrat, *Collection of Czechoslovak Chemical Communications*, 1995, **60**, 1756–1764.

[220] S. Sajjadi and B. W. Brooks, *Journal of Applied Polymer Science*, 1999, **74**, 3094–3110.

[221] S. Sajjadi and B. W. Brooks, *Journal of Applied Polymer Science*, 2000, **79**, 582–597.

[222] S. Sajjadi and B. Brooks, *Chemical Engineering Science*, 2000, **55**, 4757–4781.

[223] S. Sajjadi, *Journal of Polymer Science Part A: Polymer Chemistry*, 2000, **38**, 3612–3630.

[224] S. Sajjadi and B. W. Brooks, *Journal of Polymer Science Part A: Polymer Chemistry*, 2000, **38**, 528–545.

[225] M. Al-Bagoury and E.-J. Yaacoub, *Journal of Applied Polymer Science*, 2003, **90**, 2091–2102.

[226] M. Al-Bagoury and E.-J. Yaacoub, *European Polymer Journal*, 2004, **40**, 2617–2627.

[227] M. Mayer, J. Meuldijk and D. Thoenes, *Chemical Engineering Science*, 1994, **49**, 4971–4980.